MEASUREMENTS OF VELOCITY COMPONENTS IN THE WAKE OF A FULL-SCALE HELICOPTER ROTOR IN HOVER

Donald W. Boatwright

Mississippi State University

Prepared for:

Army Air Mobility Research and Development Laboratory

August 1972

AD

USAAMRDL TECHNICAL REPORT 72-33

MEASUREMENTS OF VELOCITY COMPONENTS IN THE WAKE OF A FULL-SCALE HELICOPTER ROTOR IN HOVER

By

Donald W. Boatwright

August 1972

EUSTIS DIRECTORATE
U. S. ARMY AIR MOBILITY RESEARCH AND DEVELOPMENT LABORATORY
FORT EUSTIS, VIRGINIA

CONTRACT DAAJ02-67-C-0105
THE DEPARTMENT OF AEROPHYSICS AND AEROSPACE ENGINEERING
MISSISSIPPI STATE UNIVERSITY
STATE COLLEGE, MISSISSIPPI

DISCLAIMERS

The findings in this report are not to be construed as an official Department of the Army position unless so designated by other authorized documents.

When Government drawings, specifications, or other data are used for any purpose other than in connection with a definitely related Government procurement operation, the United States Government thereby incurs no responsibility nor any obligation whatsoever; and the fact that the Government may have formulated, furnished, or in any way supplied the said drawings, specifications, or other data is not to be regarded by implication or otherwise as in any manner licensing the holder or any other person or corporation, or conveying any rights or permission, to manufacture, use, or sell any patented invention that may in any way be related thereto.

Trade names cited in this report do not constitute an official endorsement or approval of the use of such commercial hardware or software.

DISPOSITION INSTRUCTIONS

Destroy this report when no longer needed. Do not return it to the originator.

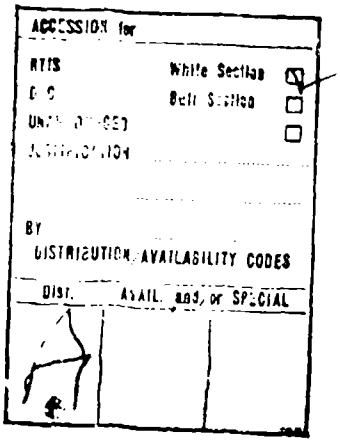

DEPARTMENT OF THE ARMY
U. S. ARMY AIR MOBILITY RESEARCH & DEVELOPMENT LABORATORY
EUSTIS DIRECTORATE
FORT EUSTIS, VIRGINIA 23604

This report has been reviewed by the Eustis Directorate, U. S. Army Air Mobility Research and Development Laboratory, and is considered to be technically sound. The report is published for the exchange of information and the stimulation of ideas. The program was conducted under the technical management of Mr. Frederick A. Raitch of the Aeromechanics Division of this Directorate.

UNCLASSIFIED
Security Classification

DOCUMENT CONTROL DATA - R & D

(Security classification of title, body of abstract and indexing annotation must be entered when the overall report is classified)

1. ORIGINATING ACTIVITY (Corporate author)

Mississippi State University
Dept. of Aerophysics and Aerospace Engineering
State College, Mississippi

2a. REPORT SECURITY CLASSIFICATION

UNCLASSIFIED

2b. GROUP

3. REPORT TITLE

MEASUREMENTS OF VELOCITY COMPONENTS IN THE WAKE OF A FULL-SCALE HELICOPTER ROTOR IN HOVER

4. DESCRIPTIVE NOTES (Type of report and inclusive dates)

Final Report

5. AUTHOR(S) (First name, middle initial, last name)

Donald W. Boatwright

6. REPORT DATE	7a. TOTAL NO. OF PAGES	7b. NO. OF REFS
August 1972	126	13

8a. CONTRACT OR GRANT NO.	9a. ORIGINATOR'S REPORT NUMBER(S)
DAAJ02-67-C-0105	USAAMRDL Technical Report 72-33
b. PROJECT NO. Task 1F162204A13903	
c.	9b. OTHER REPORT NO(S) (Any other numbers that may be assigned this report)
d.	AASE Report No. 72-59

10. DISTRIBUTION STATEMENT

Approved for public release; distribution unlimited.

11. SUPPLEMENTARY NOTES	12. SPONSORING MILITARY ACTIVITY
	Eustis Directorate U.S. Army Air Mobility R & D Laboratory Fort Eustis, Virginia

13. ABSTRACT

This report presents three-component wake velocity measurements made with a split-film total vector anemometer. The measurements were made in the wake of a full-scale OH-13E helicopter rotor which was mounted on a 60-foot rotor test tower at Mississippi State University. Time-averaged velocity distributions along wake radii at various distances below the rotor disk were measured for two conditions of disk loading and three combinations of blade pitch and rotor speed. Instantaneous velocity measurements were made across the helical vortex trails to investigate the effects of blade pitch and rotor speed on vortex structure, core size, transport velocity, and distribution of axial and tangential velocity components within the vortices. The results indicated that maximum values of induced velocity in the mean wake exceeded twice the magnitude of momentum values, and that instantaneous values of the vertical velocity component in the vicinity of the vortex trails could be as large as ten times the momentum value of induced velocity at high thrust coefficients. Velocity distributions across the tip vortices revealed longitudinal components of velocity of the same order of magnitude as the rotational components. Also, tip vortex structure and dissipation characteristics were found to be similar to the vortices shed from fixed-wing aircraft. The effects of varying the test parameters were reflected as significant changes of the flow within the rotor tip vortex trails, and as smaller variations of the velocity components of the inner wake region.

DD FORM 1 NOV 68 1473 REPLACES DD FORM 1473, 1 JAN 64, WHICH IS OBSOLETE FOR ARMY USE.

UNCLASSIFIED
Security Classification

14. KEY WORDS	LINK A		LINK B		LINK C	
	ROLE	WT	ROLE	WT	ROLE	WT
Helicopter Rotors Helicopter Rotor Wake Vortices						

ib

Task 1F162204A13903
Contract DAAJ02-67-C-0105
USAAMRDL Technical Report 72-33
August 1972

MEASUREMENTS OF VELOCITY COMPONENTS IN THE WAKE OF A FULL-SCALE HELICOPTER ROTOR IN HOVER

AASE Report No. 72-59

By

Donald W. Boatwright

Prepared by

Raspet Flight Research Laboratory
The Department of Aerophysics and Aerospace Engineering
Mississippi State University
State College, Mississippi

for

EUSTIS DIRECTORATE
U. S. ARMY
AIR MOBILITY RESEARCH AND DEVELOPMENT LABORATORY
FORT EUSTIS, VIRGINIA

ABSTRACT

This report presents three-component wake velocity measurements made with a split-film total vector anemometer. The measurements were made in the wake of a full-scale OH-13E helicopter rotor which was mounted on a 60-foot rotor test tower at Mississippi State University. Time-averaged velocity distributions along wake radii at various distances below the rotor disk were measured for two conditions of disk loading and three combinations of blade pitch and rotor speed. Instantaneous velocity measurements were made across the helical vortex trails to investigate the effects of blade pitch and rotor speed on vortex structure, core size, transport velocity, and distribution of axial and tangential velocity components within the vortices. The results indicated that maximum values of induced velocity in the mean wake exceeded twice the magnitude of momentum values, and that instantaneous values of the vertical velocity component in the vicinity of the vortex trails could be as large as ten times the momentum value of induced velocity at high thrust coefficients. Velocity distributions across the tip vortices revealed longitudinal components of velocity of the same order of magnitude as the rotational components. Also, tip vortex structure and dissipation characteristics were found to be similar to the vortices shed from fixed-wing aircraft. The effects of varying the test parameters were reflected as significant changes of the flow within the rotor tip vortex trails, and as smaller variations of the velocity components of the inner wake region.

FOREWORD

This investigation was sponsored by the Eustis Directorate, U. S. Army Air Mobility Research and Development Laboratory under Contract DAAJ02-67-C-0105, DA Task 1F162204A13903. This report presents the results of Phase III as outlined in the contract. The Phase III period of effort extended from September 1970 through September 1971.

The author wishes to acknowledge the work of Mr. John Owens, who designed and perfected the electronics of the rotor tower data acquisition system. Also, grateful acknowledgment is made of Mr. Stan Miley's work in data reduction and computer programming.

TABLE OF CONTENTS

LIST OF ILLUSTRATIONS

LIST OF SYMBOLS

C_Q	rotor torque coefficient; $C_Q = \frac{Q}{\rho \pi R^2 (\Omega R)^2 R}$
C_T	rotor thrust coefficient; $C_T = \frac{T}{\rho \pi R^2 (\Omega R)^2}$
d	axial distance along a helical vortex path measured from the blade tip, ft
n	number of rotor revolutions or events
Q	rotor torque, ft-lb
R	rotor radius, ft
r	radial spanwise distance from the hub, ft
r_c	vortex core radius, ft
r_v	vortex radius, ft
T	rotor thrust, lb
V_R	instantaneous total velocity magnitude, ft/sec
$\bar{V}_R$	mean value of total velocity magnitude, ft/sec
v_a	vortex velocity measured parallel to y axis, ft/sec
v_t	vortex velocity in the xz plane, ft/sec
v_x, v_y, v_z	local instantaneous velocity components, ft/sec
$\bar{v}_x$, $\bar{v}_y$, $\bar{v}_z$	mean values of instantaneous velocity components, ft/sec
x, y, z	fixed axes of rotor tower coordinate system
x', y', z'	axes of probe sensor coordinate system
ε	angle between mean and instantaneous resultant velocity vector, deg or rad
Θ_{75}	blade collective pitch at three-quarter span station, deg or rad
v_o	absolute value of momentum induced velocity; $v_o = \Omega R \sqrt{\frac{C_T}{2}}$, ft/sec
ρ	air density, lb-sec^2/ft^4

σ_{V_R/V_o}	standard deviation between instantaneous and mean resultant velocity magnitude
σ_ε	standard deviation of the angle between instantaneous and mean resultant velocity vectors, deg or rad
ϕ_A, ϕ_B, ϕ_C	angles between the resultant velocity vector and the perpendicular to anemometer probe sensors, deg or rad
ψ	blade azimuth angle measured counterclockwise from x axis, deg or rad
Ω	rotor angular velocity, rad/sec

INTRODUCTION

Theoretical methods of predicting rotor performance require detailed knowledge of the characteristics of the rotor wake so that mathematical models of the wake can be formulated. While partial wake characteristics can generally be obtained through flow visualization techniques, these techniques are insufficient to adequately describe the relationships between the inner shed vortex sheets and the trailing tip vortices. Also, flow visualization techniques are difficult to apply to full-scale rotors. While numerous model test programs have been conducted in the past few years which have depended primarily on flow visualization for description of the wake, the requirement for detailed information not available through flow visualization remains, particularly for full-scale rotors.

Some attempts have been made in the past to use hot-wire or hot-film anemometry as a method of providing supplementary information to that obtained through flow visualization. However, until the recent development of the three-dimensional probe, only partial information could be obtained with the single and x-array systems that were available. Furthermore, hot wires have proved to be difficult to use because of their delicacy and the constant threat of contamination of the sensor elements when exposed to an environment such as that in a rotor wake. As a result, past efforts to measure the rotor wake with hot-wire or hot-film anemometry have not been extensive, and have failed to provide true three-dimensional wake data.

Because of the need for full-scale, experimental wake data, and due to recent development of the "total vector" or three-dimensional anememeter, a test program was conducted at Mississippi State University to measure the flow field velocity distributions of a rotor in the hover configuration. It was originally planned that velocity components would be measured using a dozen or more of the total vector probes to obtain instantaneous velocity distribution along specific wake radii; however, because of funding limitations, only a single probe system could be obtained for these initial tests. As a result, it was necessary to sample the data at each station for a number of revolutions of the rotor, and to present the results in terms of the mean distributions of velocity at specific azimuth positions of the rotor blades. The single probe did permit an examination of the local instantaneous flow variations, however, and proved to be particularly useful for this purpose in the region of the tip vortices.

This project was initiated in September, 1970, with wake measurement tests being conducted from April through August, 1971. The measurements were made by utilizing an OH-13E engine and main rotor assembly which was installed on the full-scale rotor test tower at Mississippi State University. Objectives of the wake measurement tests were as follows:

1. To obtain the mean distributions of velocity components in the wake of the OH-13E rotor installation with the rotor operating

at selected values of the tip speed and collective pitch.

2. To examine the structure of the rotor tip vortices from measurements of velocity distribution across the helical vortex trails.

3. To determine the time-dependent positions, transport velocities, and dissipation characteristics of the rotor tip vortices with distance below the rotor disk.

4. To evaluate the total vector anemometer and rotor tower instrumentation systems.

Test data were acquired by traversing the total vector probe along an instrumentation boom which extended radially into the wake. This boom was positioned at preselected distances below the rotor disk. Analog probe output was stored on magnetic tape during tests, and was later converted to digital form by use of a Hewlett-Packard A to D converter and computer system.

DESCRIPTION OF TEST FACILITY AND EQUIPMENT

ROTOR TOWER

The tests presented in this report were conducted on the full-scale rotor test tower that was designed and built under the Phase I and Phase II portions of Contract DAAJ02-67-C-0105. An overall view of the tower is presented in Figure 1. The top of the tower is 58.3 feet above ground level, and is only 3.9 feet in diameter. These dimensions permit the testing of full-scale rotors with a minimum of tower and ground plane interference.

In its current state of development, no drive system has been installed in the tower. For this reason, an OH-13E rotor and engine assembly was installed on the tower for the Phase III test program. These tests represented the initial tests to be conducted on the tower.

Access to the top of the tower was achieved by utilizing a stairway system within the tower or by the use of an access gantry which was mounted on a railway extending outward from the tower base.

For the current wake measurement tests, it was necessary to design a support for the total vector probe which would permit positioning of the probe at selected radial stations. The supporting structure was required to have sufficient strength to support approximately 10 pounds of instrumentation while maintaining a high degree of rigidity in the unsteady wake. After consideration of several schemes, it was concluded that a cantilevered, triangular boom would be required to obtain the strength and rigidity characteristics that were desired. In addition, a cantilevered boom would provide the most feasible means of positioning the probe at various distances below the rotor disk through the use of vertical attachment beams welded to the outer structure of the tower. The final design incorporated a track along which the probe could be traversed, and was equipped with a support platform for the circuit control box of the anemometer system. The boom was designed to position the probe sensors 20 inches above the structure to minimize the flow interference effects of the boom.

A sketch of the rotor tower showing the instrumentation boom and the wake survey measurement boundaries is presented in Figure 2.

OH-13E TEST INSTALLATION

An assembly consisting of the main rotor, engine, and drive system of an OH-13E helicopter was installed on the top of the rotor tower for wake measurement tests. The assembly rested on four load cells which were used to determine rotor thrust. The system also included a fifth load cell which was used to measure the torque of the engine and main rotor.

Cyclic pitch controls of the rotor were locked in the zero-cyclic position. Engine instrumentation and controls, which included a collective pitch meter, were installed on the second level of the tower. The collective pitch meter responded to the output of a potentiometer which was activated by vertical movement of the swashplate. Collective pitch control was achieved with an electric motor drive system on the swashplate.

During tests, rotor angular velocity was determined from a binary counter which was triggered by a magnetic sensor on the rotor shaft. The rotor was a standard OH-13E rotor having the following characteristics:

disk area	969 sq ft
blade area (each)	17.67 sq ft
diameter	35.125 ft
root chord	1.167 ft
tip chord	0.845 ft
airfoil section	NACA 0015
blade twist	-4.25 deg (average)

The blades of the rotor were found to be slightly mismatched, with one blade having -4.0 degrees twist and the other -4.5 degrees twist. As a result, cyclic pitch was locked such that the incidence of the blade tips would be equal. In this report, all values of collective pitch, azimuth angle, and elapsed time are in reference to the blade having -4.0 degrees of twist.

TOTAL VECTOR ANEMOMETER SYSTEM

A Thermo-Systems, Inc. Model 1080 total vector anemometer system was used for measurements of the rotor wake velocity components. This system included a Model 1296F probe which had three sensor "rods". Each rod held a split-film sensor, such that a total of six hot-film anemometers were used to determine the direction and magnitude of a velocity vector. The three sensor rods were mounted on the support stem of the probe to form a mutually perpendicular array, with each sensor inclined at an angle of 54.73 degrees with respect to the support stem. With this arrangement, the sensor rods described a cone bisected by the support stem of the probe. During tests the probe was mounted upright in the rotor wake such that each sensor rod was depressed below the plane of the rotor disk by an angle of 35.27 degrees as a result of the coned arrangement of the sensor array. The temperature in the vicinity of the sensor array was measured by a small thermocouple located between the sensor rods.

The three sensor rods were identified as sensors A, B, and C. For data reduction purposes, it was necessary to define the angular relationship between the orthogonal axes system described by the sensors and an axes system which was fixed to the rotor tower. The axes lying coincident with sensor rods A, B, and C were designated as axes x', y', and z', respectively, to distinguish this coordinate system from the fixed tower axes x, y, and z. An enlarged view of the sensor array is shown in Figure 3 in addition to an overall view of the total vector probe and control circuit box of the anemometer system.

The probe was factory calibrated, with calibration constants and data reduction equations being provided by the manufacturer. The anemometer system was capable of measuring velocity magnitude and direction over a full 360-degree solid angle in three-dimensional flow fields. The split-film sensors of the probe allowed unambiguous determination of magnitude and direction of the instantaneous velocity vector. Probe output consisted of six simultaneous velocity-dependent analog voltages and one 0- to 5-volt analog temperature signal. Power required by the system was 110 volts ac.

A block diagram of the data acquisition and reduction systems is shown in Figure 4. The seven analog voltages from the probe were recorded on magnetic tape, using the signal from a magnetic pickup on the rotor mast as an rpm and blade position reference. A binary counter and relay system was used to automatically record the probe output voltages for 25 revolutions of the reference blade. Since it was necessary to condition the probe output signals in order to record them on magnetic tape, calibration of the recorder was required prior to each test. This procedure consisted of recording measured voltages which were applied simultaneously to each of the seven probe output channels.

Data supplied by the manufacturer for the anemometer system indicated a frequency response of 750 Hz, a velocity range of 0 to 300 ft/sec in air, and sensitivity of 0.1 ft/sec. Spatial resolution of the probe was specified as being less than 0.5 inch, spherical.

DATA REDUCTION EQUIPMENT

Conversion of analog signals to digital velocity information was made with a Hewlett-Packard Model 5610A A to D converter and Model 2114A computer as indicated in the block diagram of Figure 4. This system was capable of sampling each of the seven data channels at a rate of 500 bits per second without loss in accuracy of the computed results.

CALIBRATION PROCEDURES

LOAD CELLS

Prior to wake measurement tests, a static calibration was performed on the load cell system which was used to measure rotor thrust and torque. The calibration was accomplished by application of torque to the engine and rotor assembly while maintaining values of constant static thrust. A weighted platform and pulley arrangement was used for application of torque to the system. Thrust loads were varied by means of a hydraulic jack and aircraft scale.

The calibration revealed that indicated thrust was approximately 4.0 percent less than applied thrust, and was independent of rotor torque throughout the range of thrust values that could be obtained for normal operating conditions of the rotor. Because of the design of the system, however, the four thrust cells restrained rotation of the engine mounting assembly which caused the output of the single torque cell to be dependent on thrust loading.

During tests, corrected rotor torque was determined from curves of indicated versus applied torque which were plotted for each thrust increment of 100 pounds. Rotor thrust was determined by summing the indicated values of each thrust cell and by correction of this value for system error.

Empirical and flight test data were compared to the resulting performance curve of the test installation as shown in Figure 7. The empirical curve was derived from similar curves of Reference 1, and the hover test data were obtained from flight test results of References 2 and 3. The deviation of the performance curves at large thrust coefficient was attributed to possible errors of measuring rotor torque and to geometric differences of the helicopters and rotor tower installation. The possibility of errors in rotor torque measurements should not have affected the current tests, since only thrust coefficient was used as a significant test variable.

ANALOG DATA CIRCUIT

Output voltages of the total vector probe ranged from 0 to 20 volts dc for the 0- to 300-ft/sec range of velocity. In order to record these voltages on magnetic tape, it was necessary to scale the probe signals to a range of ± 1.0 volt. This was accomplished by potentiometers in each of the seven output channels of the probe. The scale factors of each data channel were determined by application of known voltages to the probe input side of the circuit, and by recording the output voltages on the tape recorder. This procedure was followed prior to each of the velocity measurement tests. In addition to providing reference voltages from which the voltage scale factors could be determined, the procedure also accounted for any changes in the electronic components of the system

which may have occurred over the test period.

PROBE POSITION INDICATOR

The total vector probe could be remotely positioned at any desired radial location in the wake. Probe position was varied by the use of a traversing mechanism which was mounted on the track of the instrumentation boom. The traversing carriage was driven by a small, reversible electric motor which was activated from the control room of the rotor tower. A high-turn potentiometer, located on the traversing carriage, was used to sense the radial location of the probe as indicated by a microammeter which was calibrated to indicate the radial distance of the probe from the center of the rotor hub.

Prior to each velocity measurement test, the potentiometer was adjusted to provide the correct indication of the starting location of the total vector probe. Tests showed a tendency of the carriage to coast slightly after the electric motor was de-energized, such that small adjustments were often required to accurately position the probe at a desired location. The traversing speed of the carriage could be adjusted between 0 and 0.5 ft/sec. The probe and traversing carriage are shown installed on the instrumentation boom in Figure 5.

TOTAL VECTOR PROBE

The total vector anemometer system, consisting of the probe and control circuit box, was calibrated by the manufacturer prior to delivery. Due to the need for special calibration equipment, it was not possible to calibrate the system at Mississippi State University. As a check against possible contamination or damage to the probe sensors and system circuitry, measurements of the zero-velocity output of each data channel were made prior to each test run for comparison to those supplied by the manufacturer.

On one occasion, it was necessary to return the system to the manufacturer for recalibration due to a shift of the zero-velocity voltages on two of the seven data channels. In this case, the problem was attributed to the effects of humidity on the electronic components of the circuit. The probe, itself, remained intact and showed no effects of sensor contamination upon completion of the wake measurement tests.

As a check of probe accuracy, several tests of the probe were made in the low-speed wind tunnel at Mississippi State. Other tests were conducted with an apparatus which utilized a centrifugal blower as a velocity source. In the latter case, honeycomb sections and screens were used to achieve a flat, exit velocity profile across a 2-inch-diameter pipe that was connected to the blower. In these tests, the probe sensor axes were fixed at selected angles relative to the flow. Probe output was measured throughout a velocity range of 0 to 118 ft/sec in the wind tunnel and a range of 0 to 63 ft/sec with the blower apparatus. The velocity components that were computed from analog probe data were compared with test

values as determined with a calibrated airspeed indicator and from angular measurements of probe orientation. The assumption was made that the direction of the mean flow coincided with the longitudinal axes of the test sections of the wind tunnel and blower systems. This assumption was based on the results obtained from tests in which tufts and flow vanes were used to determine the direction of the mean flow.

HELICOPTER INSTRUMENTS AND BINARY COUNTER

Manifold pressure and tachometer gages were calibrated on a standard aircraft instrumentation test set. However, rotor speed was determined from the binary counter during tests, rather than from the aircraft tachometer. The counter was a standard three-digit instrument with a counting period of 1 minute. The input signal for the counter was derived from a magnetic pickup which produced one pulse for each revolution of the rotor. After the 1-minute counting period, the indicator would display for 30 seconds and then resume counting.

The collective pitch meter was calibrated from measurements made on the rotor blades with an aircraft propeller protractor.

WIND MEASUREMENT SET

Local winds were measured with a wind measuring set which was capable of producing a continuous record of both magnitude and direction of the ambient wind. Wind detectors were installed on the tower access gantry at a height of approximately 3 feet above rotor level. Prior to each test, the access gantry was moved to a position approximately 75 feet from the base of the tower.

The wind-measuring equipment was sensitive to velocities of less than 1.0 mph and was continuously monitored during wake measurements. The equipment was calibrated by placing the wind detectors in the entrance section of the low-speed wind tunnel prior to wake measurement tests.

DESCRIPTION OF TESTS

ENVIRONMENTAL CONDITIONS

Wake measurement tests were conducted at low, ambient wind conditions to minimize the effects of local winds on the wake data. However, each radial survey required approximately 30 minutes running time, such that some difficulty was encountered with variable wind conditions during the test runs. It was necessary to repeat some of the measurements because of this problem. Although an effort was made to initiate the test runs when no local winds could be detected, experience proved that this condition seldom existed. As a result, tests were initiated when ambient wind velocities were less than 3.0 mph, although in some cases gusts occurred during the data runs which exceeded this value. At the end of the test period, only those data that were least affected by ambient winds were selected for analyses.

It was also necessary to conduct measurements during conditions of low atmospheric humidity, since the electronic components of the anemometer were sensitive to moisture content of the air. The most favorable test conditions generally occurred in the early evening hours shortly after sunset.

ROTOR TEST PARAMETERS

Following performance tests, three operating conditions of the rotor were selected at which wake measurements would be made. These conditions, which were selected in order that the effects of rotor speed and blade pitch on the test data could be examined, were as follows:

Condition 1: ΩR = 625 ft/sec, θ_{75} = 6.25 deg, C_T = 0.0020

Condition 2: ΩR = 450 ft/sec, θ_{75} = 10.75 deg, C_T = 0.0040

Condition 3: ΩR = 450 ft/sec, θ_{75} = 6.25 deg, C_T = 0.0020

The collective pitch values given above were used throughout the test program, but rotor rpm was allowed to vary slightly from the selected test values. This was done since small adjustments of rotor speed tended to result in smoother operation of the engine and rotor in some instances.

In order to account for the effects of small variations of thrust, all wake velocity data were nondimensionalized by the momentum value of induced velocity as determined from thrust measurements for each test run.

DATA ACQUISITION PROCEDURE

When favorable conditions were indicated by the wind-measuring equipment, tests were initiated by using the following procedure:

1. The total vector probe and traversing mechanism were installed on the instrumentation boom at a selected radial station. The probe potentiometer was adjusted until the proper radial station was indicated by the probe position indicator.

2. With the probe sensors shielded, zero velocity output voltages of the probe were measured and checked against the values supplied by the manufacturer. Load cell output was also recorded prior to engine start.

3. After recording local temperature and pressure, the engine was started and the rotor was set at the operating test conditions of tip speed and collective pitch.

4. With the rotor operating, two calibration voltages were fed through each channel of the anemometer circuit to the magnetic tape recorder. These voltages were used to determine the calibration constants of the recorder.

5. When rotor speed stabilized, output of the thrust and torque load cells was recorded.

6. Output of the total vector probe was recorded for 25 revolutions of the rotor at selected radial stations along the length of the boom. Measurements in the vicinity of the tip were made at radial stations which appeared to coincide with the path of the tip vortices. These positions were determined from observations of the probe signals displayed on an oscilloscope.

DATA REDUCTION PROCEDURE

The analog signals from the seven data channels of the total vector probe were processed by using an A to D converter and computer. Each data channel was sampled at blade azimuth angles of Ψ = 0, 45, 90, and 135 degrees for each revolution of the rotor. Twenty-five revolutions were analyzed at each radial station. The seven probe voltages at each azimuth angle and for each revolution of the rotor were then used to compute the local instantaneous velocity components of the wake. The mean values of the instantaneous components were then computed and used to determine the local, mean resultant velocity vector at each radial station in the wake.

The equations and probe constants, required for calculation of the wake velocity components, were supplied by the manufacturer. The first step in computing the values of these components consisted of evaluating the heat transfer to each of the three sensor rods, A, B, and C. For sensor A, heat transfer as a function of environment temperature was expressed as

$$\left(\frac{Q}{\Delta T}\right)_A = \frac{(K_1 E_1^2 + K_2 E_2^2)}{T - T_e} \qquad (1)$$

where K_1, K_2 = calibration constants for channels 1 and 2 of sensor A

E_1, E_2 = bridge voltages of channels 1 and 2

T_e = environment temperature

T = sensor temperature

Heat transfer to sensors B and C was calculated in a similar manner by using the calibration constants and bridge voltages associated with each channel. The environment temperature, T_e, was determined from the output of a thermocouple located between the probe sensors.

After evaluation of heat transfer equations, the "effective" velocity for each sensor was calculated.

$$V = \left(\frac{Q}{B\Delta T}\right)^n \qquad (2)$$

where V = "effective" velocity at "standard" conditions

B, n = constants determined from probe calibration

The "effective" velocity was defined as the velocity normal to the sensor which would produce the same output reading. "Standard" conditions were defined at a temperature of 70 degrees Fahrenheit and a barometric pressure of 14.7 psia.

The "effective" velocity for each of the three probe sensors was used to evaluate the resultant velocity magnitude.

$$V_s = \frac{V_A^2 + V_B^2 + V_C^2}{2 + k^2} \qquad (3)$$

where V_s = magnitude of the resultant velocity vector at "standard" conditions

V_A, V_B, V_C = "effective" velocities for sensors A, B, and C

k = constant defined as a function of V_s

The value of V_s was then corrected for variations in temperature and pressure.

$$V_R = V_s \left(\frac{P_s T}{P T_s}\right) \qquad (4)$$

where P, T = test values of barometric pressure and temperature, respectively

P_s, T_s = "standard" values of pressure and temperature, respectively

The next step, after finding the velocity magnitude, V_R, was to determine the angles between the velocity vector and the sensor axes. For example, the magnitude of the angle between V_R and the perpendicular to sensor A could be calculated from the relationship

$$|\phi_A| = \arcsin \left[\frac{1 - (V_A/V_s)^2}{1 - k^2} \right]^{\frac{1}{2}} \tag{5}$$

Similarly, the magnitude of angles ϕ_B and ϕ_C could be found by using the corresponding values of V_B and V_C that were previously determined. The sign of the angles was determined by comparing the magnitudes of the two output voltages obtained from each sensor by using a procedure furnished by the manufacturer. At this point, the velocity components along each of the three orthogonal probe sensors could be calculated.

The final step of the data reduction procedure consisted of a transformation of velocity components from the sensor axes to the fixed coordinate system of the rotor tower. Making use of the angular relationships between the tower and sensor coordinate systems as shown in Figure 6, expressions for the velocity components in the tower coordinate system were found to be

$$v_x = 0.7071\ V_R\ (\sin \phi_B - \sin \phi_C) \tag{6}$$

$$v_y = V_R\ [0.8165 \sin \phi_A - 0.4082\ (\sin \phi_B + \sin \phi_C)] \tag{7}$$

$$v_z = -0.5774\ V_R\ (\sin \phi_A + \sin \phi_B + \sin \phi_C) \tag{8}$$

Equations 6, 7, and 8 were evaluated at each radial measurement station at blade azimuth angles of 0, 45, 90, and 135 degrees. The instantaneous velocity components were calculated at each azimuth angle for each of the 25 sets of wake data recorded at each measurement station. The arithmetic mean of each velocity component was then computed as

$$\bar{v}_x = \frac{1}{n} \sum_{i=1}^{n} (v_x)_i, \quad \bar{v}_y = \frac{1}{n} \sum_{i=1}^{n} (v_y)_i, \quad \bar{v}_z = \frac{1}{n} \sum_{i=1}^{n} (v_z)_i \quad (n=25) \tag{9}$$

The mean value of the resultant velocity vector was then determined from the averaged values of the velocity components.

$$\bar{V}_R = \left(\bar{v}_x^2 + \bar{v}_y^2 + \bar{v}_z^2\right)^{1/2} \tag{10}$$

The standard deviation of both magnitude and direction of the local instantaneous resultant velocity vectors with respect to the mean value was computed to allow the unsteady properties of the wake to be examined. Deviation of the magnitude of the nondimensionalized resultant velocity vector was calculated from the expression

$$\sigma_{V_R/v_o} = \left[1/(n-1) \sum_{i=1}^{n} \left[(V_{R_i} - \bar{V}_R)/v_o\right]^2\right]^{1/2} \tag{11}$$

The above equation differs slightly from the usual definition of "standard deviation" in that the summation of the squared differences is divided by "n-1" instead of "n" occurrences. This procedure was used since it is generally considered to produce better results when the number of occurrences is relatively small.

Deviation of the direction of the resultant velocity vector was denoted as σ_ε, where ε was defined as the angle between the local instantaneous velocity vector and the mean value, $\bar{V}_R$. This angle was calculated from the dot product of the instantaneous and mean velocity vectors. Standard deviation of the angle ε was expressed as

$$\sigma_\varepsilon = \left[\frac{1}{n-1} \sum_{i=1}^{n} \varepsilon_i^2\right]^{1/2} \quad (n=25) \tag{12}$$

Computed values of the mean velocity components and standard deviation parameters are presented in the Appendix of this report.

DATA CHARACTERISTICS

ACCURACY OF TEST DATA

Results of the wind tunnel and blower tests of the total vector probe indicated that accuracy of the probe varied with respect to the orientation of the probe sensors to the main flow direction. The probe was most accurate when its shank was aligned with the flow such that angular symmetry existed between the sensors and main flow direction. This condition would occur during actual tests when the resultant wake velocity vector was directed downward and was parallel to the vertical axis of the rotor tower.

Tests conducted with the probe sensors at various angles to the resultant flow indicated that velocity magnitude and angular errors were largest when the direction of the resultant flow was perpendicular to one of the probe sensors. Typical results of the probe tests are shown in Figures 8 and 9.

Angular deviations of the velocity vectors that were calculated from probe measurements exhibited considerable data scatter for all tests, and were generally larger than shown in Figure 9 when the probe was angled to the main flow. Because of data scatter, the accuracy of the probe was expressed in terms of the standard deviations of the data.

Calculated values of resultant velocity magnitude determined from the probe measurements fell within a range of ± 6 percent of the test values as shown in Figure 8. The more conservative estimates of probe error as determined from standard deviations of the test data are presented below for two conditions of probe orientation. In case (b), the direction of the resultant velocity vector was essentially perpendicular to one sensor of the probe.

Resultant Velocity Magnitude Error (0-118 ft/sec)

(a)	probe shank aligned with flow	± 3.0% V_R
(b)	probe shank angled to flow	± 4.1% V_R

Angular Error (angle between actual resultant velocity vector and vector calculated from probe output)

(a)	probe shank aligned with flow	± 2.5 deg
(b)	probe shank angled to flow	± 8.4 deg

The above results were obtained by feeding the probe analog signals through the data acquisition and reduction system of the current test program. For this reason, these values were considered to be valid for the entire data system.

The results of the probe tests were consistent with the accuracy data supplied by the manufacturer, and should have been representative of the accuracy of velocity measurements in the inner wake flow where the resultant velocity vector has a large downward component parallel to the probe shank. However, velocity measurements made in the upflow region outside of the tip vortex trails and within the tip vortices were expected to be subject to errors in excess of the values stated above due to flow interference caused by the body of the probe.

Other tests of the probe traversing carriage, collective pitch meter, and binary rpm counter resulted in the following accuracy limitations of test parameters:

(a)	radial position of probe	± 3 in. ($\Delta x/R$ = ± 0.0142)
(b)	collective pitch setting	± 0.25 deg
(c)	rotor angular velocity	± 3 rpm

WIND EFFECTS

In attempting to correlate the test data at various vertical stations beneath the rotor, it was obvious that the data at some stations were affected by wind. In spite of the precautions taken to reduce wind effects to a minimum, ideal conditions were not obtained in all instances during the measurements at each vertical station. The effects of wind were observed as radial shifts of the velocity distributions - either inboard or outboard - depending upon wind direction. Other inconsistencies of the data that were noted during comparison of velocity components in the plane of the rotor were also attributed to the possible addition of wind components to those of the wake proper. The above effects were most apparent in data obtained at stations z/R = -0.5, -1.0, and -2.0.

An analysis of the wind conditions which existed during tests revealed that wake deflection at the two lower stations was the result of wind velocities that were less than the 3.0-mph limitation established for tests. Only at station z/R = 0.5 did wind variations exceed this limitation. Unfortunately, test runs at these stations could not be repeated due to the absence of more favorable test conditions before termination of the project. Although data at the above stations were noticeably affected by wind gradients, these data are included in the appendix since they are subject to particular analyses and still exhibit the major characteristics of the wake flow.

PROBE PERFORMANCE

The total vector probe provided velocity data of good quality and proved to be sufficiently responsive to the large range of velocity fluctuations in the wake. Velocity fluctuations of ± 180 ft/sec were measured

within the tip vortices at a response rate of approximately 230 Hz. The probe appeared equally as responsive to velocities of the outer wake in the ± 10 ft/sec range. The symmetry of the velocity distributions measured across the tip vortex trails indicated that errors of velocity measurement associated with the probe in reversed flow regions were not as large as anticipated.

LIMITATIONS TO ANALYSES

The limited number of vertical measurement stations and the displacements of the wake due to ambient wind resulted in difficulties of data interpretation, particularly since no prior wake information was available for the test installation. Consequently, flow visualization results from previous tests proved useful as aids to data analyses. These consisted of unpublished results obtained from tests of a UH-1B tail rotor at Mississippi State University and published results such as those of References 4 and 5.

Data analyses were primarily limited to observations of the mean characteristics of the wake, since only local instantaneous measurements could be obtained with the single probe. However, instantaneous measurements proved useful in determining the time-dependent variations of velocity in the region of the tip vortex trails. Changes of the mean wake characteristics as functions of vertical distance below the rotor disk could be observed by comparisons of the mean distributions of velocity components at successive vertical stations. However, comparisons of wake phenomena at specific radial coordinates in the far wake were largely prohibited as the result of radial shifts of the wake due to ambient winds.

DISCUSSION OF TEST RESULTS

GENERAL DESCRIPTION OF THE WAKE

In the near wake at z/R = -0.1, the radial distributions of total and induced velocity were characterized by sharp velocity peaks at the radial positions of the tip vortex paths. Inboard of these positions, the decrease of total velocity magnitude was essentially linear, resulting in a near triangular distribution as shown in Figures 10-17. In the far wake below z/R = -0.3, the velocity components became more evenly distributed across the vortex paths as the tip vortices expanded and dissipated. The changing characteristics of the velocity distributions with increasing distance below the rotor may be observed in Figures 10, 18, 19, and 20.

Radial velocities of the inner wake, $\bar{v}_x$, generally fell within a range of ± 5 ft/sec for all tests, and tended to zero toward the hub. These components exhibited a characteristic negative-to-positive sign change with increasing distance below the rotor, which indicated the contraction and subsequent expansion of the wake.

Mean tangential velocity components measured parallel to the y axis, $\bar{v}_y$, were of approximately the same magnitude as the radial components throughout the wake. An exception occurred directly beneath the rotor disk, where tangential components of 10 ft/sec were measured. A comparison of the wake velocity components at four vertical measurement stations is presented in Figures 21-24.

The measurements of the velocity components at blade azimuth positions of ψ = 0, 45, 90, and 135 degrees clearly indicated the oscillatory nature of the wake. The downward passage of the inboard vortex sheets across the probe resulted in variations of the magnitude of the mean wake components which were most significant in the near wake. Comparisons of the data revealed that the wake oscillations tended to damp out with increasing distance below the rotor, and were directly proportional to thrust coefficient. Azimuthal variations of the tangential velocity components in the plane of the rotor were observed to be slightly larger than those of the axial or vertical components. At a thrust coefficient of 0.004, the velocity components at z/R = -0.1 revealed time-dependent variations in magnitude as large as 3 ft/sec, or 15 percent of the momentum value of induced velocity.

The magnitude of the three velocity components measured outside the trailing tip vortices was generally less than 10 ft/sec, with tangential components tending to be slightly larger than the radial and vertical components. Entrained flow velocities near the blade tip ranged from 8.5 to 14 ft/sec, depending on the operating condition of the rotor. Below z/R = -0.5, radial velocity components of the outer wake were essentially zero, indicating essentially zero flow entrainment in the far wake.

The most significant characteristic of the velocity distribution was the change in the mean distributions of the three velocity components that occurred with passage of the tip vortex trail across the vertical measurement station. The changes in magnitude of the wake components with varying position of the tip vortices are shown in Figures 10-13. In Figure 10, the vortex of one blade has passed below the measurement station as indicated by the negative peak of radial velocity $\bar{v}_x/v_o$. In Figure 11, slight disturbances of the velocity components indicate the approach of the next vortex. This vortex has arrived at a position very close to the measurement station in Figure 12, as shown by the sharp velocity peaks in this figure, and has continued downward to a position below the measurement level as shown in Figure 13.

In all cases, positive peaks of the wake tangential velocity component $\bar{v}_y/v_o$ were indicated within the vortex trail. The small changes of radial velocity in the vicinity of the vortex and the corresponding peaks of the vertical and tangential components of Figure 12 indicate that the mean position of the vortex was slightly outboard and at approximately the same vertical level as the probe sensors at a reference blade azimuth angle of 90 degrees.

Additional velocity distributions which show the effects of the tip vortices in Test Conditions 2 and 3 are shown in Figures 14-17 at $z/R = -0.1$. Below this position, the characteristic velocity peaks across the tip vortex trails rapidly diminished in magnitude and were seldom detected in measurements made below $z/R = -0.7$.

UNSTEADY CHARACTERISTICS OF THE WAKE

Standard deviations of the nondimensionalized total velocity vector were computed throughout the wake at each radial measurement station as previously defined in this report. The standard deviations of both magnitude and direction of the resultant wake vector are included in the compiled data of the Appendix. Values of these parameters at three distances below the rotor are plotted in Figures 25-29.

The deviation parameters clearly show the positions of the tip vortices and the growth of unsteady wake characteristics with increasing distance below the rotor disk. The large values of angular and magnitude deviation across the vortex trails were the result of a lack of uniform vortex structure or variations of the time-dependent positions of the rotor tip vortices with respect to the measurement stations. Since detailed measurements of vortices indicated that vortex structure near the rotor was essentially uniform, the large values of the deviation parameters in the vicinity of the vortex trails were concluded to be the result of unsteady variations of the path and transport velocities of the vortices.

Inspection of the data revealed that deviations of the total velocity vectors in the inner wake were small near the rotor, but large in the

far wake. These deviations of the inner wake consisted primarily of fluctuations of the magnitude of the instantaneous total velocity vectors at given azimuth angles of the rotor. Deviations of the direction of the instantaneous velocity vectors were small throughout the inner wake.

In the inner wake region at $z/R = -0.1$, standard deviations of instantaneous total velocity magnitude were approximately 2 to 4 percent of the mean values of the resultant velocity vectors, and deviation of flow direction was approximately 3 degrees. At $z/R = -0.7$, these values had increased to approximately 9 percent and 5 degrees, respectively. Exceptions to these values were apparent at particular radial stations and azimuth angles of the rotor, where values of the deviation parameters exceeded the mean values across the wake. These exceptions were most apparent from measurements near the rotor as in Figures 25, 26 and 27.

Calculations made from rotor speed and velocity distributions revealed that the points of maximum angular and magnitude deviation in the inner wake corresponded to the stations at which the trailing vortex sheets of the rotor blades passed across the probe sensors. The measurements indicated that flow within the trailing vortex sheets was more unsteady than that of the surrounding wake. Deviations of the resultant velocity vectors measured across the trailing vortex sheets became larger as distance beneath the rotor disk increased, and indicated an expansion of these sheets which eventually resulted in an unstable condition of the inner wake. Deviations of total velocity magnitude at $z/R = -1.5$ were as large as 30 percent of the mean flow value and were accompanied by angular deviations as large as 15 degrees. These conditions are illustrated in Figure 29. The observed characteristics of the inner wake appeared consistent with those shown in the flow visualization photographs of Reference 4.

The expansion of the tip vortices with distance below the rotor was apparent from a comparison of the velocity deviation parameters. At $z/R = -0.1$, the region within which instability of the vortices was measured was approximately 0.25 radii in width, or about 4.4 feet as shown in Figures 25, 26, and 27. At $z/R = -0.7$, the apparent diameter of the vortex exceeded 5 feet and continued to expand to over 10 feet at $z/R = -1.5$.

VORTEX DATA CHARACTERISTICS

Distributions of the instantaneous velocity components across a tip vortex trail at $z/R = -0.1$ are shown in Figures 30 and 31 for Test Condition 2 ($C_T = 0.004$). The axial (v_y) and vertical (v_z) velocity components of the vortex as shown in Figure 31 corresponded to the radial (v_x) components of Figure 30. These measurements show the velocity fluctuations which occurred as the vortex trail passed downward across the probe sensors. The high-velocity peaks in the distributions of radial and vertical velocity components and the rapid sign change of the radial components near $\Psi = 341$, 708, and 1068 degrees indicated

that the vortices shed from one blade passed directly across the probe sensors. Calculations of the time required for the shed vortices to arrive at the measurement station revealed that the vortices which passed directly across the probe were shed from the Number 2 rotor blade rather than from the reference blade. The path of the reference blade vortices was slightly different from the path of the vortices shed from the Number 2 blade, as shown by the smaller variations of the velocity components at Ψ = 509, 869, and 1229 degrees.

The path variations of the rotor tip vortices were possibly the result of the 0.5-degree difference in twist of the blades. Subsequent measurements of the vortices shed from the reference blade showed that the mean radial spacing between the vortex paths of the two blades was approximately 0.025R, or 5.3 inches, at vertical stations in the near wake.

In examining the velocity distributions of Figures 30 and 31, it should be noted that the velocity components include the translational velocities of the vortex. However, the measurements clearly reveal the signatures of the vortices in the flow, since the translational velocity components are small with respect to the magnitude of the axial and tangential components of the vortices.

Measurements of the velocity components in the vicinity of the vortex trails were also made for Test Conditions 1 and 3. The flow for Test Condition 1 revealed essentially the same characteristic vortex structure as measured in Test Condition 2, showing only the shifted vertical positions of the vortices with respect to azimuthal position of the reference blade and a reduction of vortex strength. The flow for Test Condition 3, at low thrust, did not reveal the well-defined vortices of the other test conditions, although the presence of the vortices in the flow was clearly indicated by characteristic peaks in the plots of the velocity components.

VELOCITY DISTRIBUTIONS ACROSS THE VORTEX TRAILS

In an effort to further examine the flow within the vortices, the data were searched in an attempt to detect the instances in which the trailing vortices passed directly over the probe. Characteristics of the probe output signals clearly indicated the stations at which the probe was near the vortex trails, but it was not possible to determine if the vortex cores actually passed across the probe sensors from an examination of the data in analog form. This problem required that numerous analog data samples be converted to digital form by the computer in order to locate vortices which revealed the velocity distributions across the core. After extensive data analysis, a few cases were found at each of the vertical measurement stations above $z/R = -0.7$, in which the vortex cores passed directly over the probe. The difficulty of obtaining these data was enhanced by the instability of the vortex trajectories and the relatively small size of the vortex cores.

Typical examples of the instantaneous velocity distributions across the core region of the vortex trails are shown in Figures 32-34. Since the vortices traveled across the probe with radial and vertical components of translational velocity and since the core centers were displaced with respect to the probe sensors, symmetrical velocity distributions were not obtained. As a result, it was necessary to assume that symmetry of the vortex structure existed in order to approximate the paths of the vortices with respect to the probe sensors as shown in Figures 32-34.

Estimates of the path velocities of the vortex cores were based on mean values of the velocity components when the vortices were above or below the measurement stations, and from considerations of symmetry of the velocity distributions across the vortices These estimates allowed the approximate radii of the vortex cores to be calculated after the paths of the vortices, with respect to the probe, had been determined. The time scale was fixed by rotor speed. By coincidence, the calculated core radii of the vortices shown in Figures 32 and 33 were exactly the same. Similar comparisons of other vortices revealed no significant differences of core size for these test conditions of equal rotor thrust.

The approximate azimuth angles which corresponded to points within the vortex cores are indicated by numerals on the blade azimuth scale and sketches of Figures 32-34. The distributions of the velocity components about these points show a characteristic increase of the radial and vertical velocity components of the vortex as the boundary of the core is approached, and peak values of axial velocity at the center of the core.

Limited capability of the computer in sampling the data at small increments of time prevented a more precise definition of the flow in the vicinity of the core boundaries. Also, the displacement of the path of the vortex cores with respect to the probe prevented direct measurement of the maximum velocities at the edge and center of the vortex cores.

In some instances, the vortex measurements revealed large velocity fluctuations in the region of the cores which were believed to have been associated with probe interference. The velocity fluctuations appeared to be largely confined to the axial velocity components of the vortex trails as shown in Figure 37. This result suggested that the stability of a vortex trail is perhaps more strongly related to the characteristics of the axial or longitudinal flow within the vortex cores than to the rotational components of the vortex.

The axial (v_y) components of each vortex increased in magnitude from the outer edge of the vortex until reaching a maximum value near the center of the core. Peak axial velocities as large as 190 ft/sec were measured in the center of the vortices. Tangential velocity values increased to a maximum at the boundary of the core and were minimum at the core center. Maximum values of tangential velocity within the

vortex trails were of approximately the same magnitude as maximum values of the axial components. The tangential velocity components of the vortices were calculated as the resultants of the measured radial and vertical velocity components at equal values of blade azimuth angle.

Attempts to determine the mean distributions of axial and tangential velocity along the diameters of typical vortices were not successful due to uncertainties related to the path coordinates of the vortices with respect to the probe. However, the tangential velocity distributions of the vortices appeared to be generally consistent with classical vortex theory as found in many texts such as Reference 6.

Measurements of the vortex velocity distributions at $z/R = -0.3$ revealed no abrupt changes in vortex structure, although axial velocities in the core had decreased significantly. At lower levels in the wake, the vortices were very sensitive to the presence of the probe, and the measured axial and tangential velocities in the core continued to decrease. Below $z/R = -0.7$, the presence of vorticity in the mean flow could still be detected from the measurements, although well-defined vortices were seldom found below this station. The measurements revealed, however, that at least some of the vortices had not completely dissipated or broken up at a distance of 1.5 radii below the rotor disk when the rotor was operating at normal thrust.

At the lower thrust level of Test Condition 3, the vortices were very weak at a distance of 0.3 radii beneath the rotor disk, and no definitive measurements of the vortices for this condition were obtained below this level.

VORTEX CORE VELOCITIES AND DIMENSIONS

The most significant feature observed from measurements of the rotor tip vortices was the rapid decline of axial velocity magnitude that occurred in the vortex cores with increasing distance below the rotor. This observation was based upon a comparison of the maximum values of axial velocity that were measured within the vortex cores. The measurements showed that the magnitude of the axial velocity components in the vortex cores decreased approximately 50 to 70 percent between stations $z/R = -0.1$ and -0.3. Extrapolation of the measurements toward the rotor disk indicated that axial core velocities would be extremely large in the immediate vicinity of the rotor. Below $z/R = -0.3$, the decline of axial velocity in the vortex cores consisted of a gradual approach to stagnation in the far wake.

Further comparisons of the maximum values of tangential velocity at the core boundaries revealed a more gradual reduction of these values below the rotor than was observed from comparisons of the maximum axial velocity components in the vortex cores. Rotational velocities varied from maximum values near 200 ft/sec in the near wake to 20 ft/sec in the far wake.

Computed radii of the vortex cores indicated a trend toward increased core size in the far wake, but results were generally inconclusive. Average core radii were approximately 0.005R, a value commonly assumed in wake analyses methods such as those of References 4 and 7. The computations were complicated as a result of the failure to obtain measurements of the vortex velocity distributions when the vortex core passed directly across the probe sensors.

MEAN PROPERTIES OF THE TRAILING VORTICES

Values of maximum tangential velocity at the edge of the vortex cores, maximum axial velocity at the center of the cores, core radii, and vortex radii were plotted as functions of vertical distance below the rotor disk to obtain the mean values of these functions. Mean properties of the trailing vortices as determined from curves faired through the experimental data are shown in the table below.

MEAN PROPERTIES OF TRAILING VORTICES

Test Condition	Vertical Station, z/R	v_t(max) ft/sec	v_a(max) ft/sec	Core Radius r_c/R	Vortex Radius r_v/R
1	-0.1	136	147	0.004	0.125
1	-0.3	87	57	0.005	0.175
1	-0.5	57	42	0.006	0.225
1	-1.5	22	30	0.007	0.35
2	-0.1	200*	193	0.004	0.10
2	-0.3	150	83	0.005	0.15
2	-0.5	116	72	0.005	0.20
2	-1.5	38	28	-	0.30
3	-0.1	57	90	0.005	0.125
3	-0.3	39	40	0.005	0.20
3	-0.5	-	-	0.006	0.25
3	-1.5	-	-	-	0.35

*Extrapolated value

Several factors concerning the values of the above table should be noted at this point. The values of vortex radii were determined from values of the standard deviation parameters which indicated the expanse of the mean wake within which the unsteady vortex-induced velocities were detected. Also, it should be emphasized that the tabulated values of maximum tangential and axial velocity were those obtained from a finite number of data samples and should not be considered optimum values. Of equal importance is the fact that the vortex velocity data include the effects of translation of the vortex trails with respect to the fixed probe. The possible effects of vortex dissipation during the time interval

required for the vortex to travel across the probe are also contained in the measurements. These factors did not appear to significantly affect the data, however, since translational components of velocity were small in comparison to the axial and tangential vortex components. Also, vortex dissipation was relatively slow with respect to the small time intervals required to traverse the vortex.

VORTEX PATH COORDINATES AND TRANSPORT VELOCITIES

The approximate coordinates of the rotor tip vortices (as functions of blade azimuth angle) were determined from the velocity distributions at each vertical measurement station in the near wake. The analysis revealed that the paths of the trailing vortices of the two blades were not identical as previously noted, and that the azimuthal spacing of the vortices varied from the expected value of 180 degrees. This resulted in the data scatter shown in the plots of the tip vortex path coordinates of Figures 35 and 36. Vortex dissipation and ambient wind effects prohibited an extension of the results to vertical stations below $z/R = -0.5$.

The time-dependent variations of vortex spacing and path coordinates were believed to have been the result of several factors. The 0.5-degree difference in linear twist of the blades, the degree of accuracy of collective pitch setting, wind effects, and errors in determining the exact vortex positions from velocity measurements were all probable factors which resulted in poor definition of the vortex path coordinates.

The calculated transport velocities of the vortices varied as the result of the path variations noted above. The results indicated, however, that the vertical displacement of the vortices below $z/R = -0.1$ was approximately equal to one-half of the maximum resultant velocity of the inner vortex sheet at equivalent distances below the rotor. As a result, the rates of vertical displacement of the vortices at stations below $z/R = -0.1$ were essentially constant. This indicated that the vortices experienced maximum acceleration between the $z/R = -0.1$ level and the blade tip. It was also observed that the vertical transport velocity of the shed vortices increased linearly with tip speed and varied approximately as the square of collective pitch ratio.

EFFECTS OF TEST VARIABLES

Comparisons of the mean wake velocity distributions revealed that the effects of varying tip speed and collective pitch were reflected primarily as changes in magnitude of the velocity components of the inner wake and rotor tip vortices, and as changes of the time-dependent characteristics of the wake. When the velocity components of the wake were nondimensionalized by the momentum values of induced velocity, no large differences between the radial distributions of the velocity components of the wake were detected which could have been directly attributed to variations of the test parameters.

Radial shifts of the wake were considered to be the result of wind effects, and were most pronounced for the condition of low rotor thrust (Test Condition 3). A comparison of data for the three test conditions also indicated that the induced inflow and tangential velocity components outside the trailing vortex boundaries tended to be slightly larger for Test Condition 3. The standard deviation parameters, however, revealed no significant differences of the unsteady flow characteristics of the wake as a result of changing test variables.

The most pronounced effects of the test variables were noted in measurements of the velocity distributions across the trailing vortices. Measured values of maximum tangential and axial velocity within the vortices increased substantially when the product of tip speed and collective pitch was increased to a maximum value in Test Condition 2. The vortices for the higher pitch condition also appeared to be slightly more restricted in size than did the vortices for the other test conditions.

Considerations of rotor thrust and circulation strength for each test condition indicated that maximum tangential velocity in the vortices should have varied directly as the product of tip speed and thrust coefficient, since differences of core radii for the various test conditions were small. The relative variations of the values of maximum tangential velocity magnitude in the vortices for Test Conditions 1 and 2 were roughly consistent with this approximation, but the corresponding values for Test Condition 3 appeared conservative. This is believed to have been the result of failure to accurately measure the velocities within the weaker and more unstable vortices with the rotor operating in the low-thrust condition.

Axial velocities in the tip vortex trails were also observed to vary as a function of the test variables. Comparisons of the data at $z/R = -0.3$ indicated that axial velocity magnitude in the vortex cores tended to vary linearly with increasing values of the product of tip speed and thrust coefficient, as did the tangential components of the vortex. Closer to the rotor, a linear relationship was obtained by comparisons of the maximum axial velocities of the vortices to the product of tip speed and collective pitch angle. At constant tip speed conditions of the rotor, the maximum axial components of the vortex trails were inversely proportional to thrust coefficient.

Only slight changes of the tip vortex path coordinates were observed for the three test conditions of the rotor. No significant differences in the extent of maximum wake contraction were detected from plots of the tip path coordinates. However, small variations of the radial coordinates indicated that maximum wake contraction occurred nearer the rotor disk when thrust coefficient was increased. No appreciable effects of tip speed on the vortex trajectories could be detected as shown by the identical vortex path coordinates for Test Conditions 1 and 3 in Figure 35.

COMPARISONS OF DATA WITH PREVIOUS RESULTS

VORTEX PATH COORDINATES

Path coordinates of the rotor tip vortices as determined from model data by Landgrebe (Reference 4) were compared to current results as shown in Figures 35 and 36. The model data were corrected to account for the differences of thrust coefficient and blade twist that existed between tests of the full-scale rotor and model. The considerable extent of azimuthal data scatter of the current results made direct comparisons of the path coordinates difficult, but certain trends could be detected. The path coordinates of the full-scale rotor agreed reasonably well with model data, except for the radial coordinates of Test Condition 2. In this case, Landgrebe's results indicated that contraction of the wake should have increased at the higher value of increased thrust coefficient, a condition not detected in the present tests. The wake of the full-scale rotor also appeared to contract to a maximum extent nearer the rotor disk than did the wake of the model rotors.

It is uncertain whether the earlier contraction of the full-scale wake could be due to the combined effects of the rotor tower and ground plane. The model data of Reference 4 indicated that the effects of a whirl test stand on path coordinates of the wake were small when the model was operating in ground effect. Also, the full-scale rotor in the current tests was operating at $z/R = 3.87$, a height at which ground plane effects should have been negligible. However, results obtained by locating cylinders of various sizes in the wake of a hovering model rotor did indicate that an expansion of the wake of 3.5 to 4.0 percent could possibly have occurred due to the effects of the rotor tower on the wake (Reference 8).

It should also be noted that the path coordinates of Figures 35 and 36 do not show the effects of differences in coning angle of the full-scale and model rotors. When these differences are considered, the apparent earlier contraction of the wake of the full-scale rotor is partially accounted for, since coning angles of the model were smaller than those of the full-scale rotor. However, this correction would also result in larger axial displacement velocities of the tip vortices of the full-scale rotor than those of the model.

In view of the above factors, it would appear that radial contraction of the full-scale wake is less a function of thrust coefficient than indicated from the model tests of Reference 4, and that axial displacement rates of the tip vortices near the rotor may be slightly higher than those of model rotors. These observations need to be further substantiated by additional tests of the full-scale rotor which would permit a more direct comparison of full-scale model data.

The full-scale data showed that tip path coordinates were independent of

tip speed and that axial transport velocities of the tip vortices varied directly with the momentum values of induced velocity. These results were in agreement with model test results.

TANGENTIAL VELOCITY COMPONENTS OF THE WAKE

Comparisons of the mean tangential velocity components ($\bar{v}_y/v_o$) of the inner wake region revealed azimuthal oscillations of the magnitude of these components at all vertical measurement stations in the wake. Inconsistent variations of tangential velocity magnitude were attributed primarily to the effects of ambient wind, rather than to unsteady oscillations of the wake itself.

Comparisons of the relative variations of tangential velocity components at each vertical measurement station showed that wake skew angles were larger for Test Condition 3 than for the other test conditions. The data indicated that wake skew angles were inversely proportional to thrust level as previously observed by Lehman in Reference 5. However, comparisons of the skew angles obtained from the data of Test Conditions 1 and 2 indicated that wake skew may also vary at constant thrust as a function of both tip speed and collective pitch angle. These comparisons led to the conclusion that wake skew varies inversely with the product of tip speed and collective pitch angle. For example, at $z/R = -0.1$, the mean deflection angle of the wake from the vertical direction was approximately 16 degrees for Test Condition 3, in which the lowest combination of tip speed and collective pitch angle was employed. The wake skew angle decreased to approximately 10 degrees when tip speed was increased in Test Condition 1 while maintaining constant collective pitch. The skew angle was reduced still further to a calculated value of 7.5 degrees in Test Condition 2, in which the product of tip speed and collective pitch angle was increased to its highest value while maintaining constant rotor thrust.

The results suggest that the neglect of tangential velocity components in wake analyses techniques would be of little consequence at nominal thrust values of helicopter rotors, but that the degree of error may increase with decreasing thrust level. The degree of error due to neglect of swirl components would appear to be more directly related to tip speed and collective pitch combinations than to disk loading alone.

RADIAL COMPONENTS OF WAKE VELOCITY

The directions of the radial velocity components ($\bar{v}_x/v_o$) were generally consistent with wake contraction and expansion. Near the rotor, the mean radial components of the inner wake were directed toward the hub, indicating wake contraction. In the far wake, the direction of these components was reversed. The mean values of radial velocity across the inner wake at each vertical station were smaller than the tangential components, and appeared to vary to a greater extent as a result of

ambient wind conditions than did the tangential velocity components.

Comparisons of the radial velocity components of Test Conditions 1 and 3 showed no significant effects of tip speed on the magnitude or direction of these components. This result agreed with the previous observation that the effects of tip speed on wake contraction could not be detected. Although data scatter largely masked the effects of the test variables, comparisons of radial velocity distributions at $z/R = -0.1$ revealed that the negative radial velocities for Test Condition 2 were slightly larger in magnitude than those measured at lower thrust coefficients. This would indicate that wake contraction does vary as a function of thrust coefficient as mentioned in Reference 4, although this condition could not be detected from comparisons of the measured radial positions of the tip vortices in current tests.

VORTEX VELOCITY CHARACTERISTICS

The rates at which the maximum values of tangential velocity within the vortex cores decreased with downstream distance behind the tips of the rotor blades were approximately the same as measured in the vortices of fixed-wing aircraft by McCormick (Reference 9). The fixed-wing measurements showed that the maximum tangential velocities in the vortex decreased inversely with the square root of the distance behind the aircraft. A plot of the available data in Figure 38 shows the approximate parabolic decrease of maximum tangential velocity in the vortex cores as a function of distance measured along the vortex trails.

The positive axial velocities measured in the vortex cores with the fixed probe represented deficiencies of axial momentum within the vortex trails. The loss of axial momentum at the center of the vortices has been treated analytically by Newman (Reference 10), and has been experimentally observed by Dosanjh and others (Reference 11) in the vortices behind a half-wing in the wind tunnel. The axial velocity defect in a vortex trail is generally associated with profile drag losses of the vortex generator.

The decrease of maximum axial velocity in the vortex trails (Figure 39) indicated that the vortices had to expand with increasing distance behind the blades if the momentum losses represented by the axial velocity defects were to remain constant. This expansion of the vortices was apparent from comparisons of the velocity distributions and wake deviation parameters in the vicinity of the vortex trails. However, the expansion rates of the vortices appeared to be more closely related to the rates of maximum tangential velocity decline in the vortex trails than to the rates of maximum axial velocity decline. As shown in Figure 40, the growth of the vortex dimensions is apparently linear with respect to the square root of the distance behind the blade.

In many instances, the measurements within the vortex trails were characterized by velocity fluctuations in the core, while the outer

portions of the vortices remained relatively stable as shown in Figure 37. The rotating velocity components of the vortices appeared less affected by the presence of the measurement probe than did the axial components. These results suggested that vortex stability may be strongly related to the axial flow properties of vortices as suggested by Bergman (Reference 12) and as observed by Olsen in experimental towing tests (Reference 13).

RESULTS AND CONCLUSIONS

1. The results of the initial wake survey conducted on the Mississippi State University rotor tower revealed that the total vector anemometer and tower instrumentation systems were adequate for the acquisition of wake velocity data which are quantitatively reliable. Comparisons of the measurements with limited analytical and experimental results indicated that accuracy of the anemometer and tower systems is also sufficient to allow qualitative examinations of the behavior of time-dependent wake characteristics with variations of test parameters.

2. The wake of the hovering OH-13E rotor with linear twist was characterized by radial distributions of vertical wake velocity near the rotor which increased almost linearly from the hub to a position just inboard of the helical vortex trails. Maximum values of induced velocity in the inner wake were directly proportional to momentum values.

3. Maximum values of the vertical velocity component of the inboard vortex sheets exceeded twice the values of momentum-induced velocity in the vicinity of the rotor tip vortices and remained essentially constant with increasing distance below the rotor.

4. Mean values of the inner wake velocity components in the plane of the rotor disk were small near the hub and tended to increase toward the position of the tip vortex trails. The direction of the radial components was generally consistent with the contraction and expansion characteristics of the wake. Tangential components were largest at vertical stations nearest the rotor disk, indicating a higher swirl condition of the inner wake near the rotor than at lower stations in the wake.

5. The magnitude of the velocity components of the inner wake oscillated with respect to blade azimuth position. The amplitude of these oscillations was observed to be proportional to thrust coefficient and to vary inversely with distance below the rotor. The azimuthal variations of the radial and tangential velocity components of the inner wake tended to be larger than those of the axial components.

6. Wake skew angles near the rotor varied inversely with thrust level. Variations of wake skew which were measured at constant thrust conditions were inversely proportional to the product of tip speed and collective pitch angle.

7. The rate of vertical displacement of the rotor tip vortices was approximately one-half of the rate of maximum vertical displacement of the inboard vortex sheets. Below the point of maximum wake contraction, the vortices moved downward at a constant rate which was proportional to tip speed and the square root of thrust coefficient.

8. The flow in the region of the tip vortex trails was highly unsteady as indicated by standard deviations of the resultant wake velocity vectors. Local instabilities of the inner wake were also observed as the results of unsteady flow variations across the inboard vortex sheets. The wake became progressively unstable with the expansion of the rotor tip vortices and vortex sheets as distance below the rotor increased. The dimensions of the unsteady region across the vortex trails was observed to be proportional to the square root of the distance measured along the vortex trails to the tip of the blade.

9. Maximum tangential and axial velocities in the vortex trails were measured at the edge and center of the vortex cores, respectively. Axial velocity components of the rotor tip vortices were of the same order of magnitude as rotational components. The magnitude of the maximum tangential and axial velocities in the vortex trails varied approximately as the product of tip speed and rotor thrust coefficient.

10. Maximum tantential and axial velocities in the rotor tip vortices decreased in magnitude with increasing distance below the rotor. The rate at which the tangential components decreased was similar to that of vortices shed from fixed-wing aircraft. Maximum axial velocity in the vortices nearest the rotor decreased at a rate which exceeded that of the maximum tangential components.

11. Measurements of velocity distributions across the vortex trails indicated that the vortices tended to dissipate into the far wake rather than to "burst" or break up at specific distances below the rotor. The measurements revealed that at least some of the vortices retained their characteristic structure at distances as far as 1.5 radii below the rotor disk.

12. Comparisons of full-scale data to model data were largely inconclusive due to path variations and uneven spacing of the tip vortices of the full-scale rotor. Correlation of wake contraction coordinates with test variables could not be established from the full-scale data. Unsteady variations of the vortex path coordinates were attributed to differences of rotor blade twist, errors of collective pitch setting, and the effects of ambient wind.

13. The axial velocity components of the rotor tip vortices were more sensitive to the disturbances of the measurement probe than were the tangential components. Large fluctuations of axial flow within the vortex cores were measured when the rotational components were relatively stable. The results indicated that the stability of the vortex trails was strongly related to the characteristics of the internal axial flow in the region of the vortex cores.

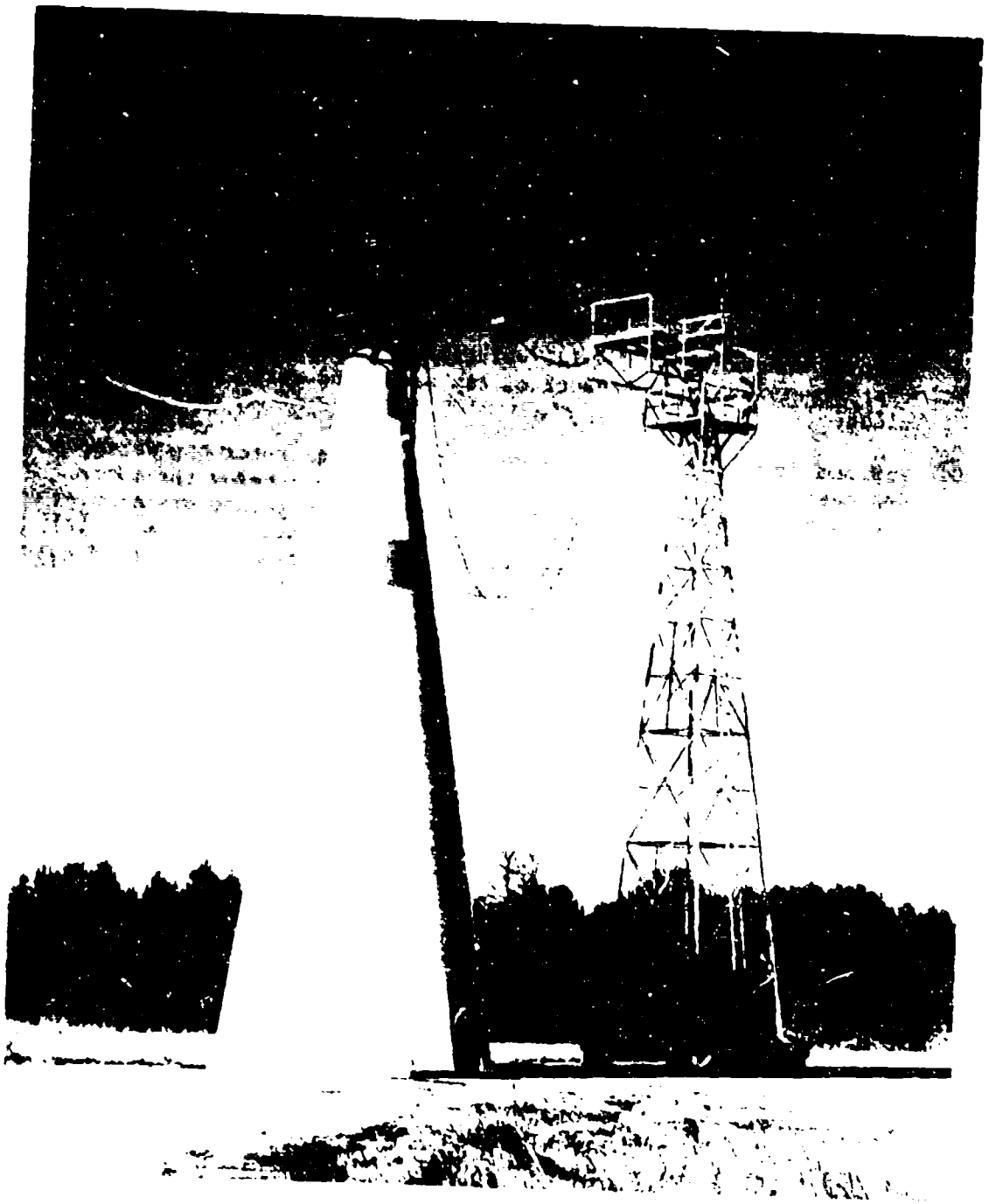

Figure 1. Rotor Tower With OH-13E Test Installation.

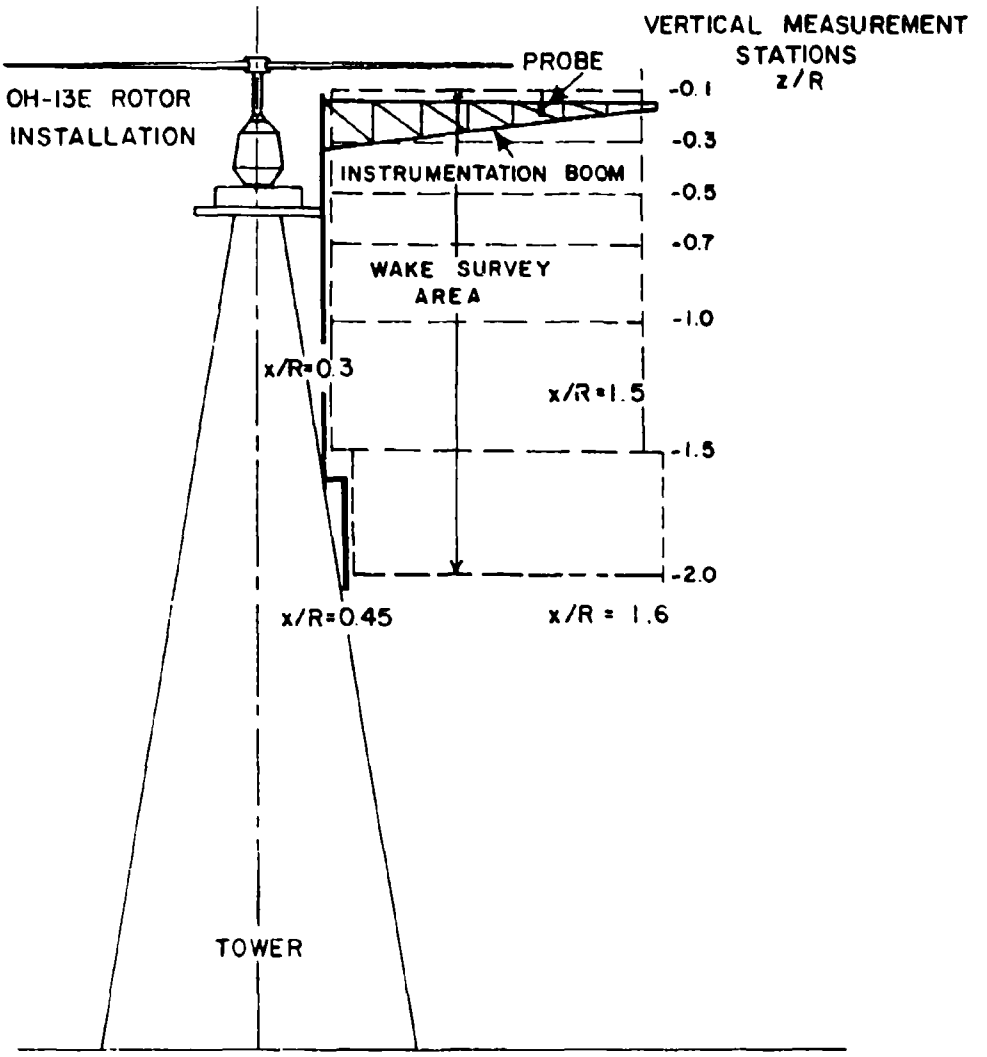

Figure 2. Sketch of Rotor Tower Showing Vertical Measurement Stations and Wake Survey Area.

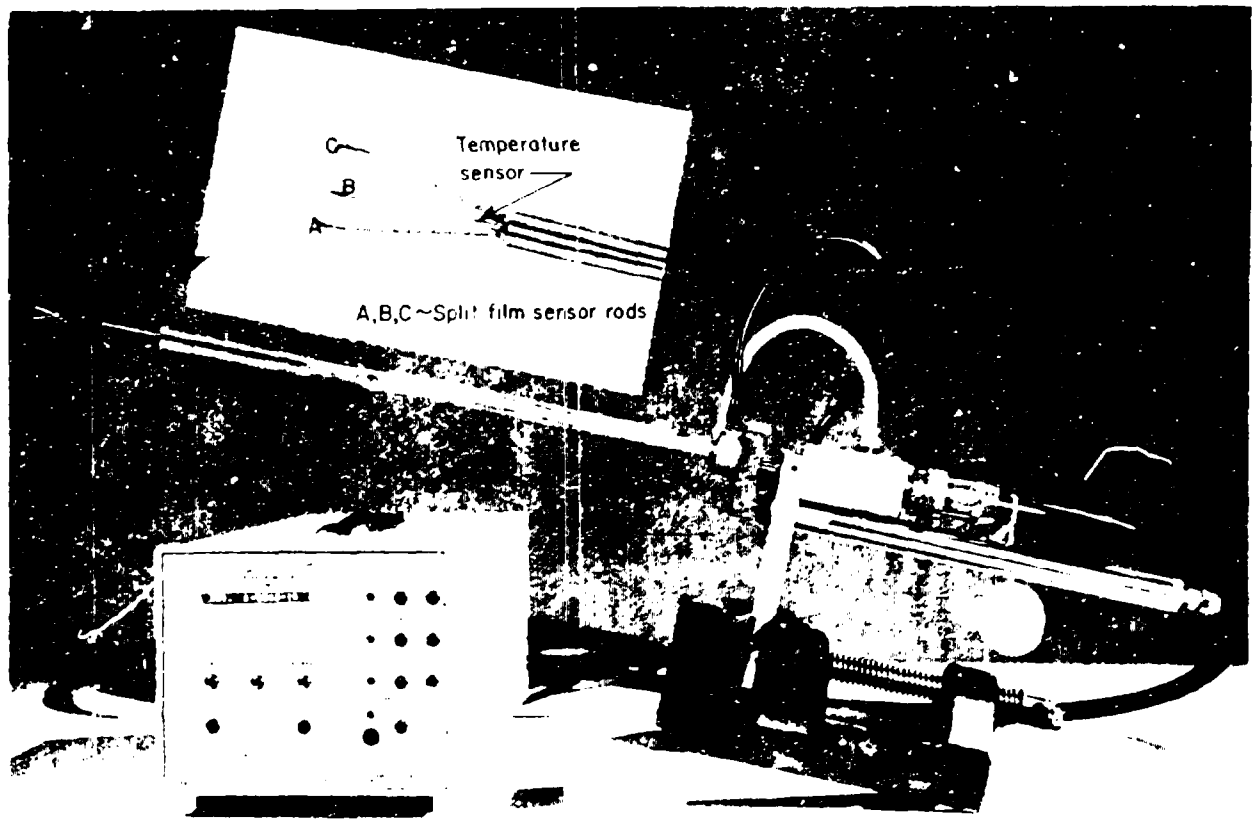

Figure 3. [illegible] Vector Probe and Control Circuit Box.

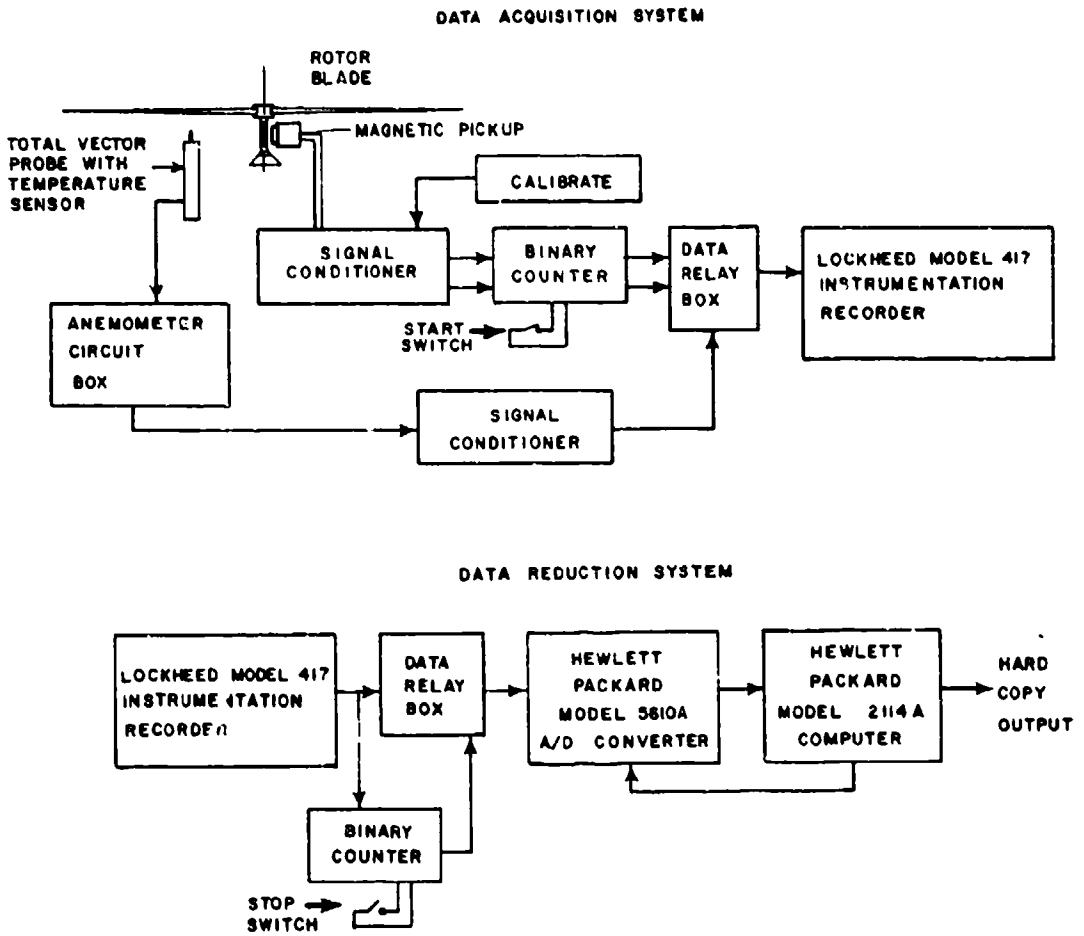

Figure 4. Block Diagram of Data Acquisition and Reduction Systems.

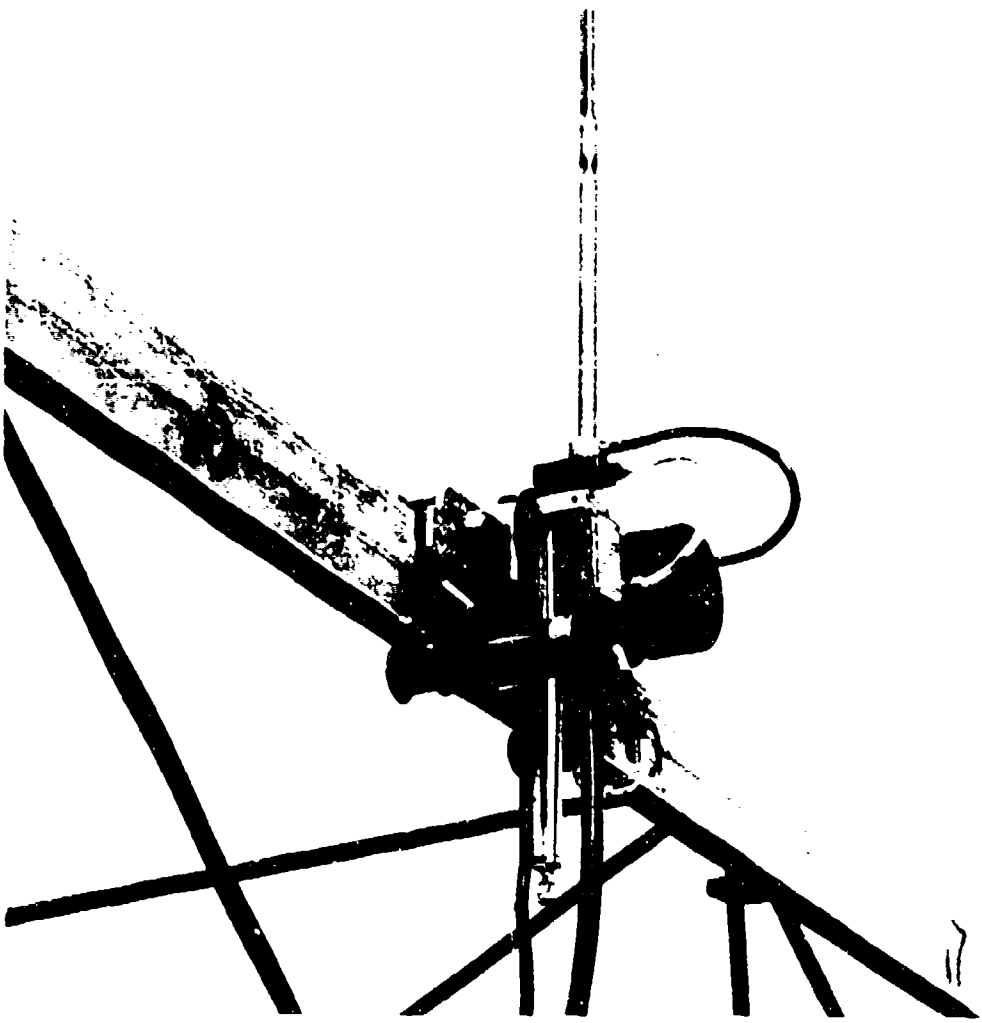

Figure 5. Test Configuration of Total Vector Probe and Traversing Mechanism.

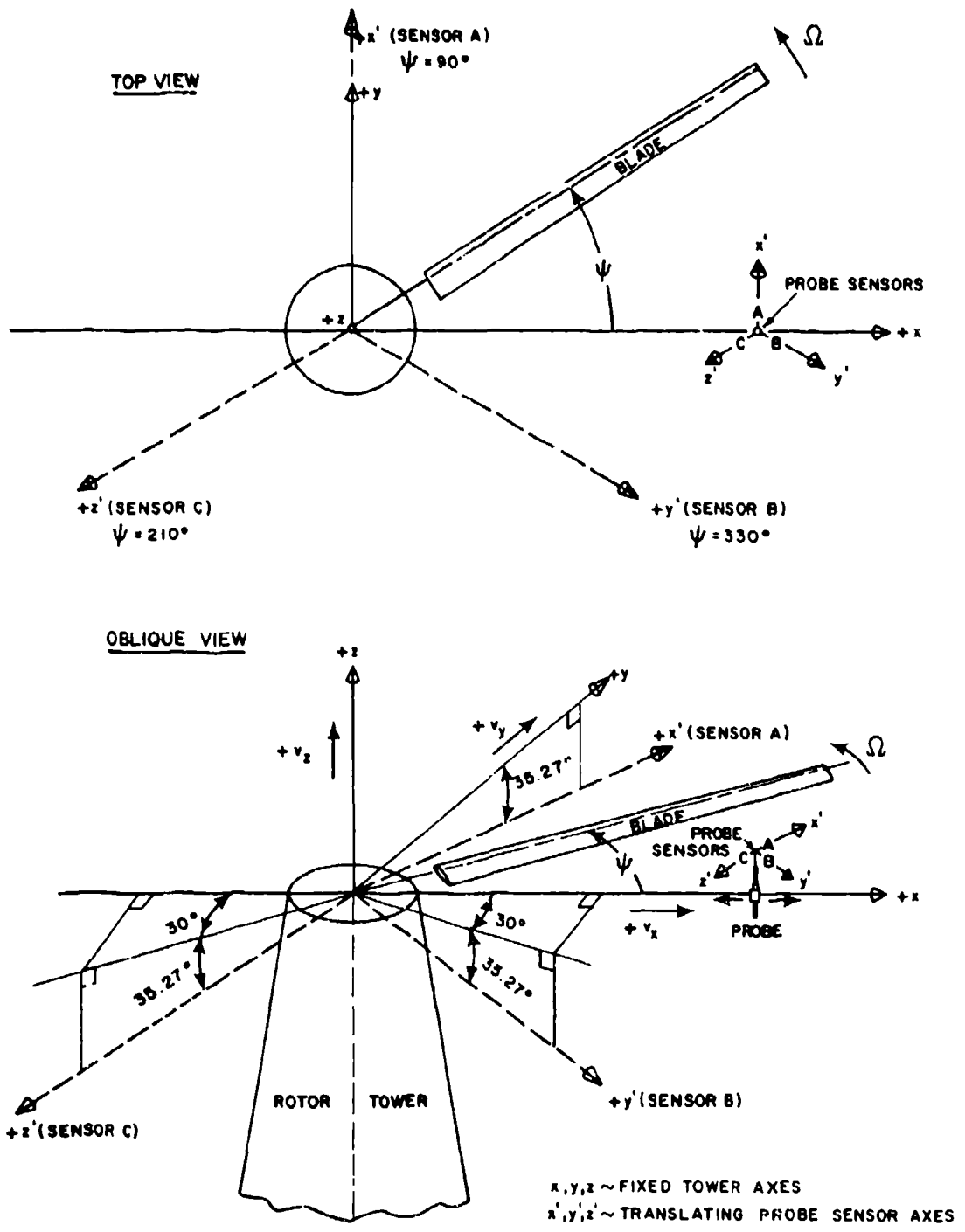

Figure 6. Rotor Tower and Anemometer Probe Sensor Coordinate Systems.

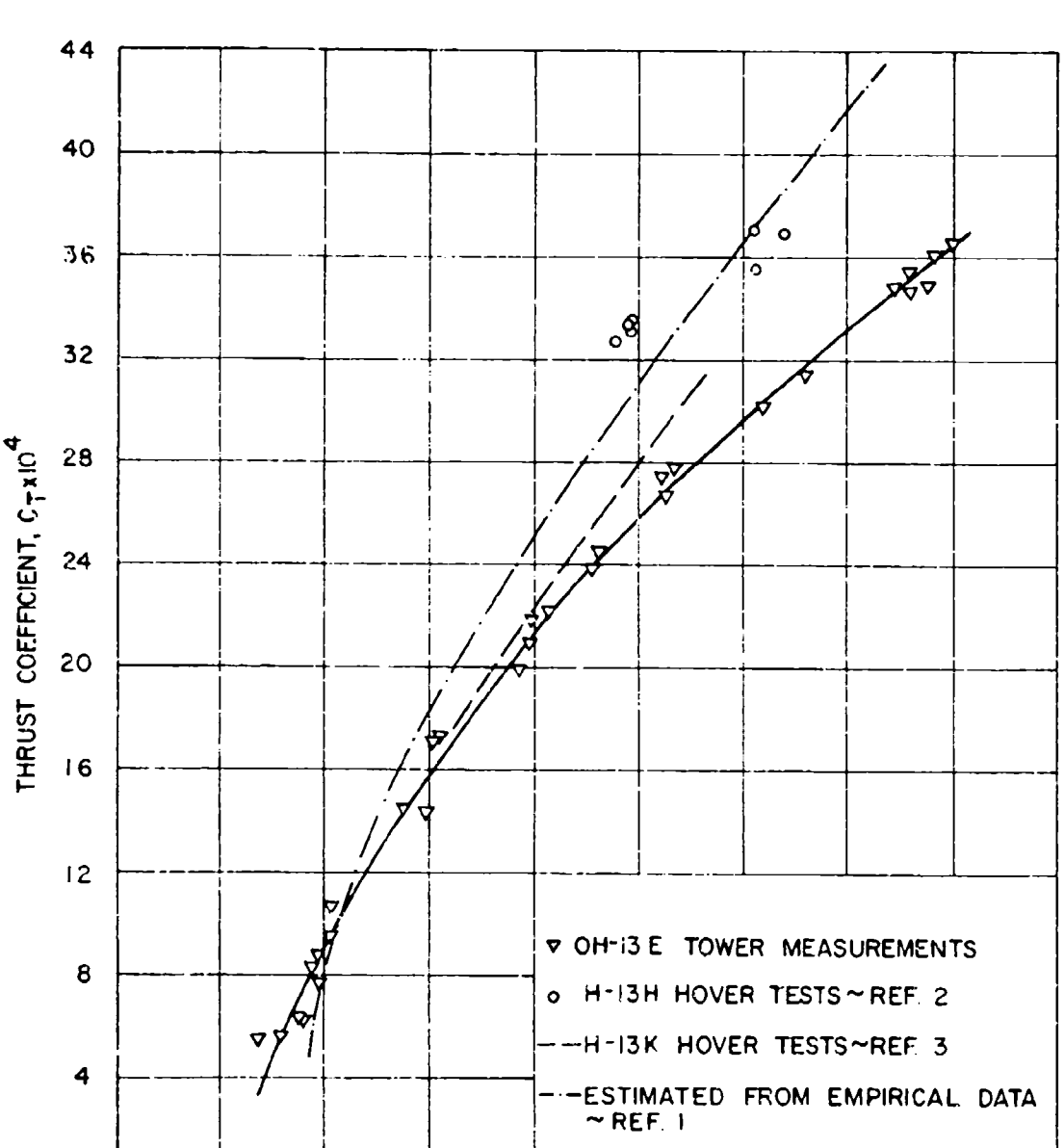

Figure 7. Comparison of Hovering Performance of the OH-13E Rotor Tower Installation With Flight Test and Empirical Data.

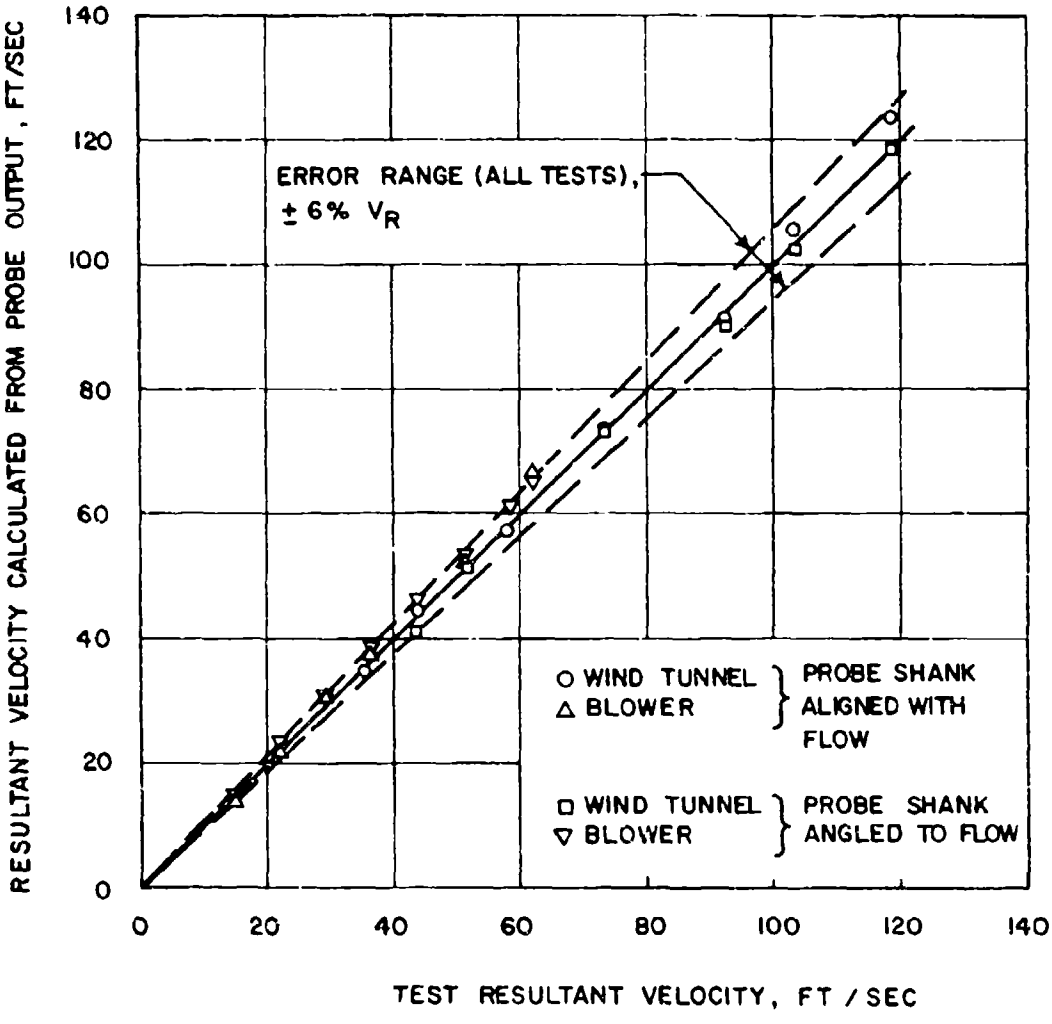

Figure 8. Velocity Measurement Error of Total Vector Probe.

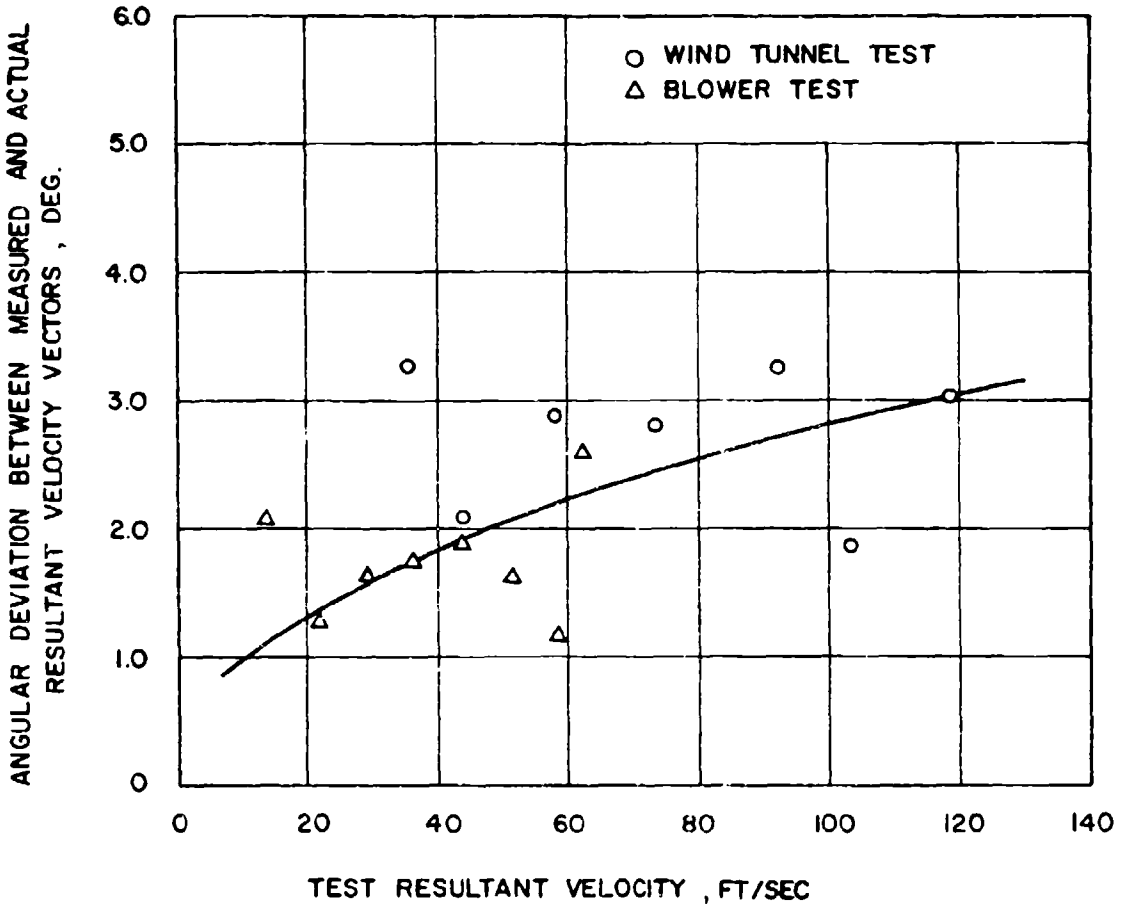

Figure 9. Angular Error of Total Vector Probe With Probe Shank Aligned With Flow Direction.

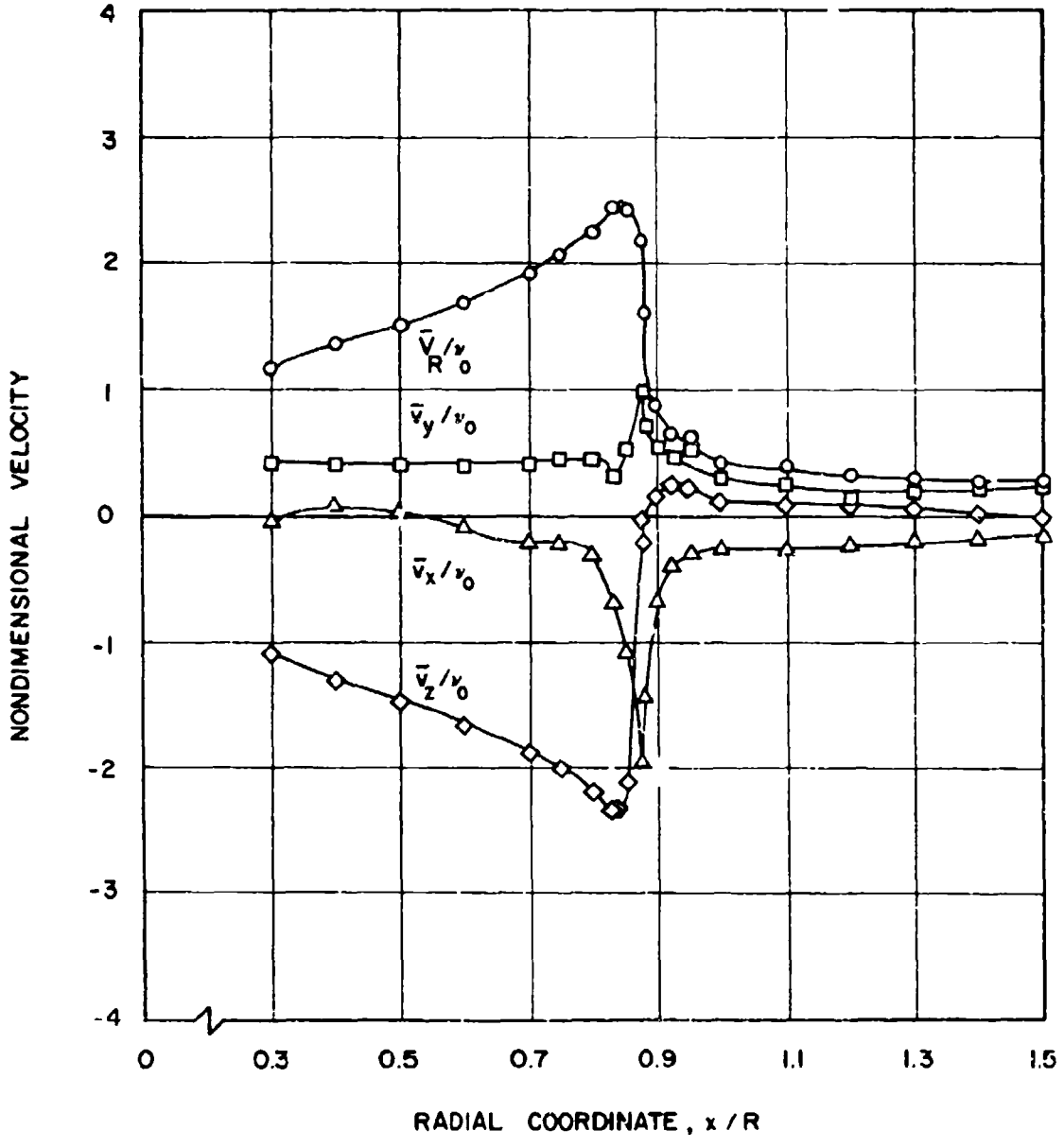

Figure 10. Radial Distribution of Mean Velocity Components and Resultant Velocity, Test Condition 1, $z/R = -0.1$, $\psi = 0$ deg.

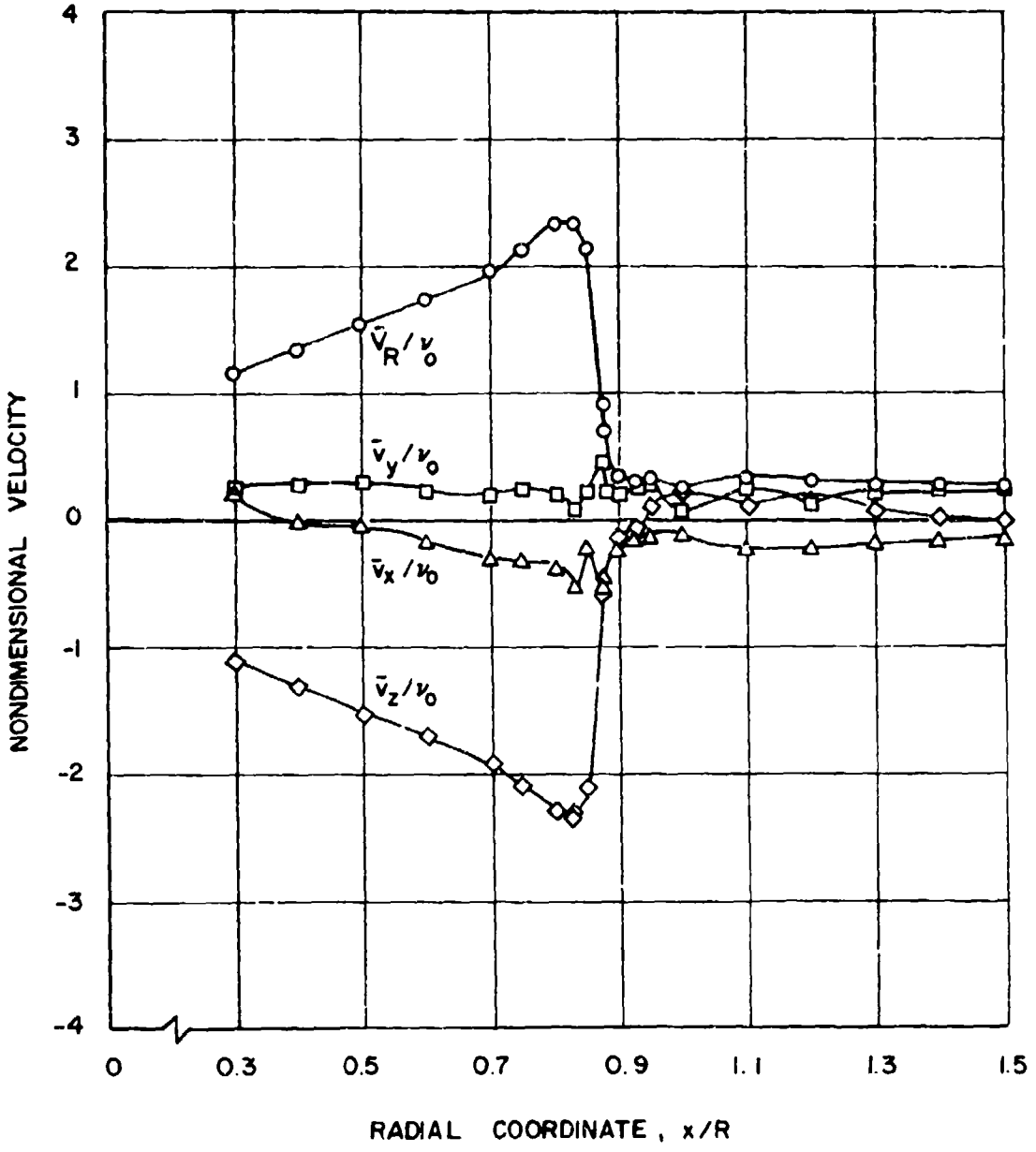

Figure 11. Radial Distribution of Mean Velocity Components and Resultant Velocity, Test Condition 1, $z/R \approx -0.1$, $\psi = 45$ deg.

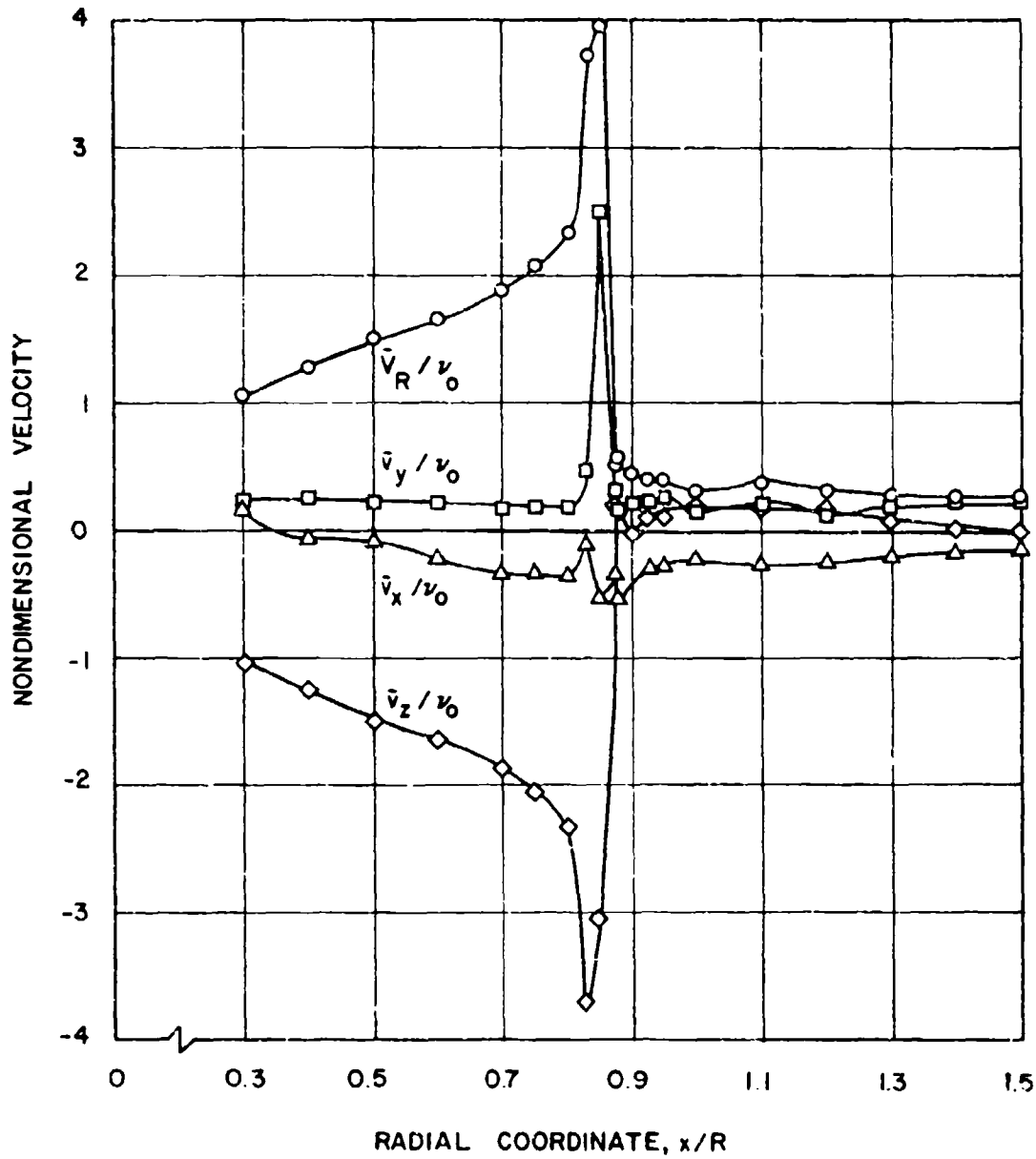

Figure 12. Radial Distribution of Mean Velocity Components and Resultant Velocity, Test Condition 1, z/R = -0.1, ψ = 90 deg.

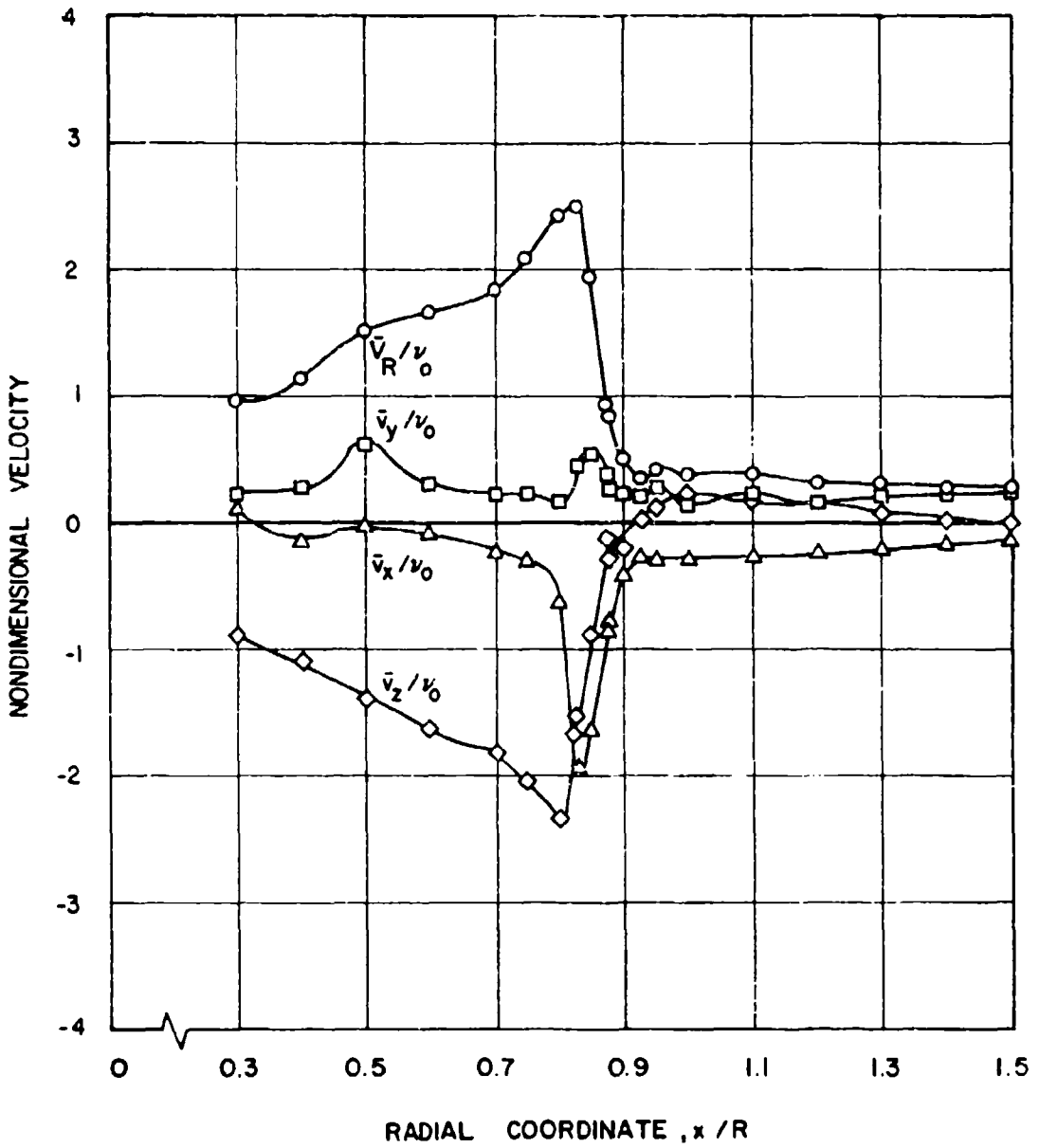

Figure 13. Radial Distribution of Mean Velocity Components and Resultant Velocity, Test Condition 1, $z/R = -0.1$, $\psi = 135$ deg.

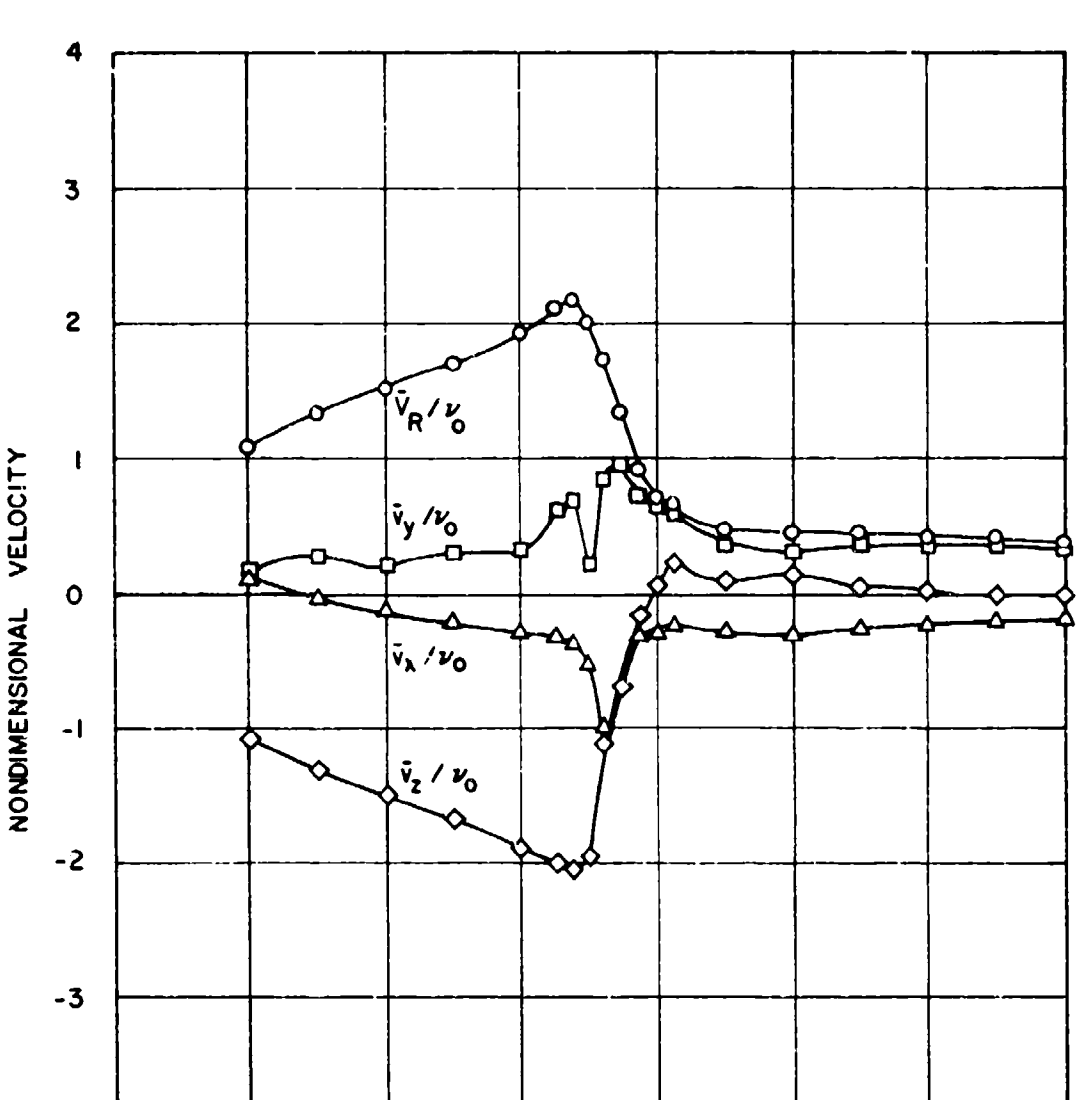

Figure 14. Radial Distribution of Mean Velocity Components and Resultant Velocity, Test Condition 2, $z/R = -0.1$, $\psi = 0$ deg.

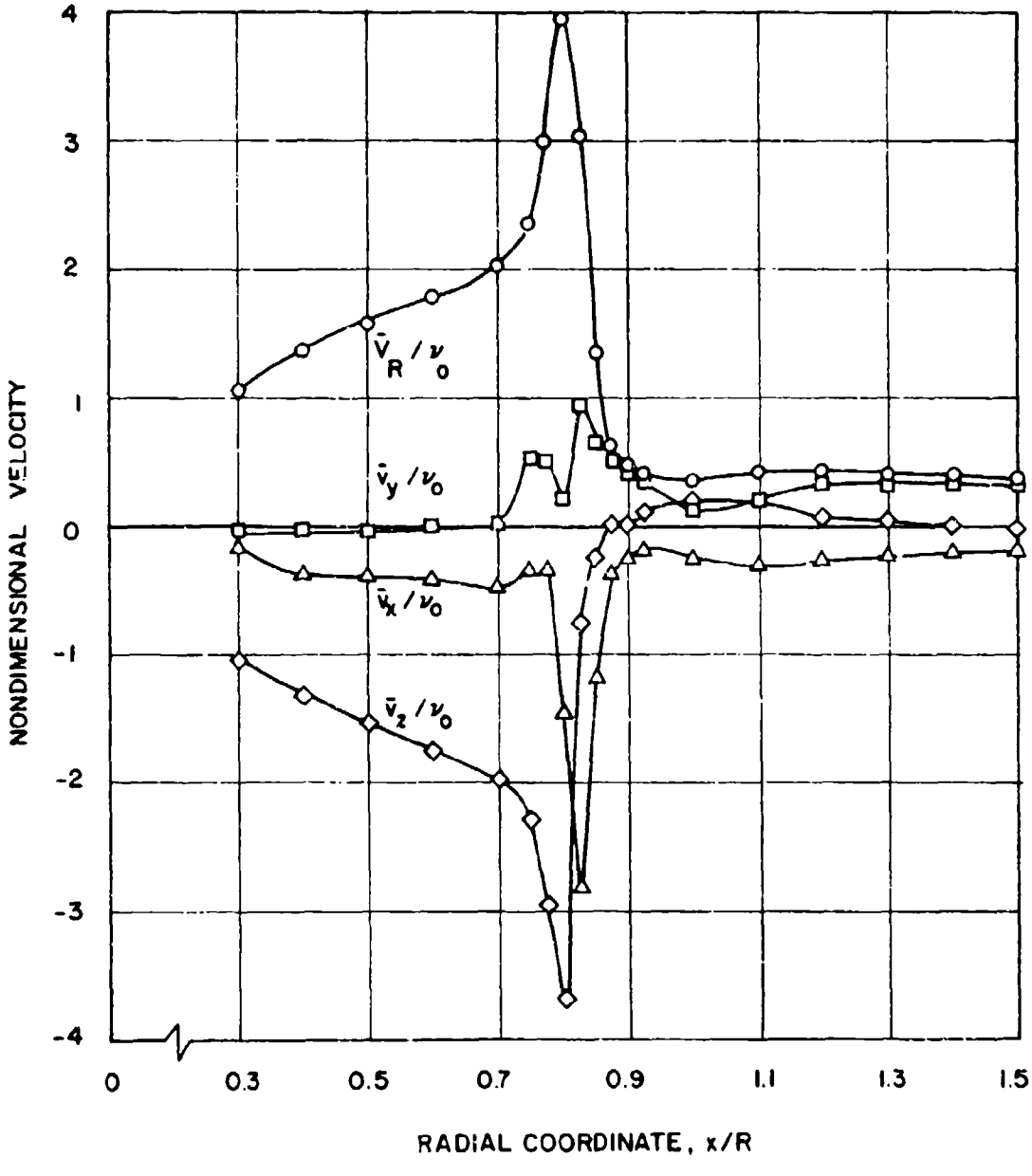

Figure 15. Radial Distribution of Mean Velocity Components and Resultant Velocity, Test Condition 2, $z/R = -0.1$, $\psi = 90$ deg.

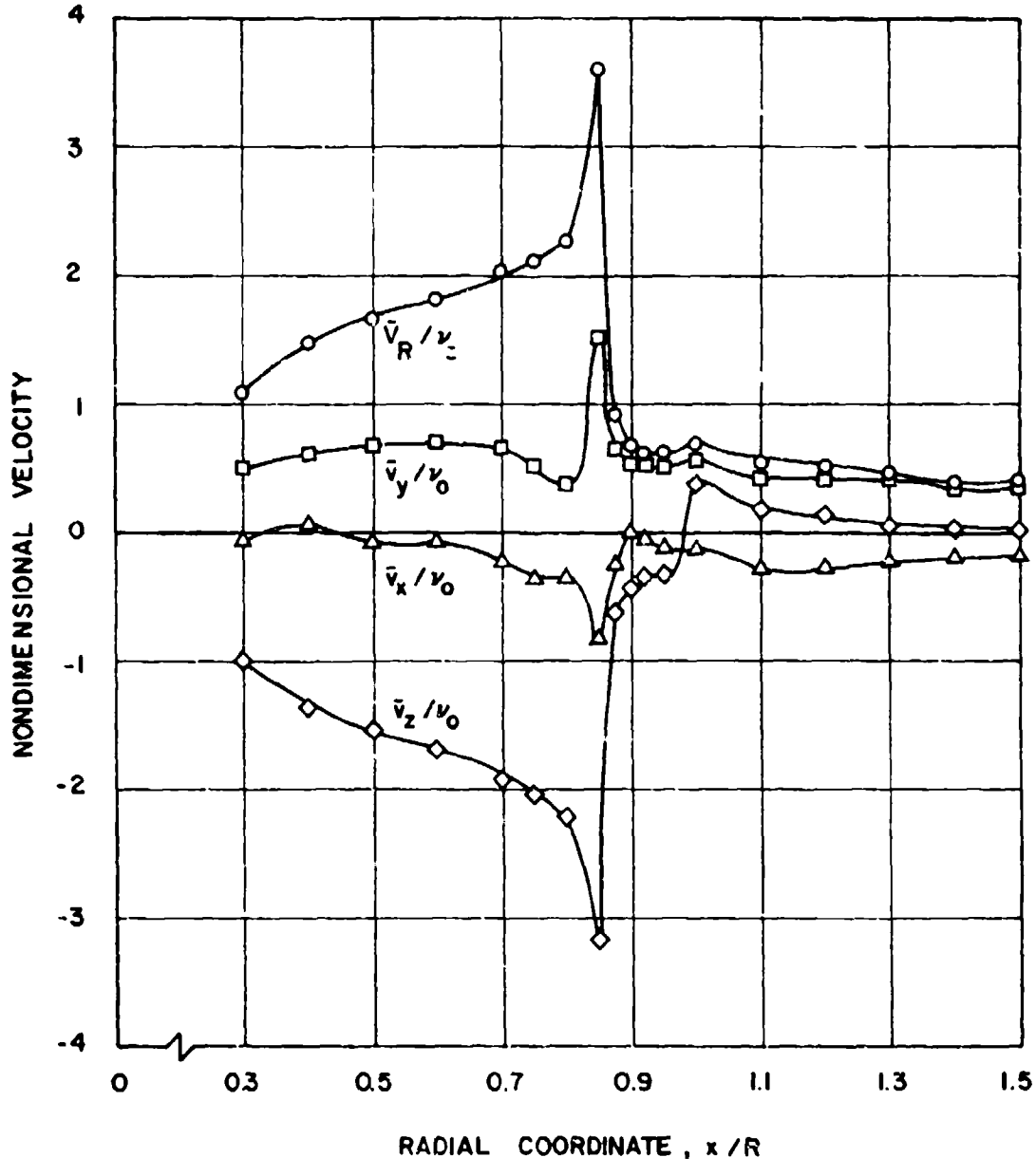

Figure 16. Radial Distribution of Mean Velocity Components and Resultant Velocity, Test Condition 3, $z/R = -0.1$, $\psi = 0$ deg.

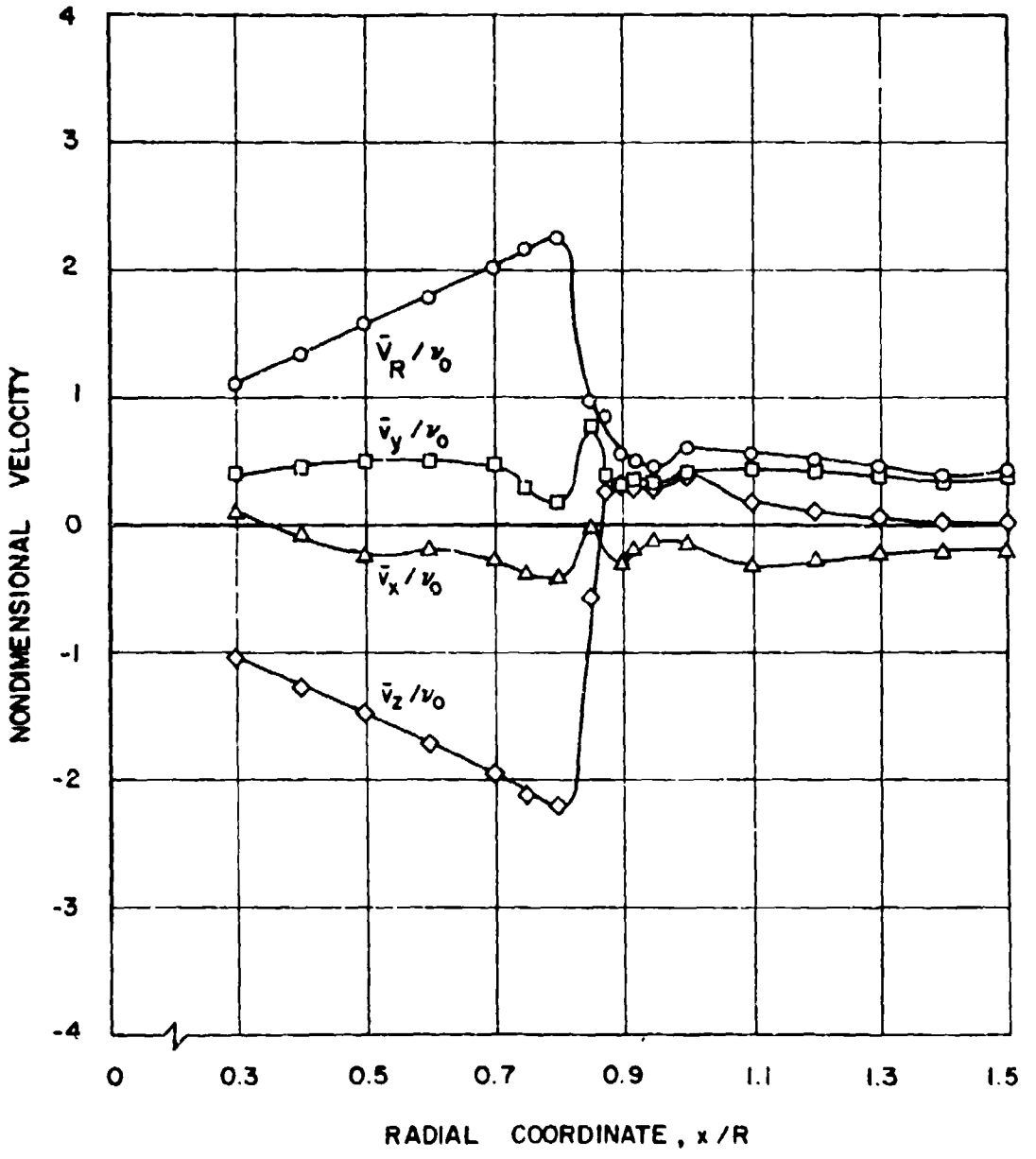

Figure 17. Radial Distribution of Mean Velocity Components and Resultant Velocity, Test Condition 3, z/R = -0.1, ψ = 90 deg.

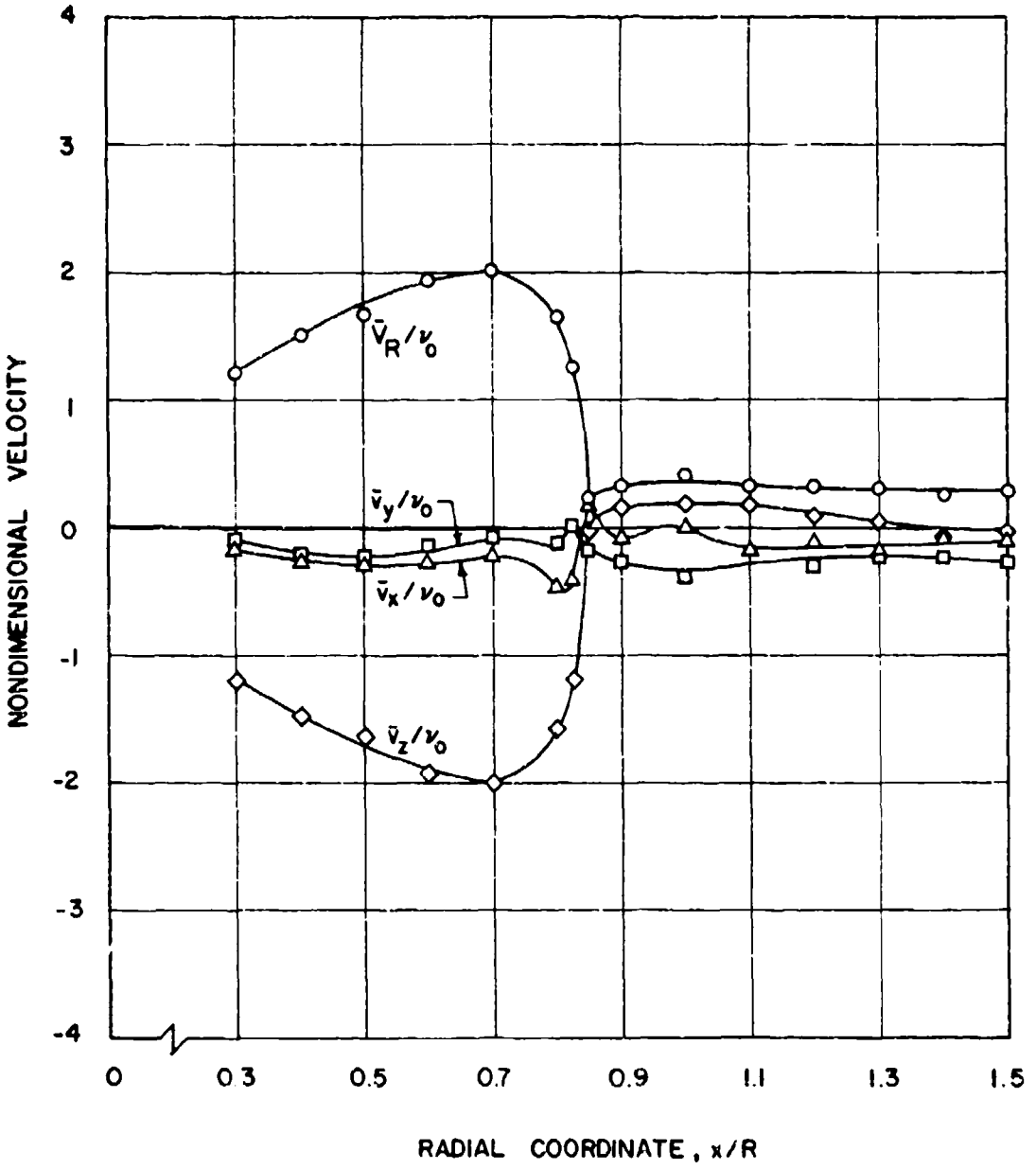

Figure 18. Radial Distribution of Mean Velocity Components and Resultant Velocity, Test Condition 1, $z/R = -0.3$, $\psi = 0$ deg.

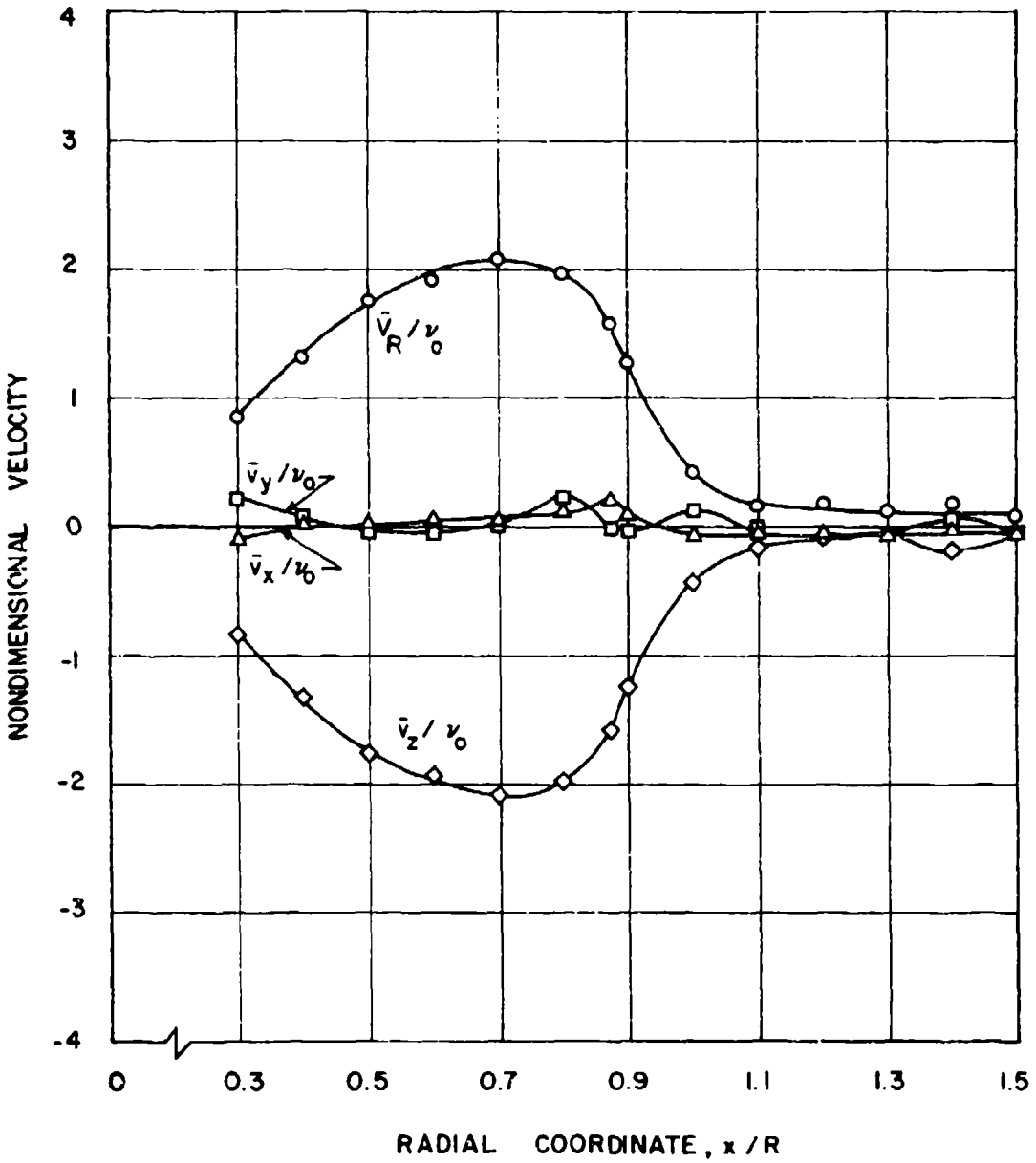

Figure 19. Radial Distribution of Mean Velocity Components and Resultant Velocity, Test Condition 1, $z/R = -0.7$, $\psi = 0$ deg.

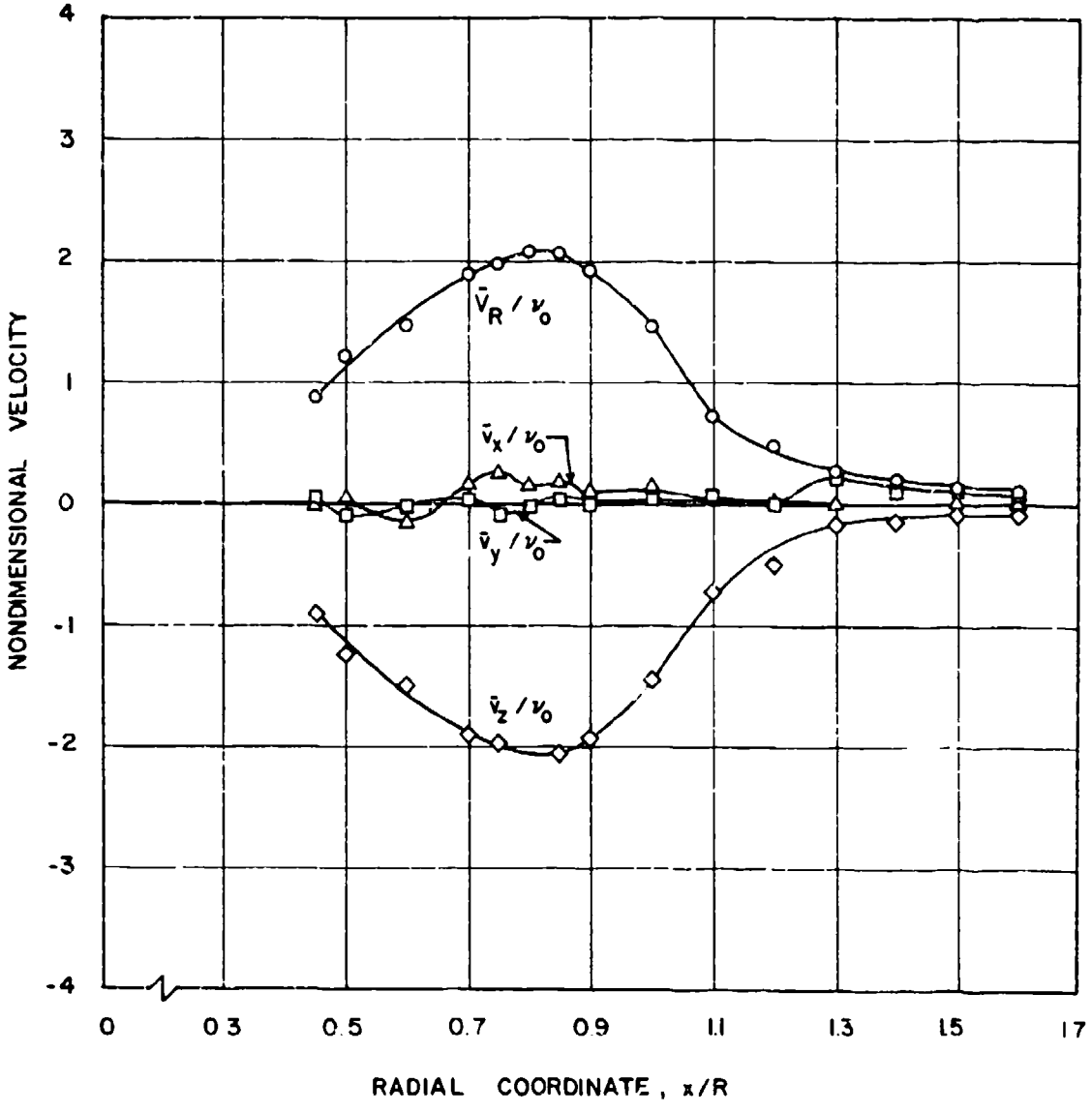

Figure 20. Radial Distribution of Mean Velocity Components and Resultant Velocity, Test Condition 1, $z/R = -1.5$, $\psi = 0$ deg.

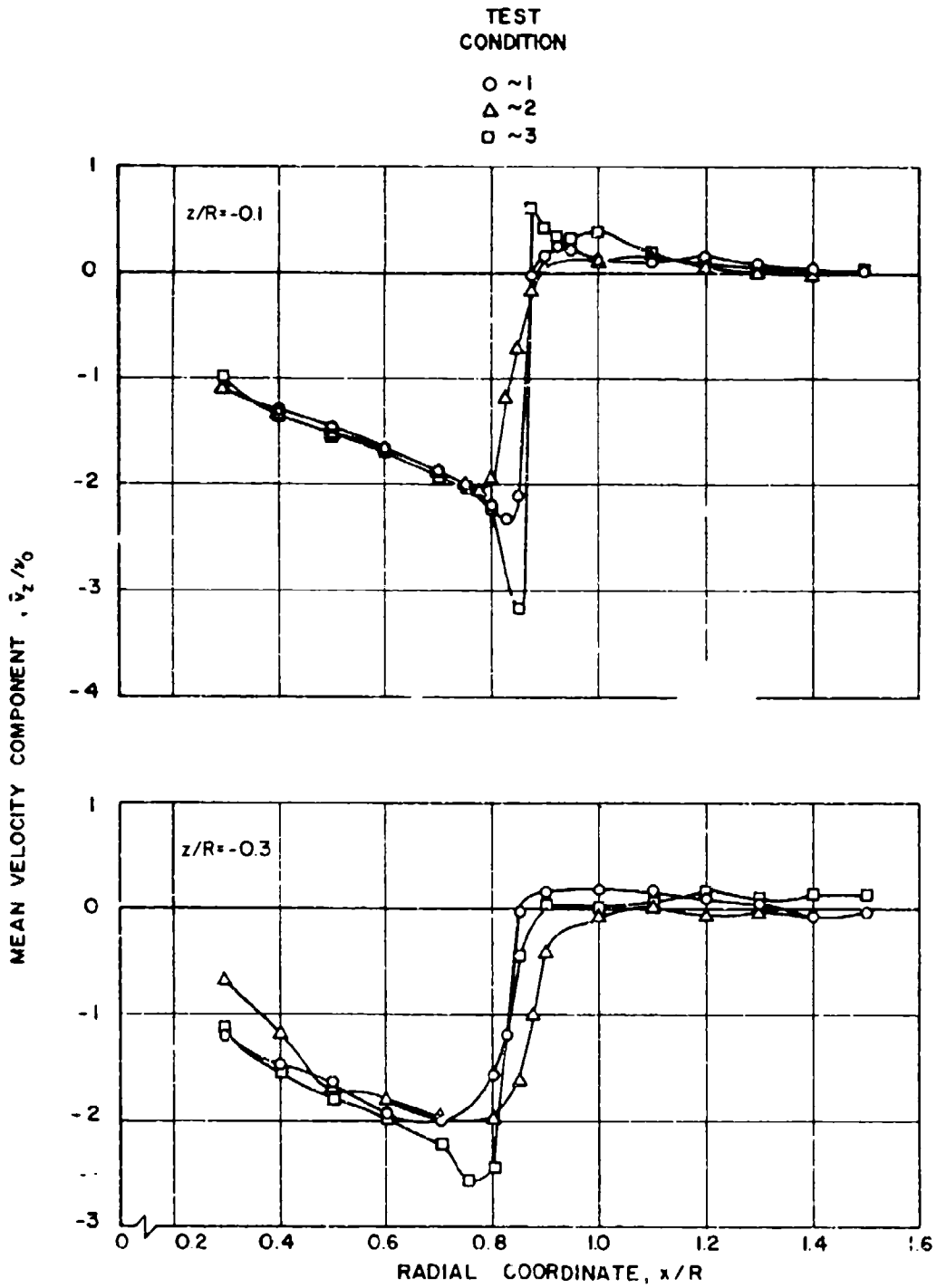

Figure 21. Comparison of Radial Distributions of Vertical Velocity Component, $\bar{v}_z/v_0$, for Three Rotor Test Conditions, z/R = -0.1 and -0.3, ψ = 0 deg.

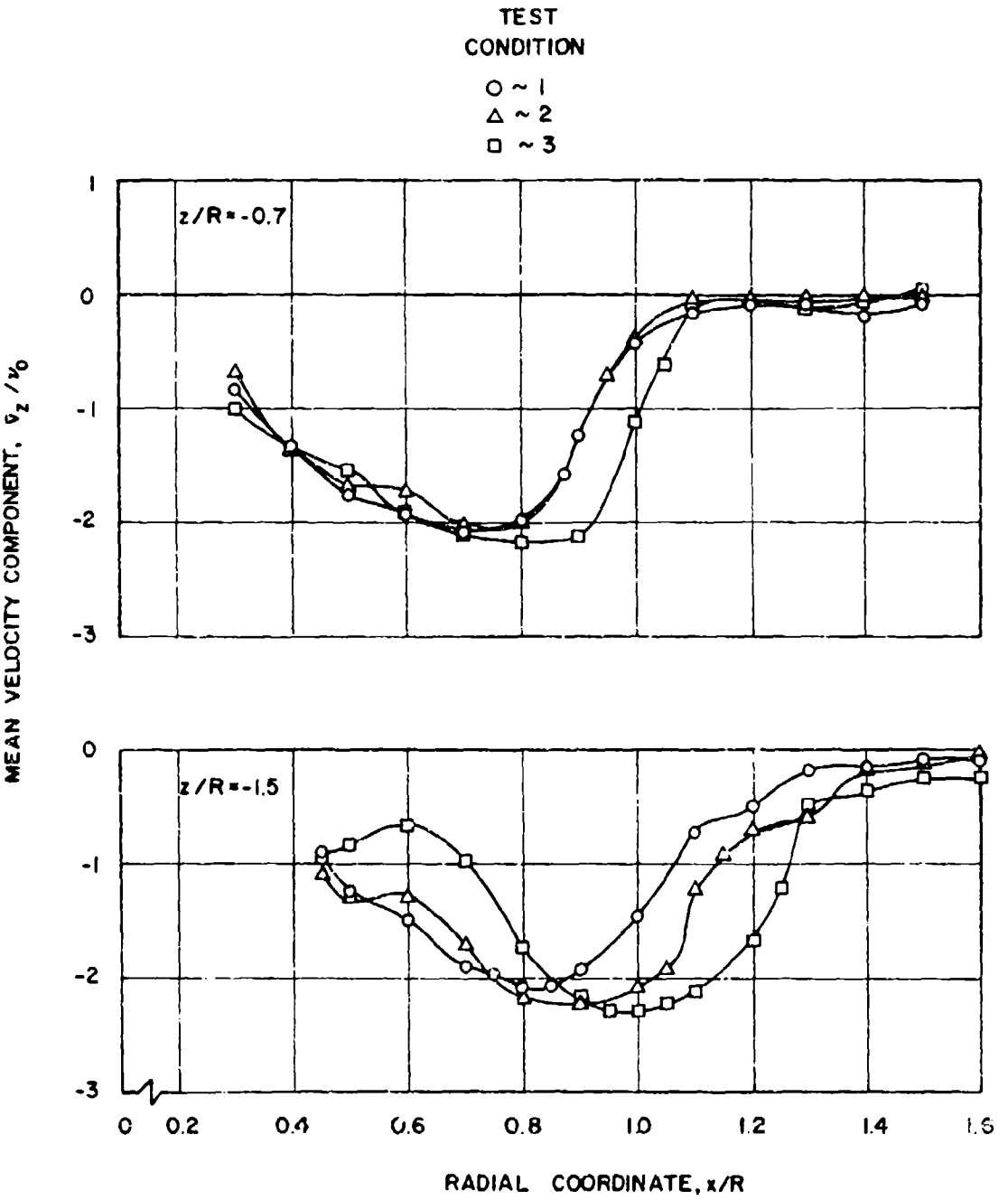

Figure 22. Comparison of Radial Distributions of Vertical Velocity Component, $\bar{v}_z/v_0$, for Three Rotor Test Conditions, z/R = -0.7 and -1.5, ψ = 0 deg.

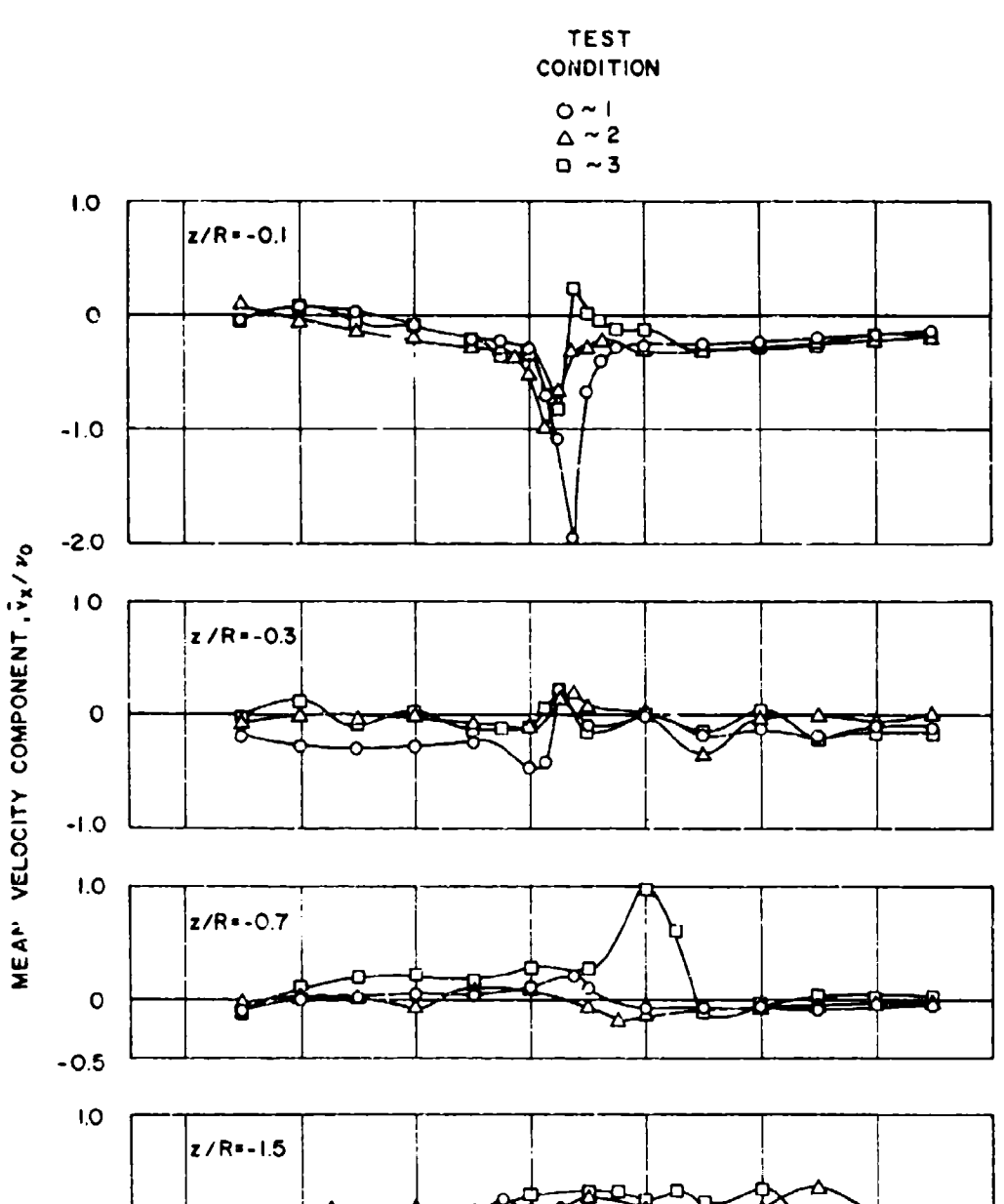

Figure 23. Comparison of Radial Distributions of Radial Velocity Component, $\bar{v}_x/v_o$, for Three Rotor Test Conditions, z/R = -0.1, -0.3, -0.7, and -1.5, ψ = 0 deg.

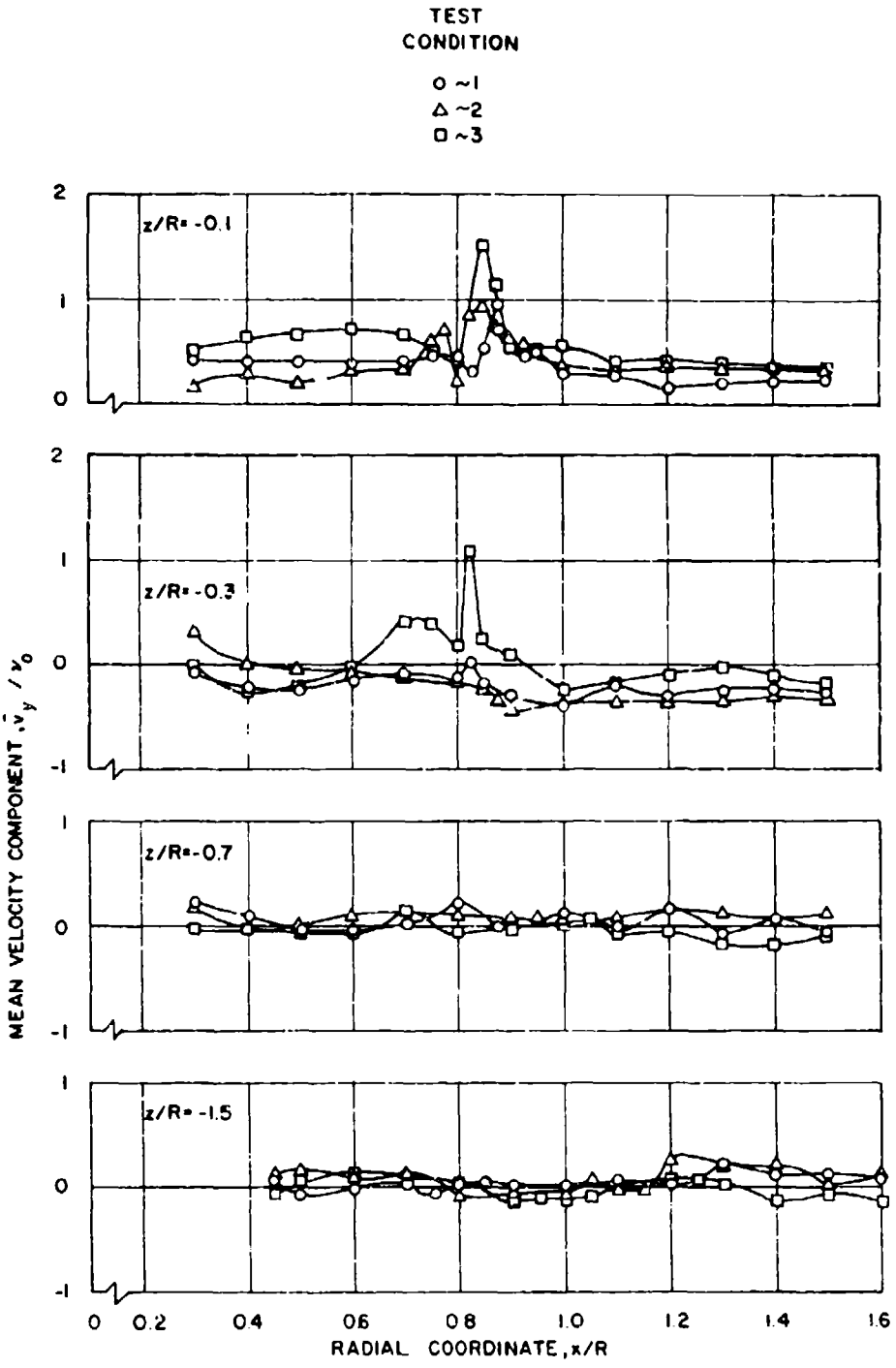

Figure 24. Comparison of Radial Distributions of Tangential Velocity Component, $\bar{v}_y/v_o$, for Three Rotor Test Conditions, z/R = -0.1, -0.3, -0.7, and -1.5, ψ = 0 deg.

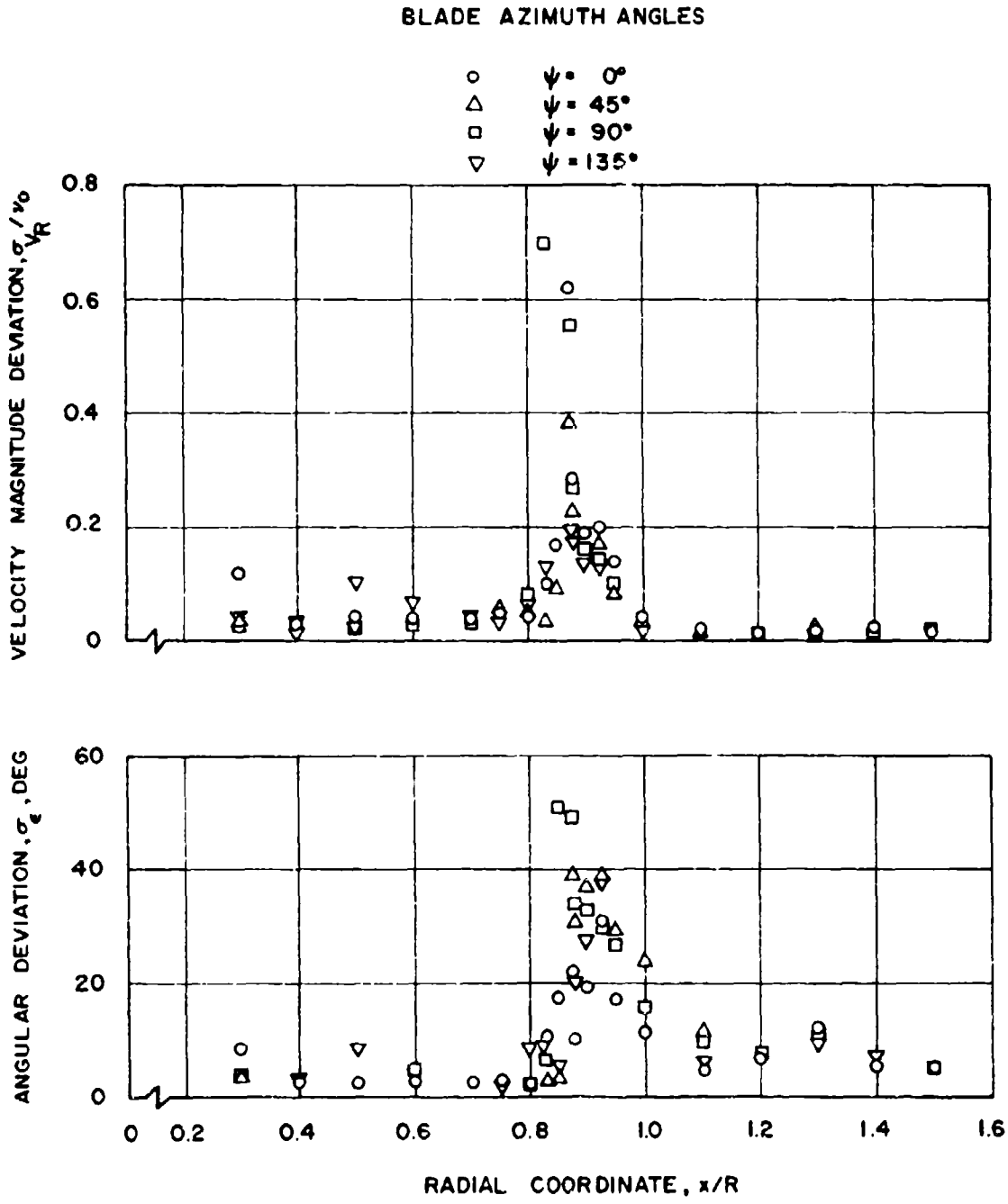

Figure 25. Standard Deviations of Instantaneous Total Velocity Vectors From Mean Values, Test Condition 1, z/R = -0.1.

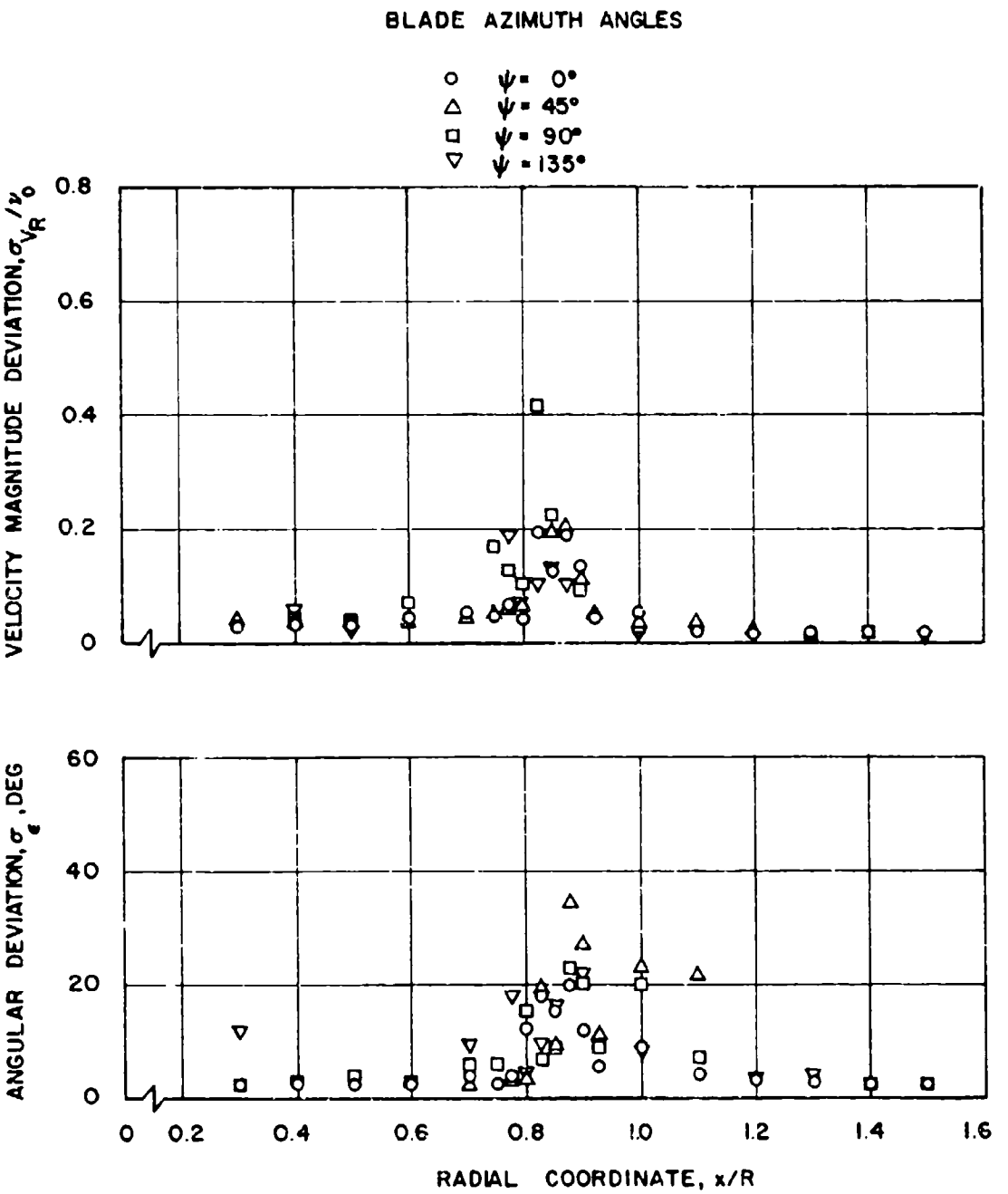

Figure 26. Standard Deviations of Instantaneous Total Velocity Vectors From Mean Values, Test Condition 2, z/R = -0.1.

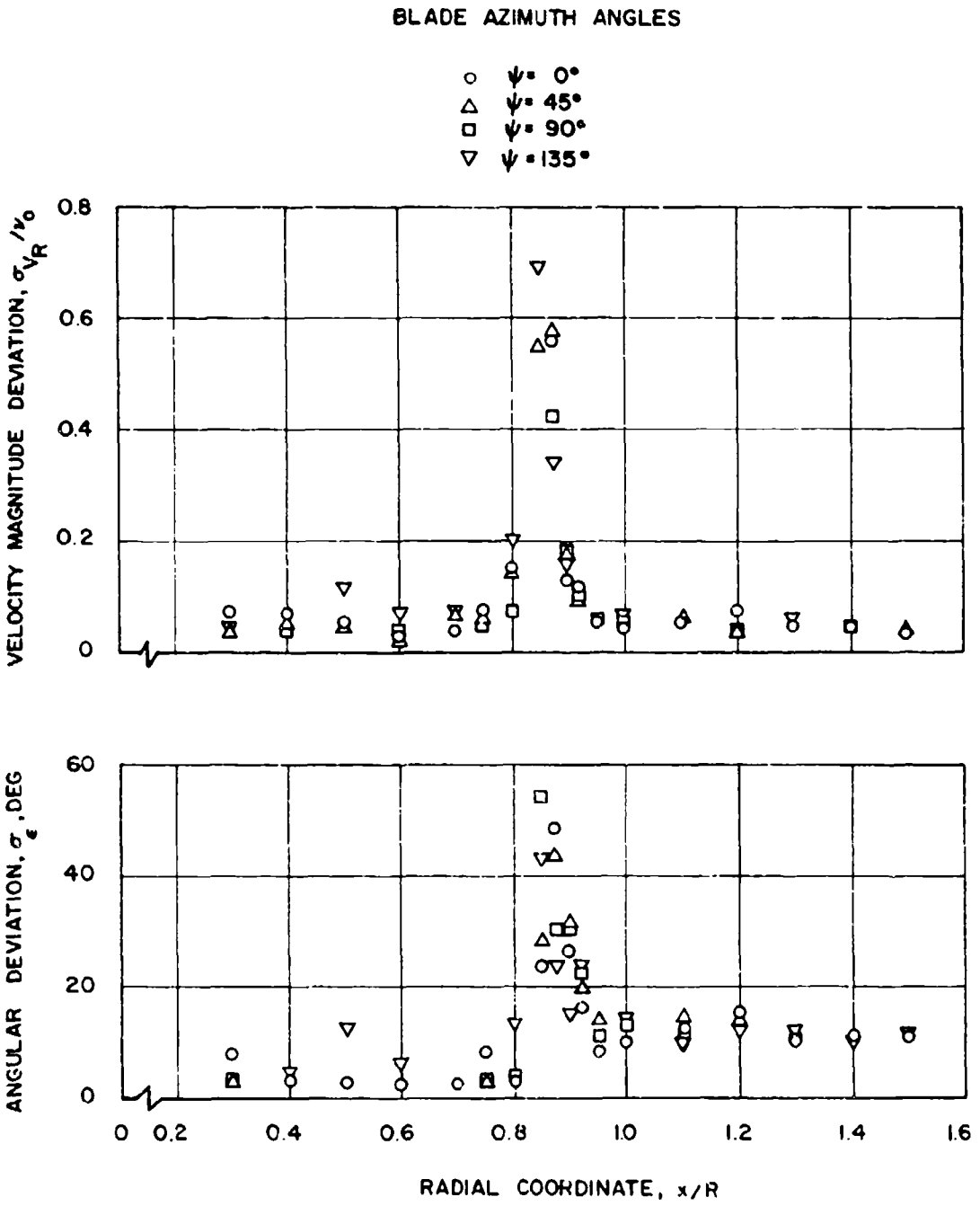

Figure 27. Standard Deviations of Instantaneous Total Velocity Vectors From Mean Values, Test Condition 3, z/R = -0.1.

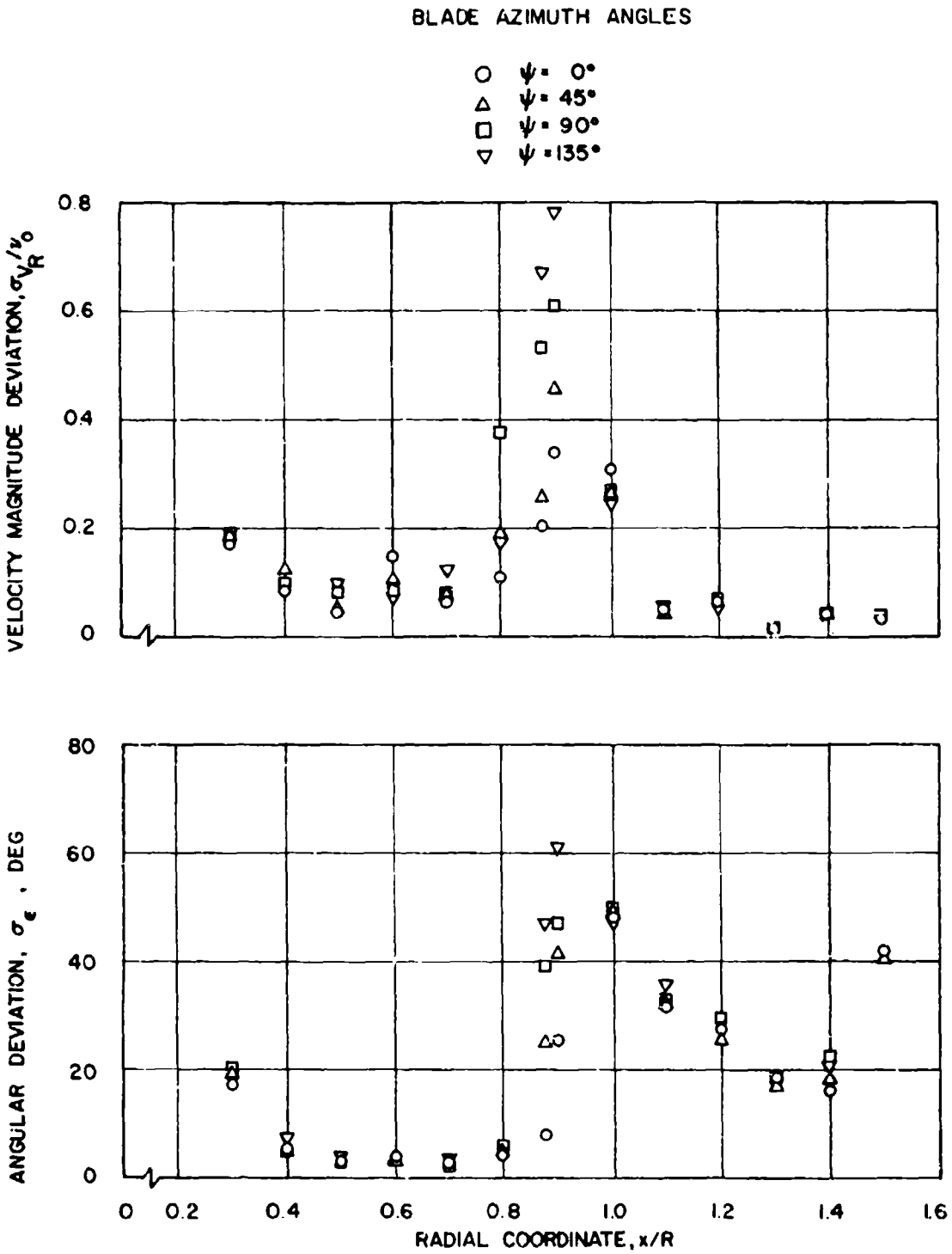

Figure 28. Standard Deviations of Instantaneous Total Velocity Vectors From Mean Values, Test Condition 1, z/R = -0.7.

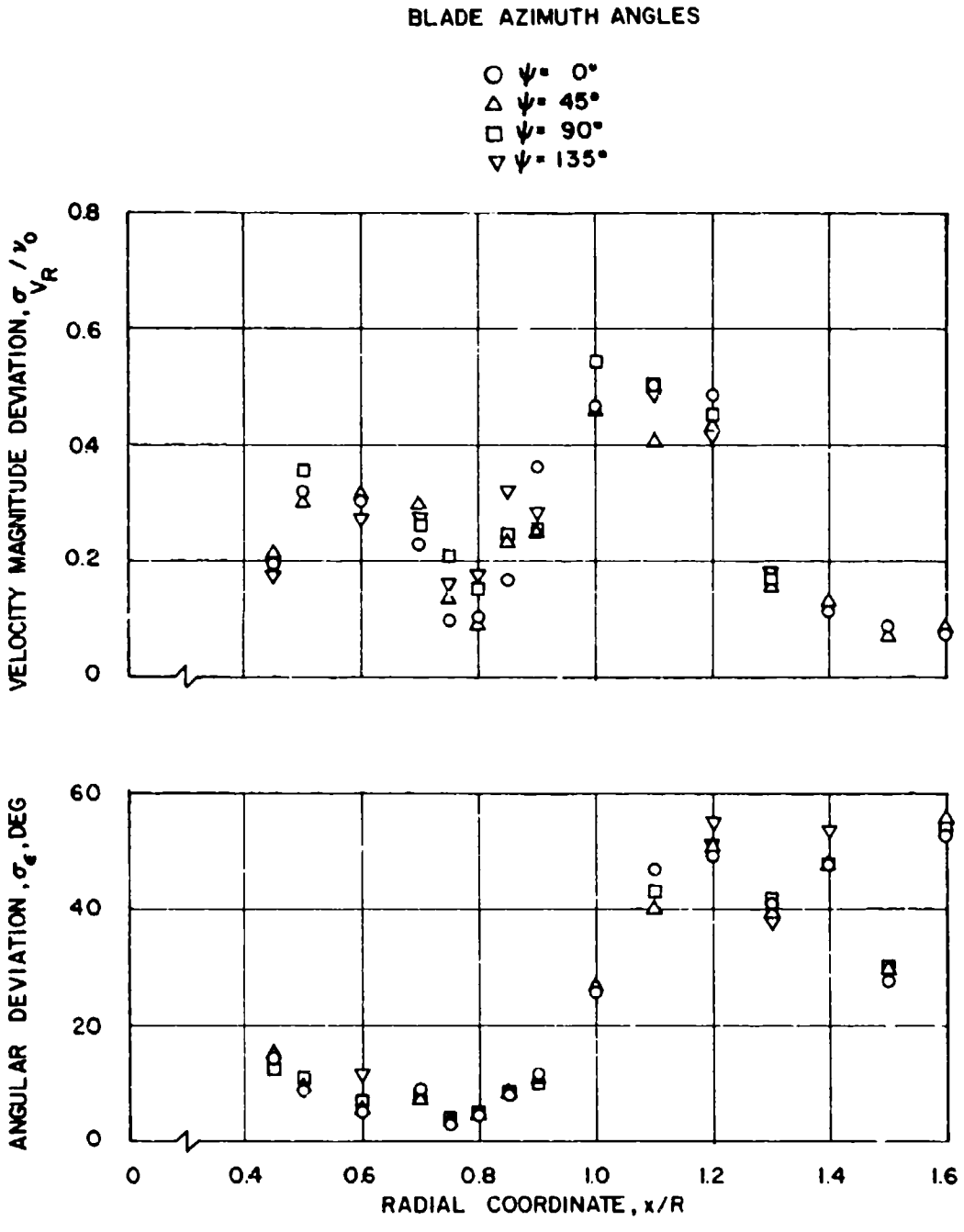

Figure 29. Standard Deviations of Instantaneous Total Velocity Vectors From Mean Values, Test Condition 1, z/R = -1.5.

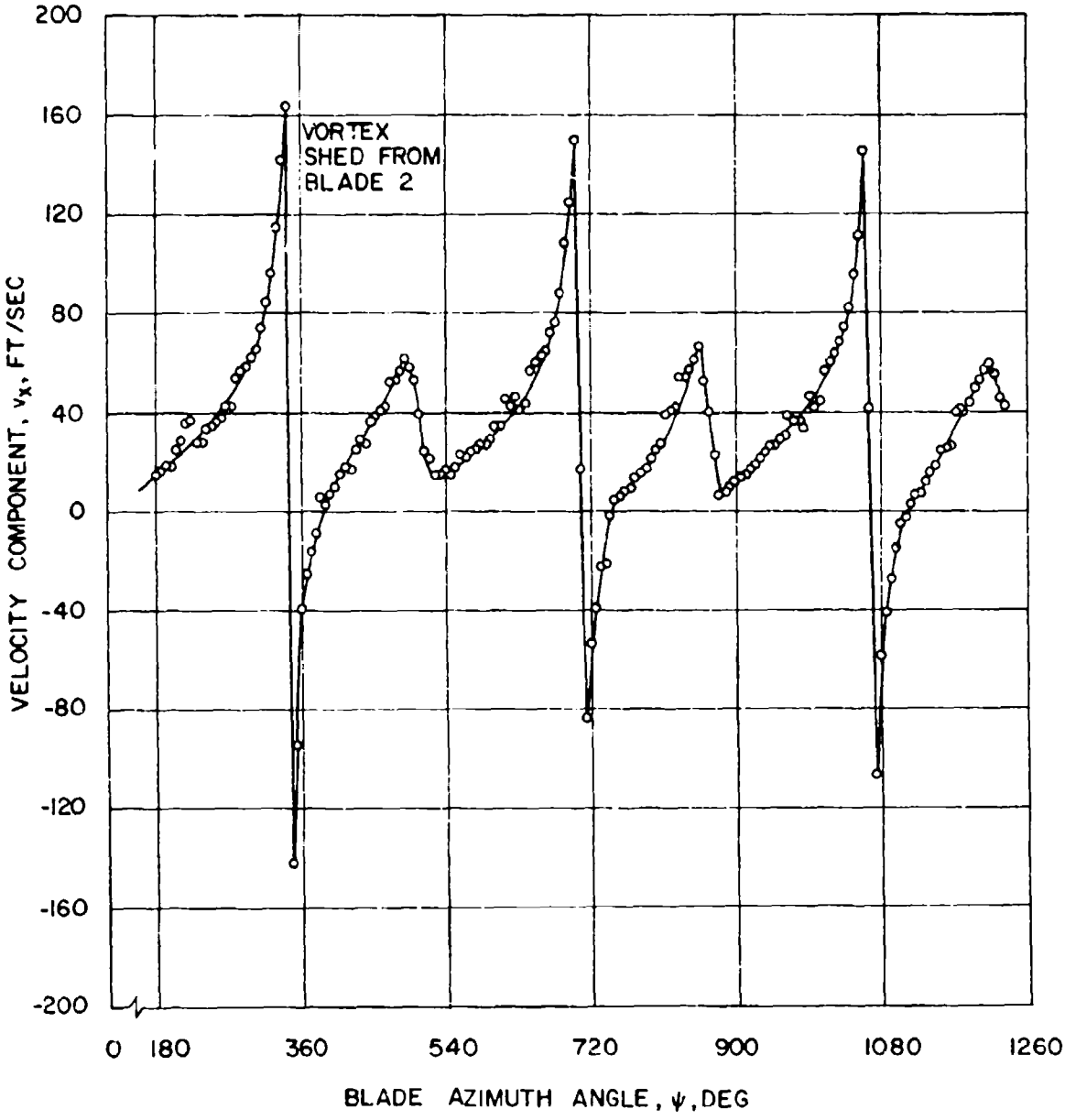

Figure 30. Instantaneous Velocity Components, v_x, Measured in the Vicinity of the Trailing Tip Vortices, Test Condition 2, $x/R = 0.85$, $z/R = -0.1$.

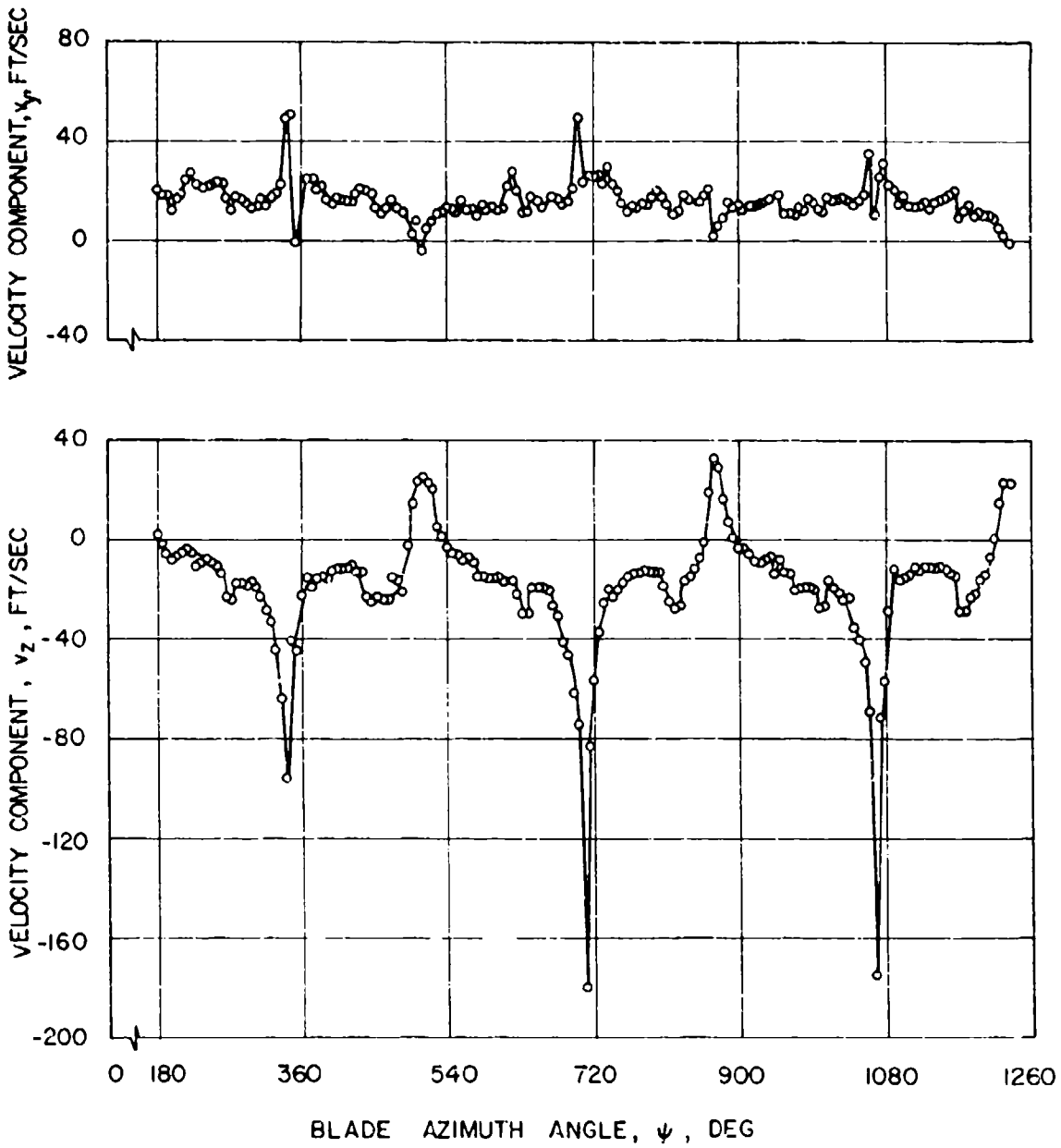

Figure 31. Instantaneous Velocity Components, v_y and v_z, Measured in the Vicinity of the Trailing Tip Vortices, Test Condition 2, $x/R = 0.85$, $z/R = -0.1$.

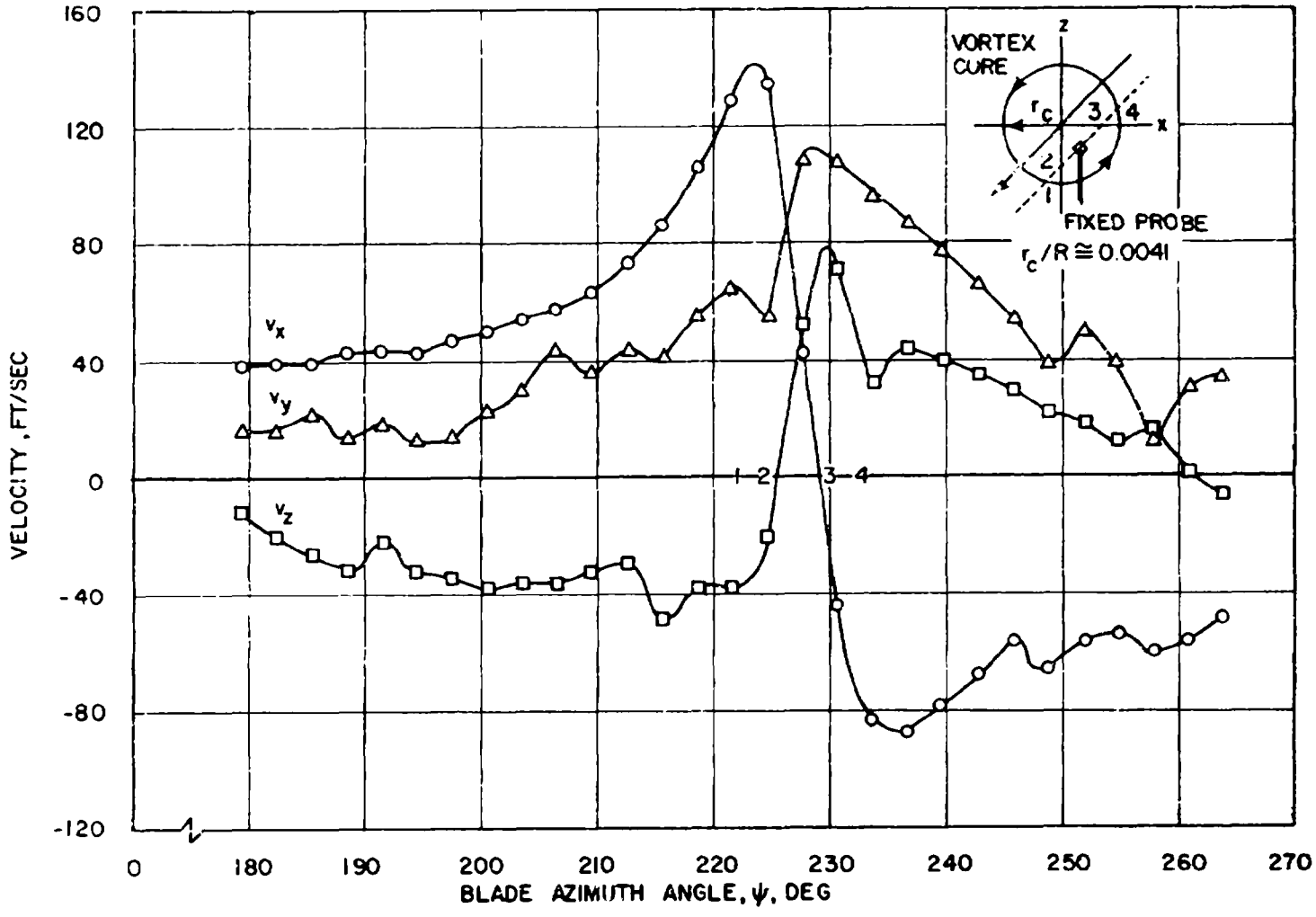

Figure 32. Distribution of Instantaneous Velocity Components Across a Trailing Vortex, Test Condition 1, x/R = 0.875, z/R = -0.1.

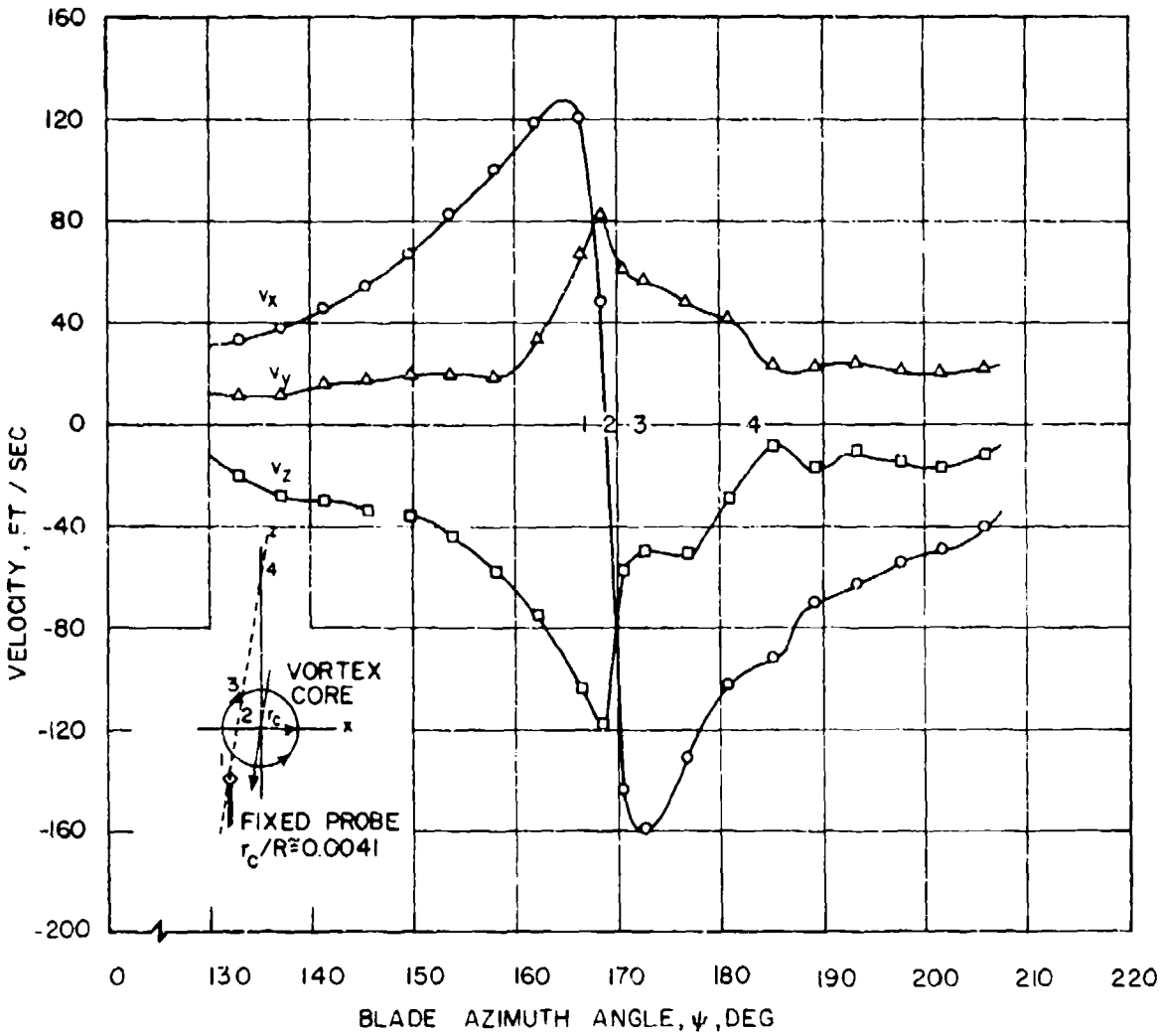

Figure 33. Distribution of Instantaneous Velocity Components Across a Trailing Vortex, Test Condition 2, x/R = 0.85, z/R = -0.1.

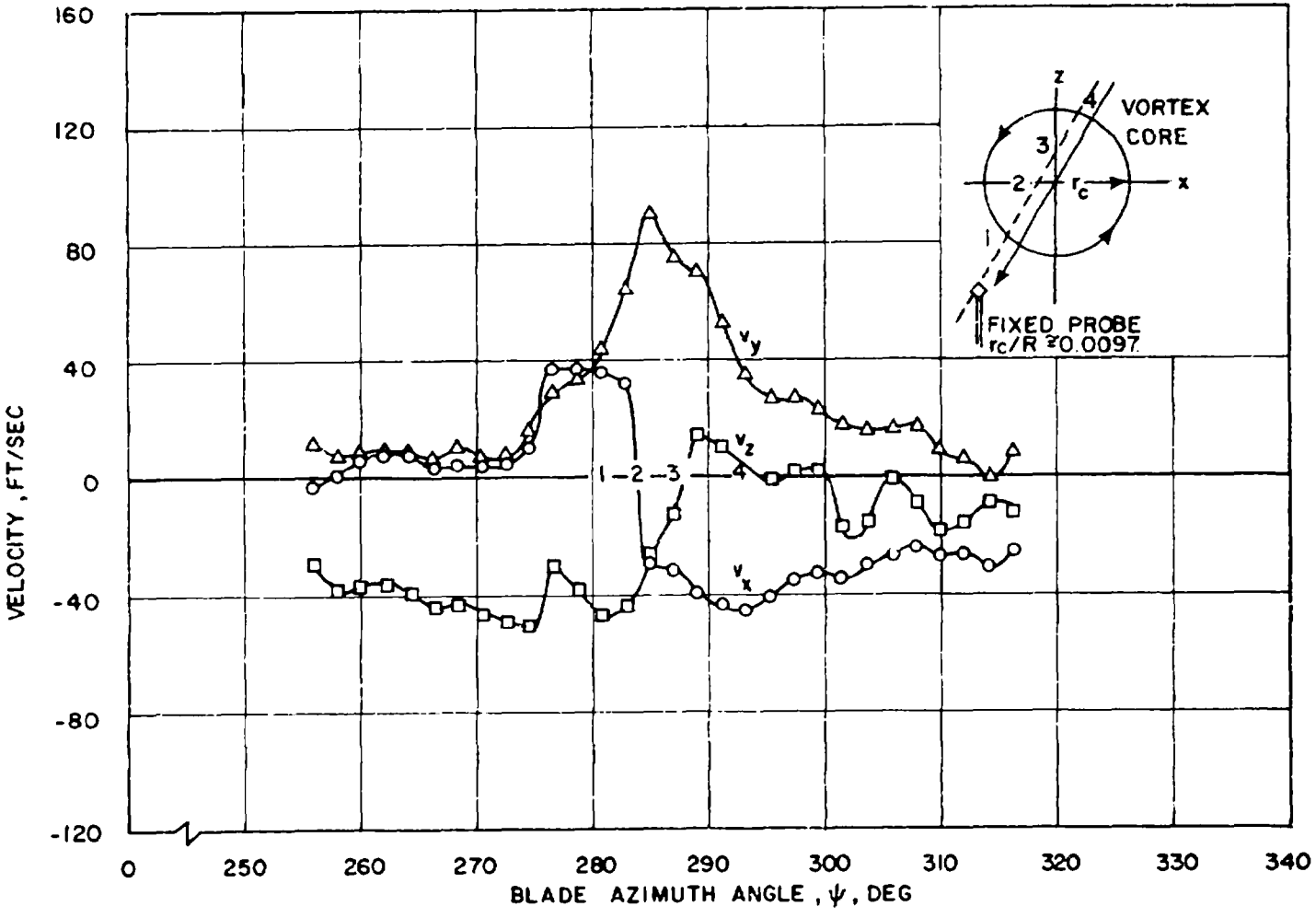

Figure 34. Distribution of Instantaneous Velocity Components Across a Trailing Vortex, Test Condition 3, x/R = 0.835, z/R = -0.1.

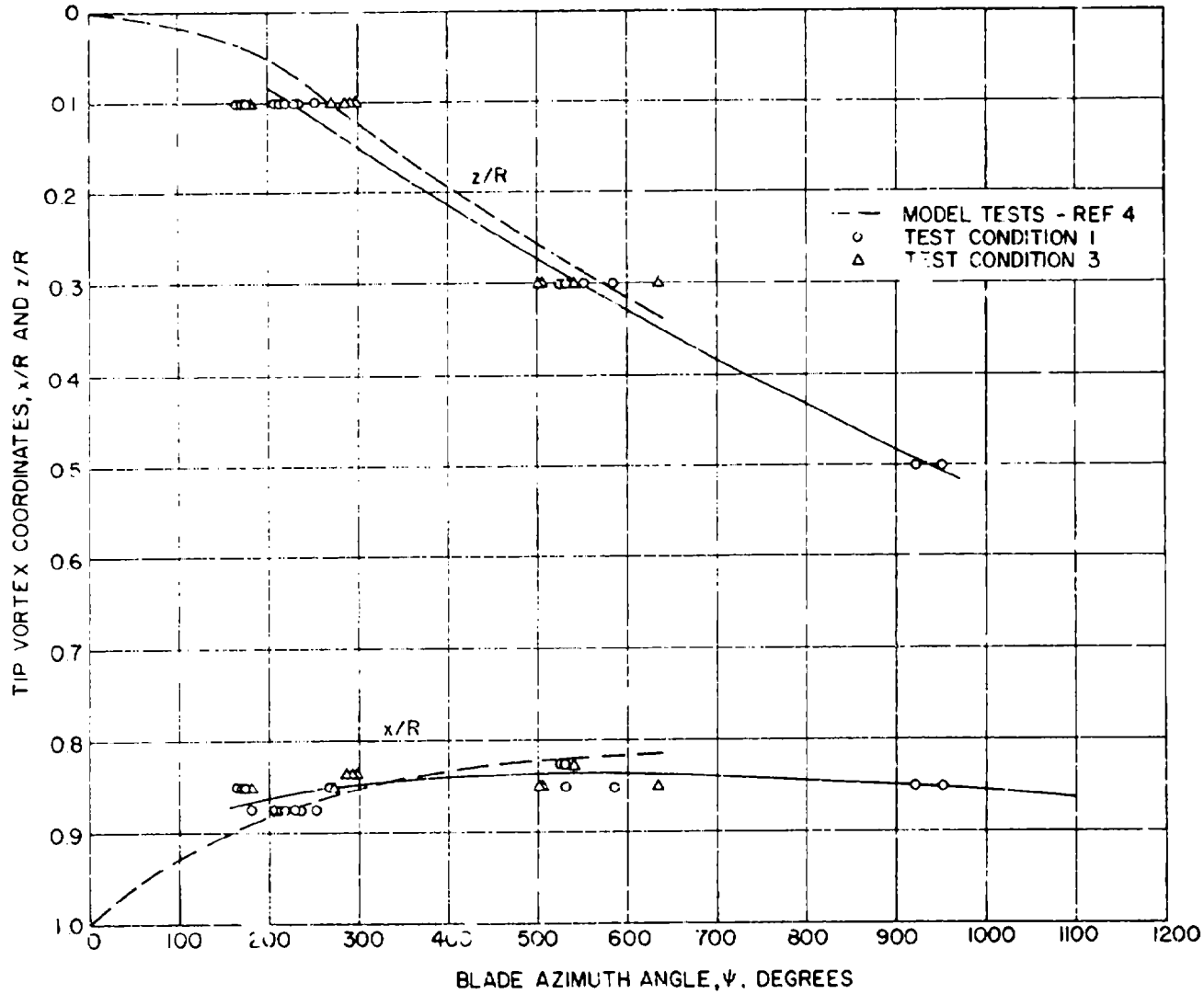

Figure 35. Tip Vortex Coordinates Determined From Vortex Analysis, Test Conditions 1 and 3.

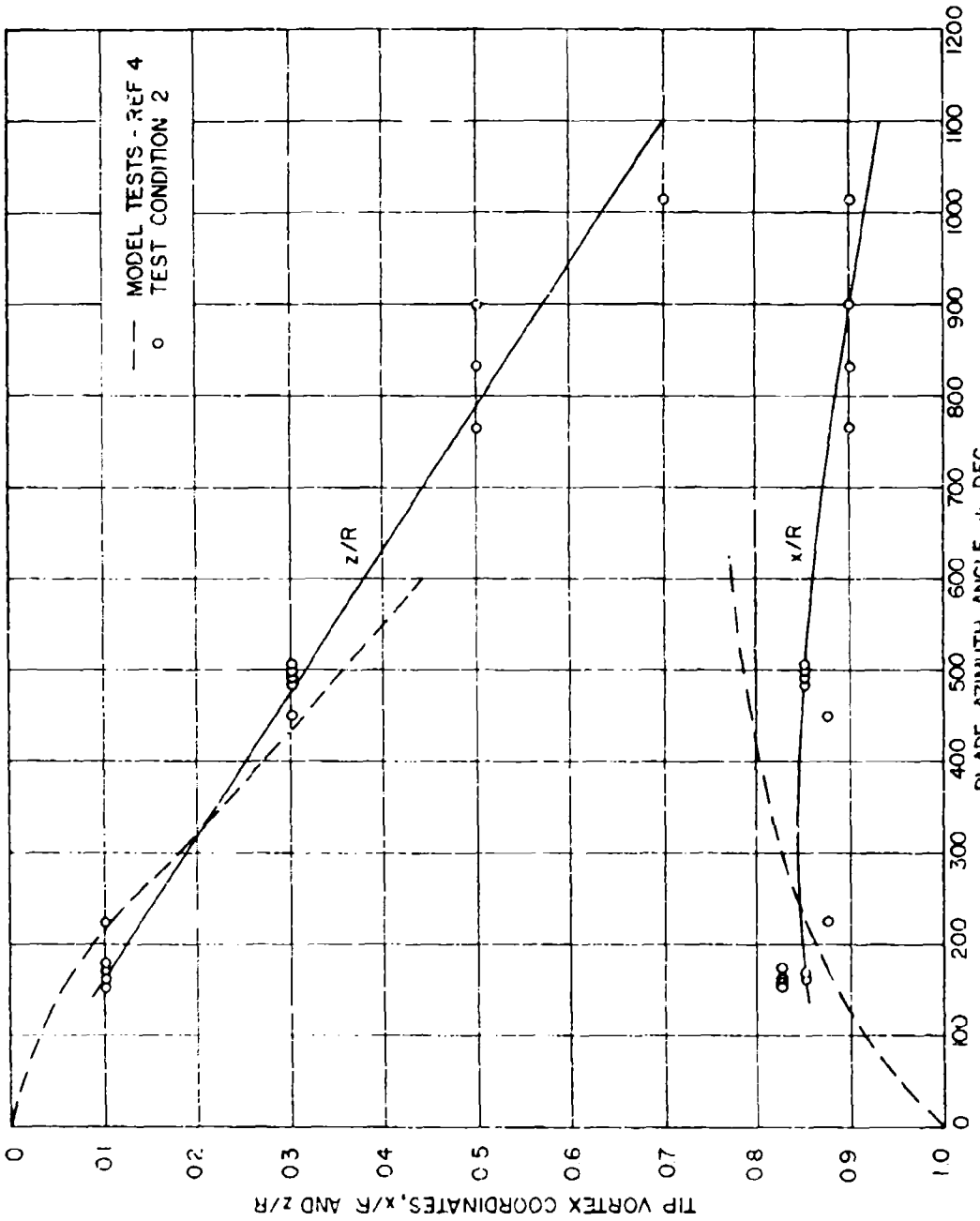

Figure 36. Tip Vortex Coordinates Determined From Vortex Analysis, Test Condition 2.

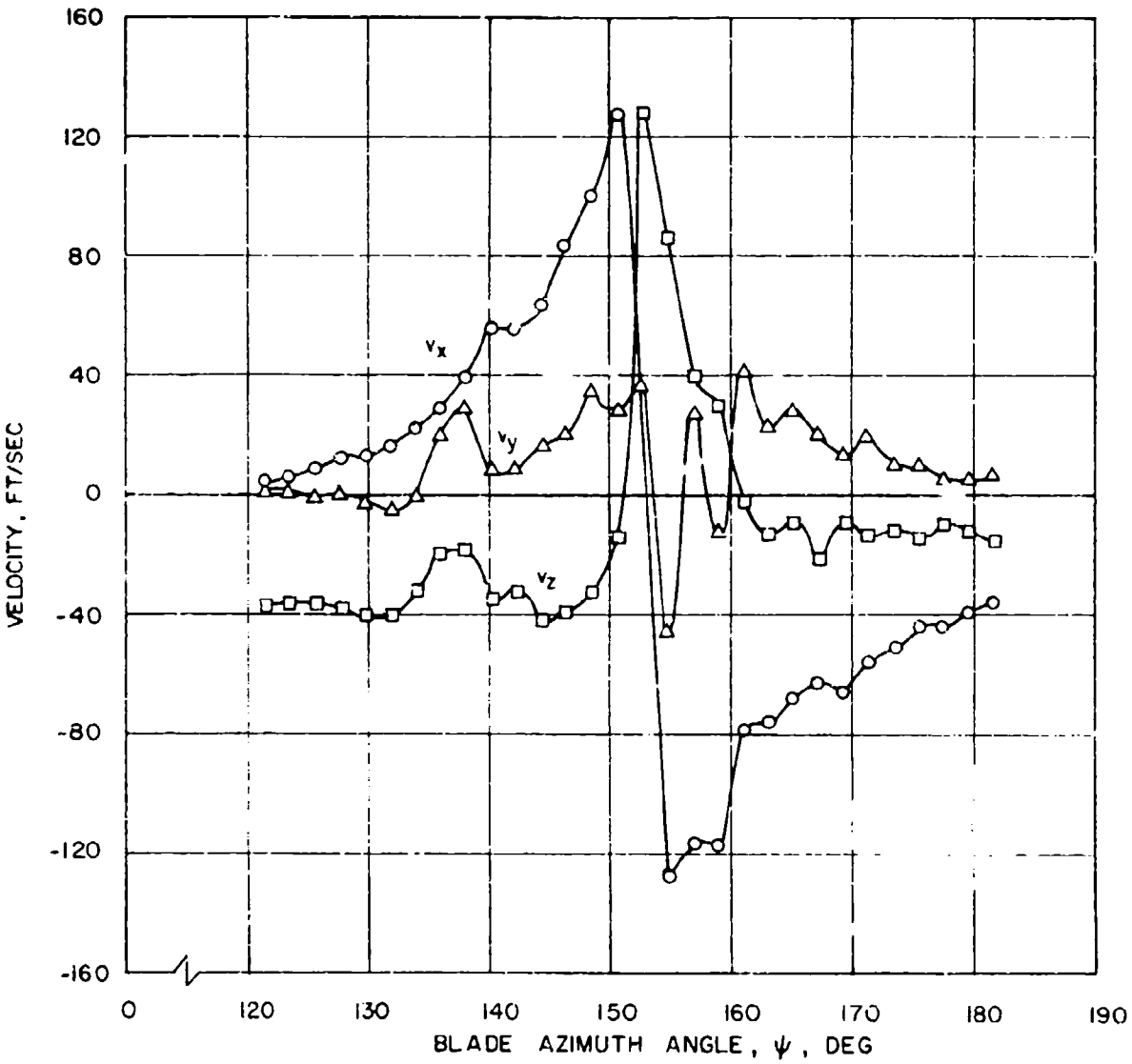

Figure 37. Distribution of Instantaneous Velocity Components Across a Vortex With Unstable Axial Flow in the Core Region, Test Condition 2, x/R = 0.825, z/R = -0.1.

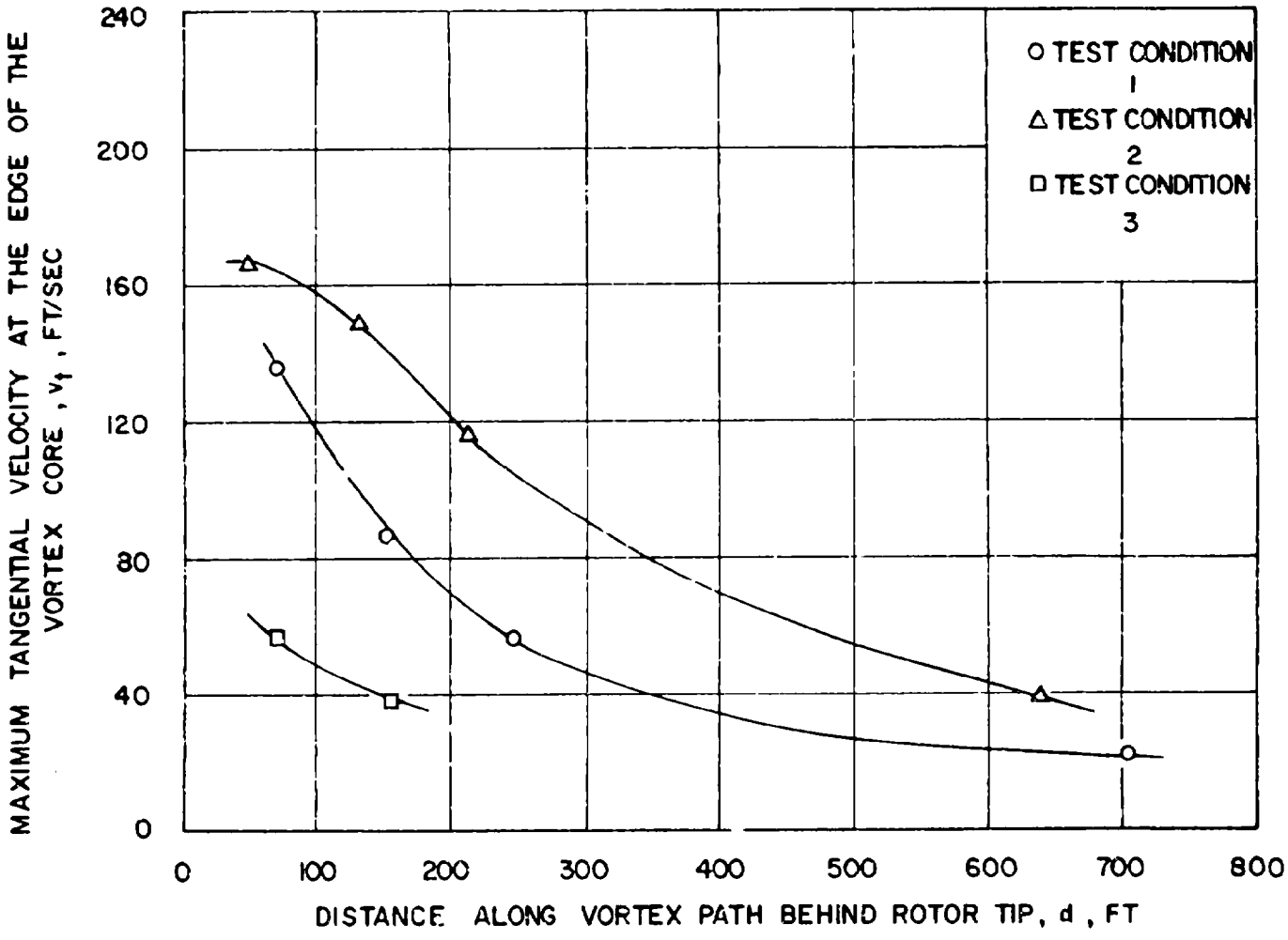

Figure 38. Decline of Maximum Tangential Velocity at the Edge of the Vortex Core With Distance Behine the Blade.

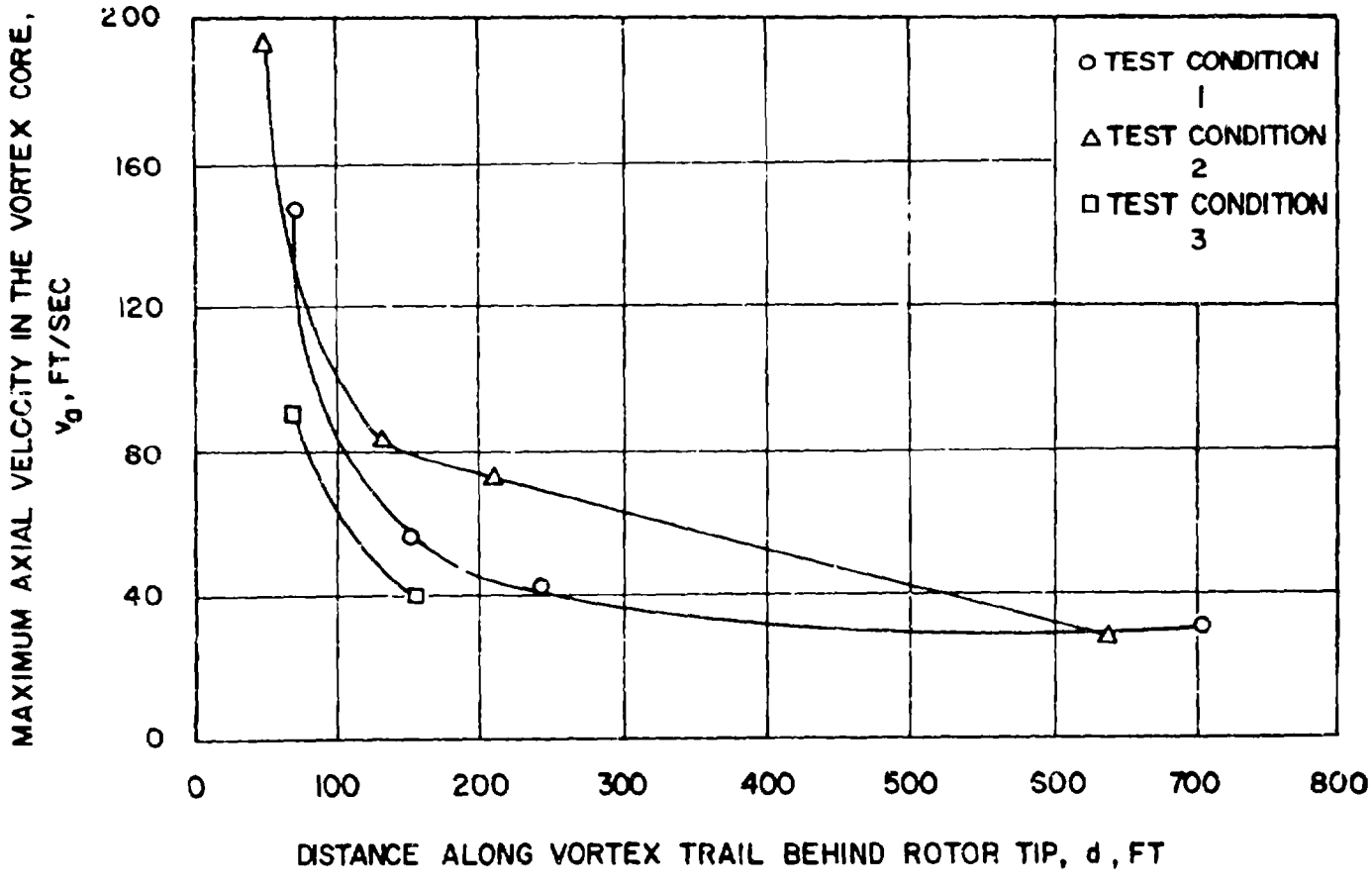

Figure 39. Decline of Maximum Axial Velocity in the Vortex Core With Distance Behind the Blade.

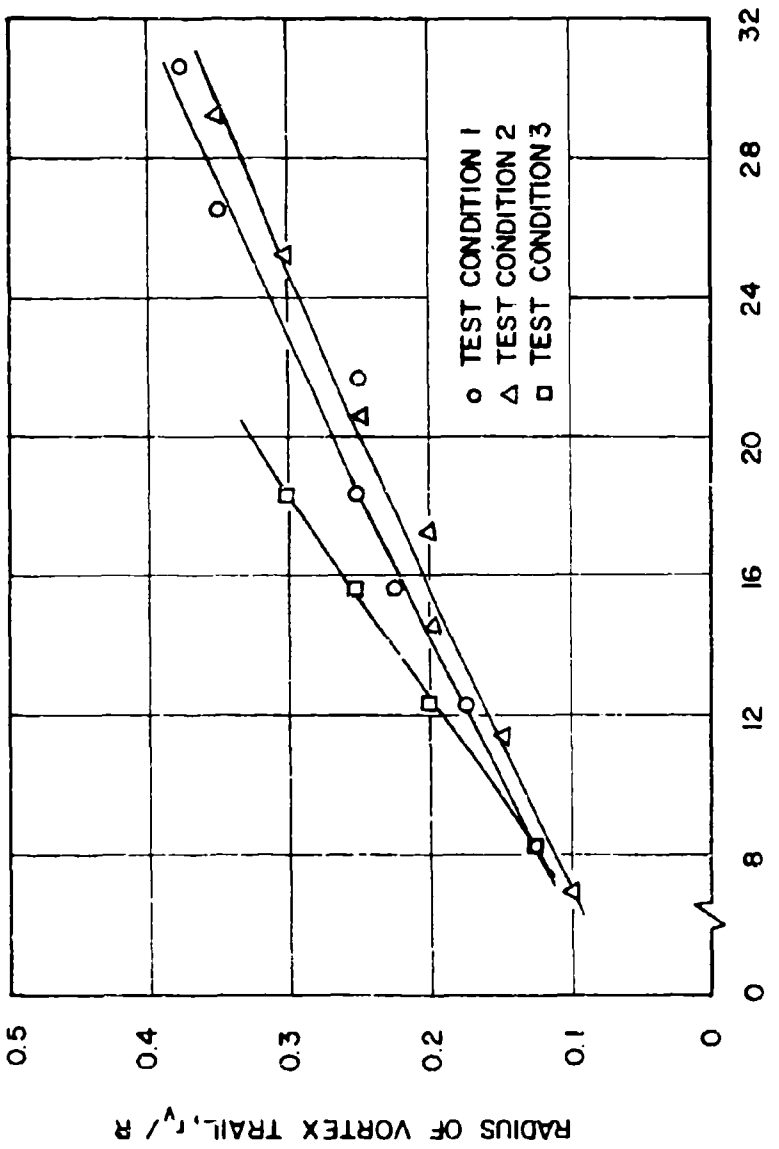

Figure 40. Growth of the Trailing Vortices Downstream of the Blade Tip.

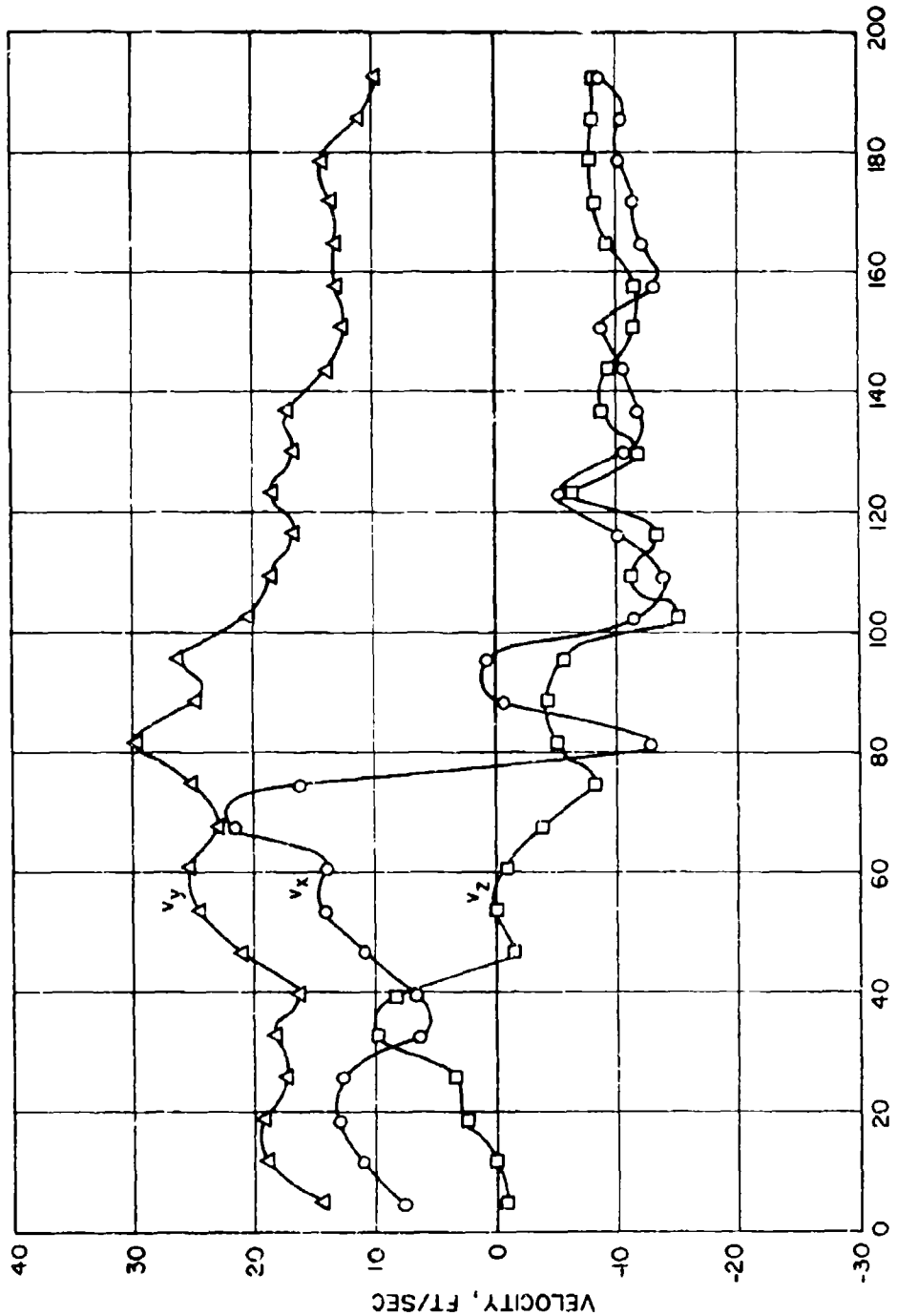

Figure 41. Vortex Signature in the Far Wake, Test Condition 1, x/R = 1.2, z/R = -1.5.

LITERATURE CITED

1. Gessow, Alfred, and Myers, Garry C., AERODYNAMICS OF THE HELICOPTER, New York, Fredrick Ungar Publishing Company, 1967.

2. Johnson, John N., and Ferry, Robert G., ARDC H-13 ADDENDUM NO. 1, PHASE IV PERFORMANCE, AFFTC-TR-57-12, Edwards Air Force Base, California, March 1958.

3. Turley, William R., and Balfe, Paul J., PERFORMANCE EVALUATION OF THE H-13K, AFFTC-TDR-62-15, Edwards Air Force Base, California, August 1962.

4. Landgrebe, Anton J., AN ANALYTICAL AND EXPERIMENTAL INVESTIGATION OF HELICOPTER ROTOR HOVER PERFORMANCE AND WAKE GEOMETRY CHARACTERISTICS, United Aircraft Corporation Research Laboratories, USAAMRDL Technical Report 71-24, Eustis Directorate, U. S. Army Air Mobility Research and Development Laboratory, Fort Eustis, Virginia, June 1971, AD 728835.

5. Lehman, August F., MODEL STUDIES OF HELICOPTER ROTOR FLOW PATTERNS, Oceanics, Inc., USAAVLABS Technical Report 68-17, U. S. Army Aviation Materiel Laboratories, Fort Eustis, Virginia, April 1968, AD 671670.

6. Milne-Thomson, L. M., THEORETICAL HYDRODYNAMICS, Fourth Edition, New York, The Macmillan Company, 1965.

7. Crimi, Peter, THEORETICAL PREDICTION OF THE FLOW IN THE WAKE OF A HELICOPTER ROTOR, PART I, DEVELOPMENT OF THEORY AND RESULTS OF COMPUTATIONS, CAL No. BB-1994-S-1, Cornell Aeronautical Laboratory, Inc., Buffalo, New York, September 1965.

8. Boatwright, D. W., SOME EFFECTS OF INTERFERENCE OF THREE-DIMENSIONAL BODIES ON THE WAKE GEOMETRY OF A HOVERING ROTOR, Mississippi State University, State College, Mississippi, AIAA Paper No. 69-228, February 1969.

9. McCormick, Barnes W., Tangler, James L., and Sherrieb, H.E., STRUCTURE OF TRAILING VORTICES, Journal of Aircraft, Vol. 5, No. 3, May-June 1968, pp 260-267.

10. Newman, B. G., FLOW IN A VISCOUS TRAILING VORTEX, The Aeronautical Quarterly, Vol. 10, May 1959, pp. 149-162.

11. Dosanjh, D. S., Gasparek, E. P., and Eskinazi, S., DECAY OF A VISCOUS VORTEX, The Aeronautical Quarterly, Vol. 13, May 1962, pp. 167-188.

12. Bergman, K. H., ON THE DYNAMIC STABILITY OF CONVECTIVE ATMOSPHERIC VORTICES, Ph.D. Thesis, Department of Atmospheric Sciences, University of Washington, 1969.

13. Olsen, John H., RESULTS OF TRAILING VORTEX STUDIES IN A TOWING TANK, Document D1-82-1004, Boeing Scientific Research Laboratories, September 1970.

APPENDIX

DISTRIBUTIONS OF MEAN WAKE VELOCITY COMPONENTS AND STANDARD DEVIATION PARAMETERS COMPUTED FROM EXPERIMENTAL WAKE SURVEY DATA, OH-13E ROTOR, HOVER CONDITION

TEST CONDITION 1, $z/R = -0.10$
$\Omega R = 631$ ft/sec, $\theta_{75} = 6.25$ deg, $C_T = 0.0021$

x/R	ψ, deg	$\bar{v}_R/v_o$	$\bar{v}_x/v_o$	$\bar{v}_y/v_o$	$\bar{v}_z/v_o$	σ_{v_R/v_o}	σ_ϵ, deg
0.3	0	1.161	-.028	.410	-1.086	.121	3.7
0.3	45	1.161	.211	.269	-1.109	.037	3.4
0.3	90	1.073	.174	.212	-1.038	.032	3.3
0.3	135	.972	.122	.231	-.937	.042	3.6
0.4	0	1.359	.077	.411	-1.293	.031	2.8
0.4	45	1.336	-.014	.293	-1.303	.019	2.6
0.4	90	1.281	-.056	.283	-1.248	.029	2.6
0.4	135	1.145	-.139	.292	-1.098	.035	2.9
0.5	0	1.515	.029	.401	-1.460	.044	2.7
0.5	45	1.535	-.040	.255	-1.513	.025	2.6
0.5	90	1.505	-.085	.232	-1.484	.024	2.6
0.5	135	1.518	-.024	.624	-1.383	.106	8.7
0.6	0	1.694	-.079	.396	-1.646	.041	2.8
0.6	45	1.734	-.163	.238	-1.709	.040	2.6
0.6	90	1.672	-.206	.226	-1.644	.031	4.6
0.6	135	1.660	-.077	.306	-1.630	.071	3.5
0.7	0	1.927	-.209	.412	-1.871	.041	2.6
0.7	45	1.945	-.299	.200	-1.912	.044	2.6
0.7	90	1.897	-.328	.186	-1.860	.036	2.6
0.7	135	1.843	-.226	.229	-1.815	.044	2.6
0.75	0	2.071	-.222	.455	-2.008	.050	3.0
0.75	45	2.127	-.304	.226	-2.093	.058	2.6
0.75	90	2.093	-.326	.204	-2.057	.050	3.0
0.75	135	2.082	-.286	.247	-2.047	.042	2.6
0.8	0	2.260	-.297	.445	-2.195	.046	2.6
0.8	45	2.331	-.378	.200	-2.291	051	2.6
0.8	90	2.346	-.349	.195	-2.312	.085	2.8
0.8	135	2.430	-.630	.174	-2.340	.075	8.9
0.83	0	2.444	-.685	.318	-2.325	.101	10.7
0.83	45	2.333	-.518	.079	-2.273	.037	3.2
0.83	90	3.724	-.101	.486	-3.691	.700	6.8
0.83	135	2.500	1.928	.467	-1.522	.133	9.3

x/R	Ψ, deg	$\bar{v}_R/v_o$	$\bar{v}_x/v_o$	$\bar{v}_y/v_o$	$\bar{v}_z/v_o$	σ_{V_R}/v_o	σ_ε, deg
0.85	0	2.422	-1.076	.533	-2.103	.171	17.6
0.85	45	2.129	-.220	.236	-2.105	.092	3.6
0.85	90	3.966	-.547	2.505	-3.026	2.714	50.9
0.85	135	1.946	-1.638	.550	-.895	.167	5.6
0.875	0	2.167	-1.942	.961	-.022	.621	22.0
0.875	45	.930	-.526	.473	-.603	.382	39.1
0.875	90	.527	-.336	.336	.227	.556	49.3
0.875	135	.944	-.852	.384	-.130	.193	21.6
0.88	0	1.604	-1.425	.710	-.196	.285	10.0
0.88	45	.701	-.448	.235	-.485	.229	30.9
0.88	90	.589	-.539	.180	.154	.270	34.1
0.88	135	.850	-.762	.264	-.268	.175	20.1
0.9	0	.873	-.671	.535	.161	.192	19.2
0.9	45	.352	-.246	.218	-.127	.138	36.9
0.9	90	.465	-.396	.243	-.005	.164	33.0
0.9	135	.512	-.408	.234	-.203	.137	27.5
0.925	0	.658	-.390	.462	.258	.201	31.1
0.925	45	.310	-.179	.245	.065	.170	39.0
0.925	90	.401	-.296	.245	.115	.146	29.8
0.925	135	.352	-.283	.208	.023	.136	38.7
0.95	0	.614	-.279	.502	.215	.141	17.2
0.95	45	.325	-.150	.263	.117	.087	29.6
0.95	90	.402	-.266	.269	.136	.106	26.9
0.95	135	.430	-.280	.299	.131	.105	27.5
1.0	0	.420	-.259	.308	.123	.045	11.4
1.0	45	.255	-.112	.080	.215	.037	23.8
1.0	90	.324	-.222	.150	.181	.034	15.7
1.0	135	.379	-.276	.147	.213	.029	11.2
1.1	0	.389	-.250	.278	.109	.024	4.7
1.1	45	.350	-.232	.234	.119	.020	11.9
1.1	90	.383	-.265	.219	.169	.021	9.7
1.1	135	.399	-.275	.238	.163	.023	6.0
1.2	0	.320	-.227	.163	.156	.014	6.7
1.2	45	.315	-.223	.128	.182	.011	6.4
1.2	90	.322	-.231	.129	.183	.014	7.6
1.2	135	.325	-.237	.158	.157	.016	7.5

x/R	Ψ, deg	$\bar{v}_R/v_o$	$\bar{v}_x/v_o$	$\bar{v}_y/v_o$	$\bar{v}_z/v_o$	σ_{v_R}/v_o	σ_ϵ, deg
1.3	0	.294	-.194	.202	.089	.019	12.3
1.3	45	.297	-.194	.205	.092	.024	12.1
1.3	90	.294	-.195	.200	.091	.017	11.3
1.3	135	.303	-.200	.209	.088	.023	10.5
1.4	0	.279	-.162	.224	.039	.024	5.4
1.4	45	.277	-.163	.220	.043	.023	5.6
1.4	90	.276	-.161	.221	.038	.019	5.6
1.4	135	.274	-.164	.217	.035	.023	7.3
1.5	0	.281	-.139	.244	-.003	.016	5.2
1.5	45	.284	-.140	.247	-.003	.013	5.1
1.5	90	.276	-.138	.239	-.000	.018	5.2
1.5	135	.281	-.138	.244	-.003	.015	5.1
TEST CONDITION 2, z/R = -0.10 ΩR = 436 ft/sec, θ_{75} = 10.75 deg, C_T = 0.0039							
0.3	0	1.091	.114	.163	-1.073	.032	2.7
0.3	45	1.138	-.070	.023	-1.136	.042	2.7
0.3	90	1.050	-.156	-.031	-1.038	.033	2.9
0.3	135	.962	-.100	.062	-.955	.109	12.0
0.4	0	1.342	-.049	.283	-1.311	.034	2.8
0.4	45	1.428	-.233	.048	-1.408	.038	3.0
0.4	90	1.364	-.373	-.020	-1.312	.043	2.9
0.4	135	1.346	.100	.100	-1.339	.061	3.3
0.5	0	1.520	-.137	.203	-1.500	.031	2.7
0.5	45	1.632	-.296	.007	-1.605	.037	2.6
0.5	90	1.569	-.394	-.044	-1.518	.040	2.9
0.5	135	1.497	-.079	.034	-1.495	.028	2.7
0.6	0	1.705	-.198	.304	-1.666	.047	2.6
0.6	45	1.830	-.370	.074	-1.790	.041	2.6
0.6	90	1.790	-.401	.015	-1.745	.074	4.2
0.6	135	1.678	-.199	.103	-1.662	.034	2.6
0.7	0	1.941	-.284	.329	-1.892	.053	2.6
0.7	45	2.123	-.444	.057	-2.076	.047	2.6
0.7	90	2.023	-.471	.035	-1.967	.044	2.9
0.7	135	2.010	-.385	.094	-1.970	.049	2.6
0.75	0	2.119	-.306	.638	-1.997	.040	2.8
0.75	45	2.299	-.366	.341	-2.244	.049	2.7
0.75	90	2.353	-.334	.549	-2.263	.169	6.2
0.75	135	2.232	-.472	.322	-2.158	.053	2.8

x/R	Ψ, deg	$\bar{V}_R/v_o$	$\bar{v}_x/v_o$	$\bar{v}_y/v_o$	$\bar{v}_z/v_o$	σ_{V_R}/v_o	σ_ϵ, deg
0.775	0	2.182	-.372	.701	-2.032	.070	4.1
0.775	45	2.438	-.361	.442	-2.371	.063	3.9
0.775	90	3.003	-.340	.511	-2.940	.129	3.4
0.775	135	2.268	-1.028	.611	-1.926	.189	18.0
0.8	0	2.010	-.515	.231	-1.929	.042	4.0
0.8	45	2.371	-.159	.147	-2.361	.068	2.6
0.8	90	3.955	-1.454	.235	-3.671	.106	6.0
0.8	135	1.757	-1.390	.333	-1.021	.067	9.6
0.825	0	1.743	-.982	.862	-1.154	.195	18.1
0.825	45	2.044	.686	.435	-1.876	.198	19.5
0.825	90	3.047	-2.802	.942	-.739	.417	7.1
0.825	135	1.448	-1.102	.578	-.740	.105	9.9
0.85	0	1.350	-.652	.959	-.690	.126	15.4
0.85	45	1.090	.724	.644	-.500	.196	9.6
0.85	90	1.360	-1.169	.654	.233	.227	8.9
0.85	135	1.040	-.677	.664	-.428	.129	16.3
0.875	0	.823	-.304	.749	-.156	.179	20.0
0.875	45	.442	.075	.420	-.115	.204	34.6
0.875	90	.631	-.368	.512	.027	.183	23.0
0.875	135	.600	-.302	.488	-.177	.104	23.0
0.9	0	.718	-.299	.648	.075	.136	12.2
0.9	45	.364	.004	.363	-.016	.114	27.2
0.9	90	.473	-.247	.403	.017	.095	20.5
0.9	135	.448	-.182	.398	-.097	.094	22.0
0.925	0	.679	-.233	.588	.249	.046	5.9
0.925	45	.355	-.040	.338	.102	.052	11.3
0.925	90	.413	-.188	.347	.123	.048	9.5
0.925	135	.439	-.224	.359	.117	.040	8.6
1.0	0	.480	-.289	.370	.104	.055	9.0
1.0	45	.271	-.106	.106	.226	.037	23.2
1.0	90	.352	-.248	.132	.211	.028	20.1
1.0	135	.435	-.306	.165	.261	.023	8.3
1.1	0	.460	-.303	.312	.150	.020	4.2
1.1	45	.363	-.256	.121	.227	.036	21.7
1.1	90	.427	-.300	.211	.218	.023	7.4
1.1	135	.462	-.322	.251	.216	.022	4.2

x/R	Ψ, deg	$\bar{v}_R/v_o$	$\bar{v}_x/v_o$	$\bar{v}_y/v_o$	$\bar{v}_z/v_o$	σ_{v_R}/v_o	σ_ε, deg
1.2	0	.450	-.257	.364	.057	.017	3.1
1.2	45	.425	-.255	.331	.078	.021	3.2
1.2	90	.438	-.265	.339	.084	.016	3.1
1.2	135	.437	-.280	.312	.122	.014	3.5
1.3	0	.419	-.228	.351	.031	.018	3.1
1.3	45	.404	-.221	.336	.033	.014	2.7
1.3	90	.409	-.231	.334	.047	.014	3.3
1.3	135	.403	-.236	.320	.062	.015	3.9
1.4	0	.402	-.195	.351	-.009	.019	2.7
1.4	45	.401	-.198	.348	-.004	.021	2.6
1.4	90	.399	-.200	.345	.001	.020	2.7
1.4	135	.395	-.202	.340	.007	.018	2.7
1.5	0	.387	-.186	.339	-.012	.018	2.7
1.5	45	.382	-.189	.332	-.003	.013	2.6
1.5	90	.374	-.186	.325	-.002	.017	2.7
1.5	135	.383	-.187	.334	-.007	.012	2.7
TEST CONDITION 3, z/R = -0.10 ΩR = 454 ft/sec, θ_{75} = 6.25 deg, C_T = 0.0020							
0.3	0	1.094	-.047	.513	-.966	.074	8.0
0.3	45	1.171	.132	.424	-1.084	.037	3.0
0.3	90	1.109	.107	.400	-1.029	.033	3.3
0.3	135	1.051	.043	.443	-.952	.043	3.4
0.4	0	1.487	.084	.613	-1.352	.070	3.3
0.4	45	1.426	-.025	.468	-1.347	.053	2.8
0.4	90	1.346	-.087	.455	-1.264	.041	3.0
0.4	135	1.245	-.142	.479	-1.141	.061	4.8
0.5	0	1.670	-.065	.681	-1.524	.054	2.9
0.5	45	1.648	-.175	.519	-1.555	.049	2.9
0.5	90	1.588	-.240	.510	-1.485	.052	2.8
0.5	135	1.629	-.022	.937	-1.332	.120	12.7
0.6	0	1.821	-.066	.706	-1.677	.032	2.6
0.6	45	1.841	-.137	.522	-1.760	.022	2.6
0.6	90	1.791	-.191	.507	-1.707	.041	2.7
0.6	135	1.809	-.029	.682	-1.675	.072	6.3

x/R	Ψ, deg	$\bar{v}_R/v_o$	$\bar{v}_x/v_o$	$\bar{v}_y/v_o$	$\bar{v}_z/v_o$	σ_{v_R}/v_o	σ_ε, deg
0.7	0	2.044	-.206	.671	-1.919	.040	2.8
0.7	45	2.045	-.270	.457	-1.975	.067	2.8
0.7	90	2.021	-.272	.470	-1.946	.043	2.7
0.7	135	1.996	-.231	.533	-1.910	.076	2.6
0.75	0	2.124	-.346	.521	-2.030	.077	8.6
0.75	45	2.203	-.365	.281	-2.154	.063	3.3
0.75	90	2.161	-.377	.293	-2.107	.053	3.6
0.75	135	2.192	-.380	.293	-2.139	.048	3.5
0.8	0	2.274	-.330	.396	-2.214	.153	3.1
0.8	45	2.388	-.481	.191	-2.332	.144	3.2
0.8	90	2.250	-.406	.184	-2.205	.073	3.9
0.8	135	2.528	-.647	.609	-2.366	.204	13.7
0.85	0	3.602	-.815	1.526	-3.159	1.510	23.8
0.85	45	2.381	-1.669	.516	-1.617	.548	28.1
0.85	90	.971	-.022	.789	-.566	1.119	54.0
0.85	135	1.110	-.937	.561	.198	.693	43.0
0.875	0	.922	.248	.649	.607	.559	48.6
0.875	45	.755	-.438	.402	.465	.577	43.5
0.875	90	.855	-.707	.399	.266	.426	30.2
0.875	135	.851	-.750	.342	.213	.341	23.8
0.9	0	.687	.008	.541	.423	.131	26.5
0.9	45	.521	-.127	.397	.313	.176	31.5
0.9	90	.560	-.297	.342	.328	.184	30.4
0.9	135	.656	-.413	.437	.264	.166	15.3
0.92	0	.633	-.050	.531	.341	.102	16.6
0.92	45	.444	-.060	.361	.251	.091	19.9
0.92	90	.506	-.185	.364	.299	.102	22.4
0.92	135	.535	-.269	.388	.252	.116	23.5
0.95	0	.629	-.123	.520	.332	.056	8.3
0.95	45	.407	-.048	.311	.259	.053	13.9
0.95	90	.464	-.126	.324	.296	.060	11.0
0.95	135	.507	-.258	.385	.206	.062	13.7
1.0	0	.696	-.158	.563	.384	.044	10.1
1.0	45	.579	-.036	.426	.390	.046	9.9
1.0	90	.603	-.144	.434	.392	.057	13.1
1.0	135	.634	-.274	.470	.325	.066	14.2

x/R	Ψ, deg	$\bar{v}_R/v_o$	$\bar{v}_x/v_o$	$\bar{v}_y/v_o$	$\bar{v}_z/v_o$	σ_{v_R/v_o}	σ_ϵ, deg
1.1	0	.553	-.291	.436	.177	.054	12.6
1.1	45	.540	-.258	.419	.221	.059	14.4
1.1	90	.571	-.312	.442	.183	.051	11.8
1.1	135	.580	-.334	.449	.153	.060	9.9
1.2	0	.517	-.265	.422	.137	.073	15.6
1.2	45	.515	-.282	.406	.142	.037	15.9
1.2	90	.519	-.281	.423	.108	.037	13.8
1.2	135	.523	-.277	.435	.087	.036	13.1
1.3	0	.469	-.233	.403	.056	.048	10.1
1.3	45	.470	-.232	.404	.064	.050	10.4
1.3	90	.460	-.225	.397	.051	.051	10.6
1.3	135	.454	-.218	.396	.039	.062	11.9
1.4	0	.395	-.188	.345	.038	.046	11.1
1.4	45	.402	-.194	.349	.050	.048	11.2
1.4	90	.395	-.195	.342	.035	.045	11.3
1.4	135	.389	-.188	.339	.025	.048	10.7
1.5	0	.408	-.177	.367	.026	.034	11.2
1.5	45	.423	-.195	.374	.029	.040	11.0
1.5	90	.425	-.189	.380	.020	.038	10.9
1.5	135	.411	-.180	.368	.023	.035	11.6

TEST CONDITION 1, $z/R = -0.30$
$\Omega R = 634$ ft/sec, $\theta_{75} = 6.25$ deg, $C_T = 0.0020$

0.3	0	1.215	-.176	-.079	-1.199	.080	6.4
0.3	45	1.237	-.186	-.214	-1.204	.041	3.3
0.3	90	1.181	-.227	-.254	-1.131	.046	3.2
0.3	135	1.122	-.240	-.251	-1.067	.050	3.4
0.4	0	1.502	-.269	-.211	-1.463	.034	2.6
0.4	45	1.467	-.326	-.102	-1.427	.089	6.6
0.4	90	1.565	-.157	-.199	-1.544	.050	2.8
0.4	135	1.513	-.176	-.209	-1.488	.045	2.6
0.5	0	1.675	-.294	-.239	-1.632	.036	2.8
0.5	45	1.735	-.204	-.165	-1.715	.081	3.2
0.5	90	1.707	-.242	-.267	-1.669	.044	2.7
0.5	135	1.665	-.285	-.267	-1.618	.032	2.8

x/R	Ψ, deg	$\bar{v}_R/v_o$	$\bar{v}_x/v_o$	$\bar{v}_y/v_o$	$\bar{v}_z/v_o$	σ_{V_R/v_o}	σ_ε, deg
0.6	0	1.943	-.267	-.147	-1.919	.059	2.8
0.6	45	1.978	-.323	-.235	-1.938	.066	2.6
0.6	90	1.942	-.366	-.249	-1.891	.071	2.6
0.6	135	1.924	-.391	-.245	-1.867	.072	3.1
0.7	0	2.016	-.230	-.077	-2.002	.410	5.8
0.7	45	2.105	-.321	-.125	-2.077	.431	7.8
0.7	90	2.002	-.453	-.128	-1.946	.365	12.4
0.7	135	1.855	-.381	-.001	-1.815	.277	12.1
0.8	0	1.641	-.456	-.121	-1.572	.738	41.3
0.8	45	1.896	-.595	-.448	-1.743	.483	19.2
0.8	90	1.930	-.696	-.172	-1.792	.531	22.6
0.8	135	1.765	-.323	-.103	-1.732	.391	21.9
0.825	0	1.261	-.403	.014	-1.194	.930	48.2
0.825	45	1.388	-.681	-.015	-1.210	.666	34.1
0.825	90	1.530	-.698	-.164	-1.351	.733	35.1
0.825	135	1.408	-.649	-.035	-1.249	.497	32.1
0.850	0	.245	.172	-.172	-.028	.587	59.5
0.850	45	.265	-.098	-.246	-.011	.570	65.7
0.850	90	.360	-.232	-.275	-.020	.400	54.7
0.850	135	.477	-.333	-.203	-.274	.362	49.0
0.9	0	.330	-.085	-.278	.156	.307	46.9
0.9	45	.380	-.115	-.344	.111	.322	51.2
0.9	90	.354	-.196	-.294	-.023	.259	50.6
0.9	135	.282	-.106	-.226	-.131	.281	54.3
1.0	0	.423	-.003	-.383	.181	.059	16.7
1.0	45	.450	.030	-.418	.162	.068	16.2
1.0	90	.455	-.014	-.422	.170	.077	17.8
1.0	135	.456	.001	-.422	.173	.054	18.5
1.1	0	.326	-.167	-.215	.179	.035	18.4
1.1	45	.325	-.146	-.248	.150	.051	21.4
1.1	90	.343	-.171	-.245	.167	.042	15.6
1.1	135	.356	-.193	-.236	.182	.033	15.6
1.2	0	.333	-.111	-.299	.095	.038	19.5
1.2	45	.332	-.085	-.308	.089	.046	20.3
1.2	90	.340	-.104	-.312	.088	.043	20.0
1.2	135	.336	-.112	-.302	.098	.044	20.3

x/R	Ψ, deg	$\bar{V}_R/v_o$	$\bar{v}_x/v_o$	$\bar{v}_y/v_o$	$\bar{v}_z/v_o$	σ_{V_R/v_o}	σ_ϵ, deg
1.3	0	.308	-.185	-.241	.048	.018	13.7
1.3	45	.302	-.168	-.244	.058	.022	16.7
1.3	90	.315	-.188	-.249	.047	.020	13.3
1.3	135	.308	-.189	-.239	.045	.025	14.6
1.4	0	.254	-.097	-.224	-.070	.144	36.9
1.4	45	.251	-.089	-.223	-.073	.163	37.9
1.4	90	.263	-.091	-.232	-.083	.178	37.6
1.4	135	.262	-.093	-.225	-.095	.197	37.9
1.5	0	.282	-.111	-.258	-.026	.116	26.7
1.5	45	.282	-.107	-.259	-.030	.133	26.7
1.5	90	.288	-.117	-.261	-.034	.157	27.6
1.5	135	.287	-.119	-.258	-.039	.188	27.9
TEST CONDITION 2, $z/R = -0.30$							
$\Omega R = 429$ ft/sec, $\theta_{75} = 10.75$ deg, $C_T = 0.0040$							
0.3	0	.724	-.055	.313	-.651	.266	29.5
0.3	45	.704	-.058	.179	-.678	.264	33.9
0.3	90	.713	-.015	.134	-.700	.278	31.3
0.3	135	.678	.020	.222	-.640	.280	34.8
0.4	0	1.168	.003	.032	-1.168	.129	6.3
0.4	45	1.396	.089	-.002	-1.393	.071	6.3
0.4	90	1.262	.038	-.133	-1.255	.058	4.2
0.4	135	1.144	-.026	-.136	-1.136	.044	4.4
0.5	0	1.681	-.028	-.018	-1.681	.022	2.6
0.5	45	1.673	-.128	-.086	-1.666	.036	2.7
0.5	90	1.623	-.167	-.118	-1.610	.065	3.7
0.5	135	1.657	.081	-.067	-1.653	.031	2.6
0.6	0	1.786	-.007	-.076	-1.785	.032	2.6
0.6	45	1.773	-.115	-.157	-1.763	.025	2.6
0.6	90	1.816	.086	.094	-1.811	.088	4.3
0.6	135	1.785	.123	-.119	-1.777	.030	2.6
0.7	0	1.970	-.065	-.141	-1.964	.047	2.6
0.7	45	2.033	-.100	-.217	-2.019	.053	2.7
0.7	90	2.065	.101	-.170	-2.056	.044	2.6
0.7	135	1.978	.036	-.160	-1.971	.044	2.7

x/R	Ψ, deg	$\bar{v}_R/v_o$	$\bar{v}_x/v_o$	$\bar{v}_y/v_o$	$\bar{v}_z/v_o$	σ_{v_R}/v_o	σ_ε, deg
0.8	0	1.985	-.119	-.184	-1.973	.113	4.4
0.8	45	2.326	.197	-.145	-2.313	.102	2.7
0.8	90	2.292	.038	-.164	-2.286	.050	2.6
0.8	135	2.123	-.022	-.181	-2.115	.035	2.7
0.85	0	1.629	.149	-.211	-1.608	.228	11.3
0.85	45	2.026	.741	-.354	-1.852	.287	9.6
0.85	90	3.261	.293	-.112	-3.246	.599	13.7
0.85	135	2.228	-.603	-.270	-2.127	.342	14.8
0.875	0	1.070	.195	-.338	-.996	.286	25.7
0.875	45	1.475	.982	-.262	-1.069	.215	17.2
0.875	90	2.041	1.862	.760	.349	3.149	45.2
0.875	135	1.829	-1.460	-.342	-1.048	.565	21.5
0.9	0	.586	.067	-.423	-.400	.115	14.4
0.9	45	.613	.420	-.430	-.123	.212	27.0
0.9	90	.573	.090	-.483	.296	.207	36.3
0.9	135	.641	-.434	-.454	.124	.188	31.4
1.0	0	.374	.024	-.366	-.075	.125	20.6
1.0	45	.448	.141	-.424	-.035	.144	19.5
1.0	90	.456	.120	-.438	.039	.159	23.6
1.0	135	.411	.005	-.407	.057	.228	31.8
1.1	0	.359	-.035	-.357	.013	.049	16.5
1.1	45	.396	.018	-.394	.024	.045	13.8
1.1	90	.402	.010	-.400	.034	.049	14.6
1.1	135	.399	-.022	-.396	.040	.051	15.4
1.2	0	.389	-.023	-.383	-.061	.052	6.8
1.2	45	.403	-.003	-.400	-.047	.048	7.4
1.2	90	.404	-.006	-.401	-.043	.049	7.5
1.2	135	.394	-.032	-.390	-.047	.055	10.6
1.3	0	.358	.006	-.357	-.019	.025	10.3
1.3	45	.373	.021	-.372	-.010	.029	8.3
1.3	90	.377	.009	-.376	-.016	.026	8.1
1.3	135	.373	-.009	-.372	-.027	.034	6.6
1.4	0	.313	-.058	-.300	-.067	.065	20.8
1.4	45	.322	-.050	-.312	-.063	.060	20.1
1.4	90	.336	-.051	-.325	-.068	.066	19.0
1.4	135	.337	-.060	-.324	-.069	.073	19.4

x/R	Ψ, deg	$\bar{v}_R/v_o$	$\bar{v}_x/v_o$	$\bar{v}_y/v_o$	$\bar{v}_z/v_o$	σ_{v_R/v_o}	σ_ε, deg
1.5	0	.331	.008	-.327	-.054	.064	12.1
1.5	45	.335	.010	-.332	-.042	.068	14.1
1.5	90	.336	.007	-.332	-.054	.058	14.9
1.5	135	.333	.002	-.329	-.056	.064	14.2
TEST CONDITION 3, z/R = -0.30 ΩR = 450 ft/sec, θ_{75} = 6.25 deg, C_T = 0.0018							
0.3	0	1.118	-.025	-.024	-1.118	.112	9.7
0.3	45	1.252	.066	.122	-1.244	.177	11.0
0.3	90	1.223	.083	.111	-1.215	.134	13.9
0.3	135	1.145	.053	.024	-1.143	.131	13.1
0.4	0	1.585	.123	-.266	-1.557	.092	2.8
0.4	45	1.537	.038	-.311	-1.505	.051	3.0
0.4	90	1.469	.019	-.329	-1.432	.079	3.9
0.4	135	1.516	.191	-.135	-1.498	.112	5.7
0.5	0	1.806	-.065	-.222	-1.791	.057	4.1
0.5	45	1.781	-.026	-.019	-1.780	.091	5.1
0.5	90	1.864	.039	-.286	-1.842	.070	3.0
0.5	135	1.805	.005	-.287	-1.782	.064	3.1
0.6	0	1.983	.036	-.027	-1.983	.103	6.7
0.6	45	2.112	.140	-.295	-2.087	.058	3.1
0.6	90	2.048	.069	-.327	-2.020	.076	3.7
0.6	135	1.986	.003	-.339	-1.956	.076	4.1
0.7	0	2.264	-.100	.402	-2.225	.200	4.8
0.7	45	2.307	-.176	.376	-2.269	.224	6.3
0.7	90	2.251	-.218	.381	-2.208	.217	5.9
0.7	135	2.236	-.261	.466	-2.171	.212	5.7
0.75	0	2.605	-.115	.393	-2.572	.487	4.5
0.75	45	2.413	-.431	.396	-2.341	.281	14.5
0.75	90	2.253	-.277	.239	-2.223	.128	6.7
0.75	135	2.088	-.299	.369	-2.033	.128	14.8
0.8	0	2.465	-.107	.186	-2.455	.267	11.0
0.8	45	2.381	-.314	-.033	-2.360	.338	14.2
0.8	90	2.278	-.356	-.138	-2.246	.227	13.4
0.8	135	2.093	-.277	.024	-2.074	.290	14.7

x/R	ψ, deg	$\bar{v}_R/v_o$	$\bar{v}_x/v_o$	$\bar{v}_y/v_o$	$\bar{v}_z/v_o$	σ_{V_R/v_o}	σ_ε, deg
0.825	0	1.642	.053	1.095	-1.222	.367	27.0
0.825	45	1.759	.185	.770	-1.571	.498	26.5
0.825	90	1.814	.244	1.090	-1.429	.463	29.2
0.825	135	1.501	-.037	.553	-1.395	.564	36.9
0.85	0	.562	.218	.248	-.455	.951	57.5
0.85	45	.649	.064	.251	-.594	.965	63.0
0.85	90	.591	-.307	.259	-.434	.861	52.3
0.85	135	.890	-.594	.207	-.629	.677	50.4
0.9	0	.174	-.140	.098	.029	.935	68.8
0.9	45	.461	-.241	-.075	-.386	.770	58.4
0.9	90	.850	-.380	.026	-.760	.826	48.7
0.9	135	1.053	-.321	-.120	-.995	.578	34.2
1.0	0	.220	-.011	-.220	.013	.367	57.9
1.0	45	.236	-.025	-.234	-.018	.399	56.0
1.0	90	.247	-.073	-.226	-.071	.428	52.3
1.0	135	.276	-.099	-.216	-.140	.464	54.4
1.1	0	.228	-.148	-.161	.066	.036	25.9
1.1	45	.236	-.131	-.193	.036	.034	24.2
1.1	90	.249	-.150	-.187	.067	.037	25.9
1.1	135	.268	-.188	-.166	.096	.033	19.5
1.2	0	.178	.024	-.032	.157	.073	43.6
1.2	45	.184	.031	-.096	.154	.075	44.4
1.2	90	.199	.032	-.110	.162	.071	38.3
1.2	135	.200	.021	-.118	.160	.073	38.2
1.3	0	.211	-.188	-.014	.093	.035	23.4
1.3	45	.200	-.175	-.024	.094	.036	25.4
1.3	90	.208	-.180	-.016	.103	.039	25.8
1.3	135	.211	-.188	-.014	.095	.034	23.3
1.4	0	.225	-.156	.098	.128	.022	13.1
1.4	45	.221	-.153	.090	.132	.022	13.4
1.4	90	.227	-.162	.096	.127	.022	9.9
1.4	135	.227	-.161	.103	.122	.020	10.7
1.5	0	.266	-.156	.173	.130	.033	19.7
1.5	45	.262	-.158	.159	.137	.039	22.3
1.5	90	.265	-.159	.173	.123	.035	17.6
1.5	135	.269	-.161	.182	.114	.036	16.4

TEST CONDITION 1, $z/R = -0.50$
$\Omega R = 634$ ft/sec, $\theta_{75} = 6.25$ deg, $C_T = 0.0020$

x/R	Ψ, deg	$\bar{V}_R/v_o$	$\bar{v}_x/v_o$	$\bar{v}_y/v_o$	$\bar{v}_z/v_o$	σ_{V_R/v_o}	σ_ε, deg
0.3	0	1.330	-.058	.486	-1.236	.044	3.5
0.3	45	1.477	.006	.430	-1.413	.062	3.5
0.3	90	1.443	-.043	.401	-1.385	.044	2.6
0.3	135	1.401	-.062	.423	-1.334	.044	2.6
0.4	0	1.594	-.087	.327	-1.558	.143	5.3
0.4	45	1.570	-.119	.306	-1.535	.112	5.2
0.4	90	1.581	-.084	.541	-1.483	.126	7.1
0.4	135	1.626	-.040	.351	-1.587	.094	4.8
0.5	0	1.745	-.194	.373	-1.694	.066	3.9
0.5	45	1.908	-.098	.385	-1.866	.058	3.4
0.5	90	1.820	-.119	.320	-1.788	.041	2.6
0.5	135	1.765	-.141	.321	-1.730	.038	2.6
0.6	0	2.044	-.166	.356	-2.006	.163	6.0
0.6	45	2.009	-.235	.219	-1.983	.107	6.5
0.6	90	1.962	-.187	.201	-1.943	.080	3.8
0.6	135	1.946	-.164	.319	-1.912	.089	5.8
0.7	0	1.927	-.251	.360	-1.876	.305	18.6
0.7	45	1.872	-.332	.229	-1.828	.307	19.6
0.7	90	1.819	-.355	.222	-1.769	.292	22.1
0.7	135	1.821	-.141	.272	-1.795	.226	16.2
0.75	0	1.673	-.409	.340	-1.586	.297	27.7
0.75	45	1.627	-.361	.239	-1.569	.262	26.5
0.75	90	1.610	-.131	.205	-1.592	.227	24.8
0.75	135	1.614	.151	.182	-1.596	.246	23.1
0.775	0	1.461	-.208	.384	-1.395	.530	32.6
0.775	45	1.402	-.299	.390	-1.313	.510	36.4
0.775	90	1.306	-.246	.242	-1.260	.404	38.7
0.775	135	1.356	-.181	.117	-1.338	.383	30.2
0.8	0	.637	-.053	.590	-.234	.383	41.5
0.8	45	.747	-.151	.605	-.411	.398	41.3
0.8	90	.629	-.078	.478	-.401	.406	51.6
0.8	135	.678	.150	.467	-.468	.456	44.7
0.9	0	.286	-.144	.205	.138	.101	32.7
0.9	45	.237	-.120	.171	.112	.104	33.7
0.9	90	.260	-.122	.183	.137	.110	38.4
0.9	135	.257	-.110	.176	.146	.128	39.0

x/R	ψ, deg	$\bar{v}_R/v_o$	$\bar{v}_x/v_o$	$\bar{v}_y/v_o$	$\bar{v}_z/v_o$	σ_{v_R/v_o}	σ_ϵ, deg
1.0	0	.351	-.065	.297	.176	.047	11.3
1.0	45	.334	-.059	.285	.164	.043	13.0
1.0	90	.334	-.062	.276	.177	.035	13.7
1.0	135	.352	-.068	.282	.200	.036	12.8
1.1	0	.273	-.148	.208	.096	.029	14.7
1.1	45	.261	-.149	.195	.088	.027	17.2
1.1	90	.267	-.154	.199	.088	.028	14.3
1.1	135	.279	-.166	.202	.096	.031	16.0
1.2	0	.268	-.129	.210	.106	.015	11.9
1.2	45	.258	-.117	.202	.109	.014	10.2
1.2	90	.262	-.129	.203	.103	.015	12.1
1.2	135	.267	-.138	.206	.099	.017	12.0
1.3	0	.275	-.149	.230	.020	.020	6.1
1.3	45	.260	-.141	.217	.020	.017	6.4
1.3	90	.269	-.149	.223	.025	.019	6.8
1.3	135	.267	-.152	.217	.030	.019	8.2
1.4	0	.234	-.121	.183	.081	.056	22.9
1.4	45	.231	-.109	.181	.092	.048	20.2
1.4	90	.239	-.117	.187	.091	.052	20.1
1.4	135	.238	-.122	.182	.092	.045	18.3
1.5	0	.291	-.173	.233	.025	.015	7.0
1.5	45	.292	-.173	.234	.023	.020	8.0
1.5	90	.287	-.173	.227	.030	.016	7.2
1.5	135	.295	-.181	.232	.029	.016	7.0

TEST CONDITION 2, z/R = -0.50
ΩR = 429 ft/sec, θ_{75} = 10.75 deg, C_T = 0.0040

0.3	0	1.319	.023	.386	-1.261	.169	6.1
0.3	45	1.412	.022	.400	-1.354	.155	5.3
0.3	90	1.358	.015	.318	-1.320	.109	5.4
0.3	135	1.299	.016	.321	-1.259	.052	5.7
0.4	0	1.655	-.043	.333	-1.621	.039	3.2
0.4	45	1.637	-.098	.292	-1.608	.032	3.0
0.4	90	1.615	-.084	.292	-1.586	.068	3.5
0.4	135	1.716	-.044	.326	-1.684	.040	2.7
0.5	0	1.826	-.097	.256	-1.806	.040	2.8
0.5	45	1.947	-.024	.492	-1.884	.094	3.4
0.5	90	1.945	-.058	.250	-1.928	.044	2.6
0.5	135	1.885	-.145	.214	-1.867	.061	2.7

x/R	ψ, deg	$\bar{v}_R/v_o$	$\bar{v}_x/v_o$	$\bar{v}_y/v_o$	$\bar{v}_z/v_o$	σ_{V_R/v_o}	σ_ϵ, deg
0.6	0	2.106	.008	.342	-2.078	.096	4.2
0.6	45	2.299	-.009	.187	-2.291	.141	2.7
0.6	90	2.244	-.242	.043	-2.230	.090	5.1
0.6	135	2.159	-.320	.013	-2.135	.053	5.1
0.7	0	1.850	.235	.171	-1.827	.149	4.5
0.7	45	2.107	.651	.136	-1.999	.322	12.5
0.7	90	2.402	-.897	1.272	-1.830	.806	34.2
0.7	135	2.145	-.938	.404	-1.886	.373	23.0
0.8	0	1.276	.896	.545	-.726	.668	39.4
0.8	45	1.025	.471	.719	-.558	.848	45.1
0.8	90	.686	-.005	.686	-.032	.653	52.8
0.8	135	.700	-.281	.620	-.165	.587	49.1
0.9	0	.141	.074	.094	.074	.300	61.6
0.9	45	.083	.013	.002	.082	.401	61.1
0.9	90	.185	-.134	.101	.079	.395	50.4
0.9	135	.225	-.156	.132	.094	.276	51.1
1.0	0	.206	-.160	.062	.114	.035	19.4
1.0	45	.192	-.142	.052	.118	.036	22.5
1.0	90	.200	-.156	.054	.114	.035	21.6
1.0	135	.194	-.152	.042	.114	.090	24.5
1.1	0	.225	-.175	.086	.113	.028	12.3
1.1	45	.203	-.159	.075	.101	.028	12.8
1.1	90	.210	-.172	.074	.096	.025	12.6
1.1	135	.225	-.188	.067	.104	.029	11.9
1.2	0	.234	-.217	.049	.072	.026	9.7
1.2	45	.220	-.207	.043	.059	.029	10.5
1.2	90	.224	-.213	.037	.057	.028	10.8
1.2	135	.239	-.231	.033	.050	.025	10.4
1.3	0	.260	-.200	.143	.084	.016	11.5
1.3	45	.257	-.185	.162	.073	.018	7.4
1.3	90	.262	-.198	.150	.084	.026	10.2
1.3	135	.255	-.202	.116	.105	.025	15.6
1.4	0	.255	-.234	.038	.094	.019	12.1
1.4	45	.249	-.225	.030	.102	.017	11.4
1.4	90	.260	-.241	.052	.083	.015	10.6
1.4	135	.263	-.248	.035	.082	.018	6.2

x/R	Ψ, deg	$\bar{v}_R/v_o$	$\bar{v}_x/v_o$	$\bar{v}_y/v_o$	$\bar{v}_z/v_o$	σ_{V_R}/v_o	σ_ϵ, deg
1.5	0	.247	-.208	.122	.053	.026	15.0
1.5	45	.245	-.205	.125	.052	.018	12.9
1.5	90	.257	-.212	.136	.050	.021	11.4
1.5	135	.257	-.219	.127	.050	.024	11.0
TEST CONDITION 3, z/R = -0.50							
ΩR = 450 ft/sec, θ_{75} = 6.25 deg, C_T = 0.0020							
0.3	0	1.705	-.101	.462	-1.638	.051	3.0
0.3	45	1.685	-.137	.438	-1.621	.061	3.2
0.3	90	1.607	-.161	.412	-1.544	.073	3.6
0.3	135	1.643	-.043	.539	-1.551	.110	6.0
0.4	0	1.802	-.204	.354	-1.755	.095	4.5
0.4	45	1.742	-.199	.390	-1.686	.087	4.8
0.4	90	1.811	-.076	.478	-1.745	.132	4.4
0.4	135	1.826	-.124	.323	-1.793	.059	3.8
0.5	0	2.073	-.123	.527	-2.001	.140	5.1
0.5	45	2.068	-.165	.294	-2.040	.087	3.5
0.5	90	2.058	-.187	.283	-2.030	.100	3.4
0.5	135	2.050	-.225	.286	-2.017	.071	3.5
0.6	0	1.689	-.052	.701	-1.536	.361	21.8
0.6	45	1.832	-.053	.570	-1.740	.229	21.7
0.6	90	1.815	.098	.477	-1.748	.308	20.5
0.6	135	1.776	-.544	.545	-1.601	.426	27.1
0.7	0	.430	-.047	.378	-.199	.302	38.6
0.7	45	.357	.002	.308	-.180	.318	46.9
0.7	90	.379	-.026	.339	-.168	.339	44.8
0.7	135	.370	-.031	.328	-.168	.314	48.1
0.8	0	.331	-.147	.295	.033	.041	12.2
0.8	45	.317	-.142	.284	.017	.047	12.1
0.8	90	.313	-.129	.282	.041	.041	13.0
0.8	135	.309	-.125	.278	.051	.035	13.4
0.9	0	.320	-.183	.259	.041	.024	5.0
0.9	45	.297	-.168	.242	.035	.021	5.0
0.9	90	.296	-.172	.237	.045	.026	5.3
0.9	135	.298	-.176	.234	.055	.019	6.4

x/R	Ψ, deg	$\ddot{V}_R/v_o$	$\bar{v}_x/v_o$	$\bar{v}_y/v_o$	$\bar{v}_z/v_o$	σ_{V_R}/v_o	σ_ε, deg
1.0	0	.239	-.167	.163	.050	.171	20.4
1.0	45	.213	-.153	.142	.041	.224	22.6
1.0	90	.204	-.151	.131	.040	.249	23.7
1.0	135	.198	-.152	.120	.040	.310	27.9
1.1	0	.322	-.233	.152	.162	.026	8.7
1.1	45	.298	-.216	.135	.156	.022	9.8
1.1	90	.302	-.214	.132	.167	.029	8.5
1.1	135	.309	-.220	.143	.162	.028	7.6
1.2	0	.360	-.267	.196	.142	.014	7.8
1.2	45	.351	-.258	.196	.133	.015	5.4
1.2	90	.344	-.252	.190	.137	.019	6.8
1.2	135	.345	-.251	.185	.145	.015	7.7
1.3	0	.372	-.304	.160	.144	.029	12.8
1.3	45	.368	-.298	.168	.136	.029	11.7
1.3	90	.354	-.280	.155	.152	.030	14.1
1.3	135	.358	-.288	.154	.146	.027	13.1
1.4	0	.412	-.334	.192	.147	.042	13.6
1.4	45	.401	-.323	.182	.151	.037	14.5
1.4	90	.397	-.314	.189	.153	.037	15.3
1.4	135	.393	-.307	.198	.145	.038	14.0
1.5	0	.397	-.303	.219	.134	.022	12.9
1.5	45	.385	-.305	.191	.137	.027	14.7
1.5	90	.388	-.291	.223	.120	.024	9.0
1.5	135	.386	-.282	.236	.119	.025	8.8

TEST CONDITION 1, z/R = -0.70
ΩR = 634 ft/sec, θ_{75} = 6.25 deg, C_T = 0.0020

0.3	0	.859	-.086	.218	-.827	.172	17.4
0.3	45	.858	-.043	.139	-.846	.186	19.4
0.3	90	.813	-.054	.194	-.788	.191	20.5
0.3	135	.865	-.094	.195	-.837	.175	18.2
0.4	0	1.323	.020	.090	-1.320	.085	5.6
0.4	45	1.334	-.011	.101	-1.330	.122	5.6
0.4	90	1.324	.022	.021	-1.323	.101	5.0
0.4	135	1.274	.020	-.015	-1.274	.117	7.3
0.5	0	1.758	.037	-.048	-1.756	.047	3.1
0.5	45	1.741	.014	-.066	-1.740	.054	3.1
0.5	90	1.704	.009	-.045	-1.704	.086	3.3
0.5	135	1.735	.025	.005	-1.735	.097	3.8

x/R	ψ, deg	$\bar{v}_R/v_o$	$\bar{v}_x/v_o$	$\bar{v}_y/v_o$	$\bar{v}_z/v_o$	σ_{v_R/v_o}	σ_ϵ, deg
0.6	0	1.924	.053	-.047	-1.922	.149	4.0
0.6	45	1.984	.077	-.080	-1.981	.109	3.2
0.6	90	1.945	.095	-.197	-1.933	.088	3.7
0.6	135	1.899	.063	-.195	-1.888	.075	3.7
0.7	0	2.083	.058	.020	-2.082	.064	3.1
0.7	45	2.069	.044	.013	-2.068	.079	2.9
0.7	90	2.046	.017	.019	-2.045	.082	2.7
0.7	135	2.083	.048	.186	-2.074	.123	3.6
0.8	0	1.984	.123	.239	-1.966	.109	4.2
0.8	45	2.131	.111	.312	-2.105	.191	4.8
0.8	90	2.390	.098	.299	-2.369	.378	5.9
0.8	135	2.328	.074	.288	-2.309	.177	6.2
0.875	0	1.582	.218	-.001	-1.567	.203	7.9
0.875	45	1.443	.439	.104	-1.370	.258	25.0
0.875	90	1.295	.512	.231	-1.166	.535	39.0
0.875	135	1.366	-.084	.150	-1.355	.671	46.9
0.9	0	1.243	.108	-.025	-1.238	.342	25.3
0.9	45	1.107	.337	.148	-.947	.460	41.4
0.9	90	.845	.443	.259	-.672	.611	47.1
0.9	135	.873	.201	.265	-.807	.783	61.0
1.0	0	.441	-.073	.135	-.414	.309	48.2
1.0	45	.375	-.117	.103	-.341	.264	49.1
1.0	90	.337	-.138	-.006	-.307	.269	49.1
1.0	135	.370	-.157	-.025	-.334	.245	47.5
1.1	0	.170	-.060	.001	-.159	.050	31.5
1.1	45	.166	-.053	-.010	-.157	.045	31.9
1.1	90	.157	-.068	-.019	-.140	.046	32.5
1.1	135	.159	-.085	-.013	-.134	.055	35.6
1.2	0	.197	-.048	.168	-.091	.064	27.5
1.2	45	.196	-.057	.163	-.092	.062	25.6
1.2	90	.190	-.057	.160	-.086	.067	29.7
1.2	135	.190	-.056	.161	-.082	.057	28.2
1.3	0	.122	-.075	-.056	-.079	.016	18.5
1.3	45	.123	-.066	-.060	-.084	.013	16.8
1.3	90	.124	-.074	-.058	-.082	.015	18.2
1.3	135	.125	-.073	-.059	-.082	.014	17.8

x/R	Ψ, deg	$\bar{V}_R/v_o$	$\bar{v}_x/v_o$	$\bar{v}_y/v_o$	$\bar{v}_z/v_o$	σ_{V_R/v_o}	σ_ϵ, deg
1.4	0	.189	-.028	.065	-.176	.043	16.3
1.4	45	.188	-.033	.066	-.173	.043	18.5
1.4	90	.182	-.031	.060	-.169	.041	22.5
1.4	135	.184	-.031	.066	-.169	.042	21.4
1.5	0	.092	-.046	-.045	-.066	.033	41.9
1.5	45	.092	-.046	-.046	-.065	.034	40.5
1.5	90	.089	-.048	-.049	-.060	.038	41.3
1.5	135	.089	-.048	-.044	-.061	.037	41.7
TEST CONDITION 2, z/R = -0.70 ΩR = 450 ft/sec, θ_{75} = 10.75 deg, C_T = 0.0039							
0.3	0	.695	-.018	.192	-.668	.248	24.6
0.3	45	.711	-.058	.200	-.680	.229	23.7
0.3	90	.673	.051	.185	-.645	.244	26.7
0.3	135	.685	.021	.171	-.663	.236	29.5
0.4	0	1.347	.027	.065	-1.345	.059	3.7
0.4	45	1.346	-.014	.099	-1.342	.073	3.5
0.4	90	1.383	.038	.069	-1.381	.085	5.3
0.4	135	1.365	.020	.082	-1.363	.107	4.7
0.5	0	1.668	.034	.035	-1.667	.041	2.6
0.5	45	1.611	.014	.030	-1.610	.048	2.6
0.5	90	1.591	.027	.037	-1.590	.058	2.8
0.5	135	1.718	.064	.027	-1.717	.044	2.6
0.6	0	1.722	-.050	.119	-1.717	.055	3.0
0.6	45	1.890	.123	.131	-1.882	.096	2.9
0.6	90	1.902	.100	.091	-1.897	.055	2.7
0.6	135	1.850	.041	.106	-1.846	.057	2.6
0.7	0	2.033	.084	.129	-2.027	.060	2.6
0.7	45	2.004	.081	.120	-1.998	.065	2.6
0.7	90	2.008	.073	.135	-2.002	.076	2.9
0.7	135	2.170	.123	.128	-2.154	.098	3.0
0.8	0	1.987	.089	.096	-1.983	.044	2.8
0.8	45	1.968	.106	.068	-1.964	.069	4.0
0.8	90	2.012	.190	.059	-2.003	.070	2.6
0.8	135	2.272	.347	.032	-2.245	.074	2.8
0.9	0	1.232	-.053	.079	-1.229	.378	25.7
0.9	45	1.325	.175	.109	-1.309	.241	17.0
0.9	90	1.598	.698	-.022	-1.438	.556	29.7
0.9	135	2.196	.699	-.094	-2.080	.691	29.3

x/R	Ψ, deg	$\bar{V}_R/v_o$	$\bar{v}_x/v_o$	$\bar{v}_y/v_o$	$\bar{v}_z/v_o$	σ_{V_R}/v_o	σ_ε, deg
0.95	0	.724	-.179	.072	-.698	.318	40.2
0.95	45	.723	.121	-.033	-.712	.387	36.9
0.95	90	.875	.672	-.052	-.557	.472	40.1
0.95	135	.993	.969	-.001	-.219	.698	43.6
1.0	0	.414	-.125	.067	-.389	.226	30.9
1.0	45	.426	.050	.122	-.405	.215	29.9
1.0	90	.401	.195	.262	-.233	.397	44.6
1.0	135	.278	.220	.112	-.128	.499	50.4
1.1	0	.133	-.098	.087	-.024	.081	36.3
1.1	45	.132	-.073	.095	-.054	.109	40.4
1.1	90	.115	-.055	.093	-.039	.111	43.9
1.1	135	.117	-.052	.102	-.024	.121	45.2
1.2	0	.172	-.055	.161	-.027	.042	19.1
1.2	45	.157	-.048	.146	-.030	.030	23.5
1.2	90	.158	-.050	.148	-.026	.033	24.5
1.2	135	.160	-.055	.148	-.021	.032	24.8
1.3	0	.134	-.043	.123	-.032	.036	24.6
1.3	45	.127	-.041	.116	-.028	.041	26.7
1.3	90	.120	-.039	.119	-.029	.045	24.8
1.3	135	.135	-.049	.123	-.023	.043	24.4
1.4	0	.080	-.016	.078	-.008	.059	39.7
1.4	45	.073	-.007	.073	-.001	.055	43.7
1.4	90	.071	-.009	.071	-.006	.061	46.3
1.4	135	.083	-.014	.082	.008	.055	39.7
1.5	0	.103	.001	.102	.013	.011	11.5
1.5	45	.104	.001	.103	.010	.012	10.5
1.5	90	.101	-.001	.100	.012	.013	11.6
1.5	135	.106	-.008	.105	.013	.014	11.1

TEST CONDITION 3, $z/R = -0.70$
$\Omega R = 450$ ft/sec, $\theta_{75} = 6.25$ deg, $C_T = 0.0019$

0.3	0	1.001	-.096	- 040	-.996	.201	12.4
0.3	45	1.000	-.085	-.077	-.994	.184	14.1
0.3	90	.954	-.115	-.011	-.947	.177	14.4
0.3	135	.951	-.119	-.027	-.943	.195	15.0

x/R	ψ, deg	$\bar{v}_R/v_o$	$\bar{v}_x/v_o$	$\bar{v}_y/v_o$	$\bar{v}_z/v_o$	σ_{v_R/v_o}	σ_ε, deg
0.4	0	1.354	.108	-.043	-1.349	.131	10.1
0.4	45	1.357	.109	-.114	-1.348	.128	12.0
0.4	90	1.368	.149	-.050	-1.359	.173	10.1
0.4	135	1.390	.133	-.019	-1.384	.095	10.7
0.5	0	1.559	.210	-.068	-1.544	.078	5.1
0.5	45	1.603	.174	-.065	-1.592	.123	6.1
0.5	90	1.586	.201	-.025	-1.573	.112	5.9
0.5	135	1.570	.219	-.082	-1.553	.074	5.6
0.6	0	1.912	.212	-.062	-1.900	.049	2.8
0.6	45	1.872	.190	-.067	-1.862	.051	2.6
0.6	90	1.933	.185	-.006	-1.925	.092	3.2
0.6	135	1.961	.207	-.068	-1.949	.053	2.8
0.7	0	2.108	.174	.143	-2.096	.099	3.4
0.7	45	2.100	.210	-.043	-2.089	.071	2.7
0.7	90	2.070	.181	-.069	-2.061	.074	2.6
0.7	135	2.018	.144	-.059	-2.012	.059	2.6
0.8	0	2.187	.287	-.071	-2.167	.066	2.9
0.8	45	2.185	.276	-.099	-2.165	.108	2.9
0.8	90	2.149	.251	-.094	-2.132	.087	2.7
0.8	135	2.215	.253	.107	-2.198	.122	3.7
0.9	0	2.130	.280	-.024	-2.112	.415	12.2
0.9	45	2.099	.206	.097	-2.087	.478	15.1
0.9	90	2.109	.117	.051	-2.105	.376	13.3
0.9	135	1.991	.120	.081	-1.986	.250	14.9
1.0	0	1.486	.979	.030	-1.118	.279	20.8
1.0	45	1.413	.896	.046	-1.092	.640	38.4
1.0	90	1.526	.087	-.148	-1.516	.548	30.1
1.0	135	1.353	-.182	-.062	-1.339	.460	34.5
1.05	0	.863	.605	.087	-.610	.377	36.2
1.05	45	.567	.440	.049	-.353	.479	48.0
1.05	90	.380	.137	.088	-.343	.769	58.7
1.05	135	.840	-.381	-.034	-.748	.383	37.8
1.1	0	.134	-.087	-.087	-.052	.158	50.9
1.1	45	.170	-.117	-.112	-.052	.191	46.1
1.1	90	.146	-.101	-.101	-.030	.180	50.9
1.1	135	.134	-.107	-.070	-.041	.149	50.6

x/R	Ψ, deg	$\bar{v}_R/v_o$	$\bar{v}_x/v_o$	$\bar{v}_y/v_o$	$\bar{v}_z/v_o$	σ_{V_R/v_o}	σ_ϵ, deg
1.2	0	.091	-.034	-.052	-.068	.100	55.8
1.2	45	.129	-.044	-.068	-.100	.107	49.4
1.2	90	.096	-.031	-.056	-.071	.120	48.5
1.2	135	.048	-.048	-.055	-.082	.117	45.4
1.3	0	.183	.032	-.180	-.010	.086	37.2
1.3	45	.196	.019	-.195	-.017	.088	33.5
1.3	90	.189	.017	-.187	-.017	.097	36.8
1.3	135	.186	-.013	-.182	-.036	.080	35.2
1.4	0	.181	.023	-.172	-.053	.027	24.0
1.4	45	.185	.021	-.178	-.048	.036	24.9
1.4	90	.186	.008	-.178	-.053	.034	22.5
1.4	135	.184	.009	-.177	-.050	.035	25.0
1.5	0	.096	.036	-.075	.048	.031	35.3
1.5	45	.092	.036	-.075	.040	.033	37.1
1.5	90	.089	.026	-.072	.046	.036	36.8
1.5	135	.090	.031	-.067	.052	.038	38.3
TEST CONDITION 1, x/R = -1.0 ΩR = 634 ft/sec, θ_{75} = 6.25 deg, C_T = 0.0019							
0.3	0	1.822	-.050	-.326	-1.792	.101	3.8
0.3	45	1.860	-.043	-.321	-1.832	.100	3.4
0.3	90	1.842	-.033	-.364	-1.805	.096	2.9
0.3	135	1.822	-.035	-.328	-1.792	.087	2.9
0.4	0	1.777	-.070	-.197	-1.764	.452	4.6
0.4	45	1.823	-.031	-.143	-1.817	.455	4.4
0.4	90	1.833	-.045	-.233	-1.817	.430	3.8
0.4	135	1.804	-.058	-.250	-1.786	.387	3.8
0.5	0	2.099	-.027	-.235	-2.085	.104	3.2
0.5	45	2.119	-.072	-.270	-2.101	.153	3.3
0.5	90	2.089	-.096	-.244	-2.072	.132	4.2
0.5	135	2.166	-.079	-.176	-2.157	.152	4.0
0.6	0	1.882	-.000	-.230	-1.868	.333	12.7
0.6	45	1.950	.023	-.268	-1.931	.279	9.6
0.6	90	1.891	-.046	-.231	-1.877	.271	11.3
0.6	135	1.960	-.121	-.325	-1.929	.305	13.8

x/R	Ψ, deg	$\bar{v}_R/v_o$	$\bar{v}_x/v_o$	$\bar{v}_y/v_o$	$\bar{v}_z/v_o$	σ_{v_R}/v_o	σ_ϵ, deg
0.7	0	1.524	.032	-.257	-1.502	.463	27.3
0.7	45	1.505	.066	-.216	-1.488	.559	26.2
0.7	90	1.399	-.044	-.098	-1.395	.420	29.0
0.7	135	1.380	-.109	-.241	-1.355	.489	31.7
0.725	0	1.210	.020	-.318	-1.167	.436	28.8
0.725	45	1.100	-.010	-.303	-1.058	.471	33.8
0.725	90	1.129	.058	-.380	-1.062	.449	28.8
0.725	135	1.180	.041	-.446	-1.091	.403	31.3
0.775	0	.803	.022	-.541	-.592	.423	35.3
0.775	45	.820	.013	-.503	-.648	.454	37.5
0.775	90	.881	-.010	-.571	-.671	.405	31.4
0.775	135	.845	.084	-.557	-.630	.421	34.3
0.8	0	.596	.041	-.466	-.369	.354	45.9
0.8	45	.517	-.033	-.381	-.348	.427	51.2
0.8	90	.604	.011	-.495	-.347	.385	45.6
0.8	135	.634	-.000	-.523	-.359	.346	36.4
0.9	0	.362	-.040	-.355	.058	.083	26.4
0.9	45	.348	-.035	-.343	.045	.076	27.0
0.9	90	.366	-.020	-.360	.060	.071	25.7
0.9	135	.350	-.008	-.344	.063	.066	25.0
1.0	0	.379	-.067	-.364	-.085	.022	8.7
1.0	45	.372	-.069	-.355	-.087	.023	8.6
1.0	90	.383	-.066	-.368	-.086	.030	8.5
1.0	135	.370	-.071	-.354	-.081	.026	8.4
1.1	0	.415	-.051	-.410	-.040	.084	14.5
1.1	45	.394	-.055	-.388	-.040	.077	16.2
1.1	90	.418	-.066	-.411	-.042	.096	15.5
1.1	135	.390	-.061	-.384	-.032	.077	14.4
1.2	0	.354	-.023	-.353	-.018	.043	11.2
1.2	45	.339	-.037	-.337	-.008	.039	12.4
1.2	90	.350	-.036	-.349	-.007	.037	12.4
1.2	135	.330	-.036	-.328	-.002	.038	13.4
1.3	0	.340	-.040	-.338	.006	.035	14.7
1.3	45	.311	-.035	-.308	.011	.027	17.5
1.3	90	.332	-.030	-.330	.024	.033	18.3
1.3	135	.307	-.049	-.303	.020	.040	19.6

x/R	Ψ, deg	$\bar{v}_R/v_o$	$\bar{v}_x/v_o$	$\bar{v}_y/v_o$	$\bar{v}_z/v_o$	σ_{V_R}/v_o	σ_ε, deg
1.4	0	.335	-.126	-.309	-.027	.070	21.8
1.4	45	.329	-.135	-.298	.029	.067	22.8
1.4	90	.342	-.140	-.311	.020	.064	19.8
1.4	135	.325	-.138	-.293	.023	.061	20.3
1.5	0	.355	-.125	-.332	-.019	.042	12.1
1.5	45	.351	-.125	-.327	-.018	.028	11.5
1.5	90	.359	-.122	-.337	-.013	.038	11.8
1.5	135	.341	-.125	-.316	-.018	.038	12.1

TEST CONDITION 2, z/R = -1.0
ΩR = 429 ft/sec, Θ_{75} = 10.75 deg, C_T = 0.0041

0.3	0	1.707	-.016	-.260	-1.687	.067	3.3
0.3	45	1.796	-.015	-.245	-1.779	.067	2.6
0.3	90	1.781	-.029	-.268	-1.761	.056	2.7
0.3	135	1.770	-.056	-.262	-1.749	.077	2.9
0.4	0	1.995	-.095	-.238	-1.978	.064	2.7
0.4	45	1.958	-.058	-.168	-1.950	.079	3.3
0.4	90	2.059	-.047	-.196	-2.049	.074	3.0
0.4	135	2.019	-.096	-.221	-2.005	.053	2.9
0.5	0	2.133	-.069	-.140	-2.127	.101	3.4
0.5	45	2.176	-.027	-.208	-2.166	.072	2.8
0.5	90	2.188	-.076	-.214	-2.176	.086	3.5
0.5	135	2.160	-.154	-.282	-2.136	.083	3.6
0.6	0	2.054	-.032	-.245	-2.039	.194	9.6
0.6	45	2.024	-.056	-.289	-2.002	.214	12.5
0.6	90	2.083	.028	-.337	-2.055	.287	8.0
0.6	135	2.109	.059	-.308	-2.085	.312	11.4
0.675	0	1.611	-.009	-.293	-1.584	.346	27.3
0.675	45	1.704	-.041	-.200	-1.692	.346	16.5
0.675	90	1.673	.045	-.329	-1.639	.321	21.6
0.675	135	1.699	.162	-.258	-1.671	.277	23.0
0.7	0	1.473	-.026	-.368	-1.426	.455	24.5
0.7	45	1.426	.152	-.445	-1.346	.371	22.9
0.7	90	1.436	.075	-.298	-1.354	.392	24.2
0.7	135	1.439	.312	-.304	-1.372	.461	28.8

x/R	Ψ, deg	$\bar{V}_R/v_o$	$\bar{v}_x/v_o$	$\bar{v}_y/v_o$	$\bar{v}_z/v_o$	σ_{v_R/v_o}	σ_ϵ, deg
0.725	0	1.200	-.068	-.406	-1.127	.438	30.0
0.725	45	1.156	-.031	-.343	-1.103	.473	28.3
0.725	90	1.143	.129	-.442	-1.047	.453	33.1
0.725	135	.885	.187	-.202	-.841	.528	43.4
0.8	0	.668	.085	-.347	-.564	.442	44.1
0.8	45	.824	.104	-.331	-.748	.477	42.7
0.8	90	.777	.085	-.297	-.713	.484	42.5
0.8	135	.818	.116	-.328	-.740	.469	44.4
0.9	0	.423	.013	-.417	-.071	.201	31.9
0.9	45	.425	-.002	-.419	-.066	.182	28.7
0.9	90	.374	-.005	-.372	-.041	.148	36.2
0.9	135	.407	-.032	-.400	-.062	.175	30.4
1.0	0	.467	.082	-.457	-.053	.236	27.0
1.0	45	.486	.049	-.483	-.021	.172	19.3
1.0	90	.452	.079	-.445	.004	.179	25.0
1.0	135	.499	.066	-.494	.027	.220	18.6
1.1	0	.389	.050	-.386	.007	.057	12.3
1.1	45	.383	.042	-.381	.007	.057	13.8
1.1	90	.378	.037	-.376	.007	.064	12.9
1.1	135	.377	.017	-.376	.010	.058	15.5
1.2	0	.399	-.008	-.390	-.047	.049	12.6
1.2	45	.402	-.003	-.399	-.046	.054	14.3
1.2	90	.404	-.008	-.401	-.045	.050	12.2
1.2	135	.403	-.012	-.401	-.043	.048	11.0
1.3	0	.384	.000	-.384	.014	.043	18.6
1.3	45	.386	-.010	-.386	.010	.042	17.8
1.3	90	.382	.004	-.382	.014	.046	18.3
1.3	135	.382	-.007	-.381	.014	.047	20.0
1.4	0	.378	-.026	-.364	-.098	.155	16.7
1.4	45	.388	-.028	-.371	-.108	.179	17.0
1.4	90	.389	-.026	-.371	-.114	.200	17.4
1.4	135	.391	-.025	-.372	-.120	.236	18.1
1.5	0	.393	.002	-.389	-.056	.112	17.0
1.5	45	.388	-.008	-.382	-.070	.139	17.3
1.5	90	.386	-.011	-.379	-.072	.185	17.8
1.5	135	.394	-.009	-.387	-.071	.186	17.7

TEST CONDITION 3, $z/R = -1.0$
$\Omega R = 450$ ft/sec, $\theta_{75} = 6.25$ deg, $C_T = 0.0020$

x/R	Ψ, deg	$\bar{V}_R/v_o$	$\bar{v}_x/v_o$	$\bar{v}_y/v_o$	$\bar{v}_z/v_o$	σ_{V_R}/v_o	σ_ε, deg
0.3	0	2.071	-.023	-.305	-2.048	.054	3.0
0.3	45	2.044	-.059	-.297	-2.021	.080	3.1
0.3	90	2.024	-.053	-.218	-2.012	.103	3.0
0.3	135	2.048	-.028	-.277	-2.029	.077	2.9
0.4	0	2.079	-.059	-.195	-2.069	.291	4.1
0.4	45	2.116	-.041	-.299	-2.095	.272	3.2
0.4	90	2.096	-.078	-.318	-2.070	.247	3.5
0.4	135	2.048	-.071	-.247	-2.032	.258	3.8
0.5	0	2.303	.017	-.182	-2.295	.154	4.8
0.5	45	2.272	-.039	-.162	-2.266	.204	5.9
0.5	90	2.259	-.068	-.115	-2.255	.175	6.0
0.5	135	2.249	.000	-.159	-2.243	.161	4.9
0.575	0	2.090	-.062	-.050	-2.088	.347	10.4
0.575	45	2.050	-.068	-.033	-2.049	.240	10.1
0.575	90	2.064	.022	-.012	-2.064	.257	11.4
0.575	135	2.106	-.021	-.080	-2.104	.242	10.2
0.6	0	2.015	-.079	-.372	-1.979	.302	16.5
0.6	45	2.013	-.037	-.374	-1.977	.320	14.9
0.6	90	1.980	-.072	-.415	-1.935	.396	14.3
0.6	135	1.979	.052	-.443	-1.928	.359	12.8
0.65	0	1.676	-.007	-.208	-1.663	.310	20.7
0.65	45	1.613	-.029	-.202	-1.600	.367	23.7
0.65	90	1.571	-.021	-.316	-1.539	.454	22.6
0.65	135	1.685	-.028	-.253	-1.666	.483	23.7
0.675	0	1.478	-.016	-.244	-1.458	.364	29.0
0.675	45	1.583	.041	-.220	-1.567	.479	20.7
0.675	90	1.595	-.057	-.161	-1.586	.486	28.1
0.675	135	1.638	-.047	-.283	-1.612	.601	27.3
0.7	0	1.207	.094	-.355	-1.150	.460	31.1
0.7	45	1.200	.092	-.383	-1.134	.328	28.6
0.7	90	1.196	.146	-.337	-1.138	.347	32.0
0.7	135	1.322	.205	-.374	-1.252	.410	28.5
0.725	0	.860	.162	-.428	-.728	.459	40.1
0.725	45	.815	.133	-.386	-.705	.490	45.5
0.725	90	.872	.144	-.323	-.797	.463	43.1
0.725	135	.909	.096	-.380	-.820	.449	41.3

x/R	Ψ, deg	$\bar{v}_R/v_o$	$\bar{v}_x/v_o$	$\bar{v}_y/v_o$	$\bar{v}_z/v_o$	σ_{V_R}/v_o	σ_ε, deg
0.8	0	.573	.157	-.420	-.357	.264	37.7
0.8	45	.565	.111	-.456	-.315	.276	38.4
0.8	90	.618	.098	-.499	-.350	.335	38.4
0.8	135	.645	.134	-.520	-.257	.328	35.0
0.9	0	.542	.082	-.495	-..06	.226	32.8
0.9	45	.530	.003	-.505	-.161	.190	32.2
0.9	90	.553	.063	-.509	-.206	.270	33.0
0.9	135	.560	.090	-.489	-.259	.243	31.0
1.0	0	.449	-.005	-.447	-.047	.047	11.9
1.0	45	.447	-.002	-.443	-.056	.052	12.8
1.0	90	.445	-.014	-.442	-.053	.052	12.1
1.0	135	.436	-.018	-.432	-.056	.056	12.0
1.1	0	.428	-.012	-.426	-.036	.033	8.0
1.1	45	.429	-.018	-.427	-.045	.029	7.5
1.1	90	.425	-.022	-.422	-.039	.035	7.1
1.1	135	.421	-.023	-.418	-.038	.031	6.9
1.2	0	.432	.007	-.432	.008	.053	21.5
1.2	45	.425	.003	-.425	.001	.051	23.5
1.2	90	.430	.015	-.430	-.002	.057	22.0
1.2	135	.430	.003	-.430	.012	.048	18.8
1.3	0	.435	.050	-.432	-.001	.083	17.9
1.3	45	.441	.064	-.436	-.006	.073	17.1
1.3	90	.444	.061	-.440	.001	.076	15.1
1.3	135	.438	.052	-.435	-.001	.067	14.8
1.4	0	.469	.006	-.469	.007	.034	11.2
1.4	45	.477	-.008	-.477	.008	.045	11.2
1.4	90	.467	-.009	-.467	.007	.041	11.8
1.4	135	.472	-.028	-.471	-.002	.046	11.6
1.5	0	.413	-.180	-.367	-.059	.031	10.6
1.5	45	.410	-.168	-.369	-.061	.032	10.6
1.5	90	.414	-.186	-.365	-.059	.039	9.9
1.5	135	.413	-.194	-.360	-.059	.041	10.1

TEST CONDITION 1, $z/R = -1.5$
$\Omega R = 634$ ft/sec, $\theta_{75} = 6.25$ deg, $C_T = 0.0021$

x/R	ψ, deg	$\bar{V}_R/v_o$	$\bar{v}_x/v_o$	$\bar{v}_y/v_o$	$\bar{v}_z/v_o$	σ_{V_R/v_o}	σ_ϵ, deg
0.45	0	.897	.001	.064	-.895	.199	14.1
0.45	45	.923	.062	.056	-.920	.212	14.7
0.45	90	.875	.043	.092	-.869	.204	12.7
0.45	135	.858	.054	.109	-.849	.177	14.5
0.5	0	1.233	.073	-.084	-1.228	.320	8.8
0.5	45	1.192	.078	-.064	-1.188	.300	9.5
0.5	90	1.209	.097	-.052	-1.204	.357	10.9
0.5	135	1.178	.108	-.079	-1.170	.307	10.4
0.6	0	1.490	.147	-.014	-1.483	.304	5.1
0.6	45	1.524	.139	.002	-1.518	.314	5.6
0.6	90	1.500	.139	.019	-1.493	.303	6.9
0.6	135	1.540	.139	-.007	-1.534	.272	11.6
0.7	0	1.900	.152	.036	-1.894	.232	9.0
0.7	45	1.887	.128	.082	-1.881	.299	7.5
0.7	90	1.874	.127	.060	-1.869	.262	7.4
0.7	135	1.890	.174	.057	-1.881	.273	8.5
0.75	0	1.991	.266	-.062	-1.972	.099	3.0
0.75	45	1.974	.258	-.063	-1.956	.140	3.5
0.75	90	2.014	.240	-.081	-1.998	.210	3.9
0.75	135	2.000	.198	-.069	-1.989	.161	4.4
0.8	0	2.091	.164	.012	-2.085	.103	4.5
0.8	45	2.066	.165	.039	-2.059	.091	5.0
0.8	90	2.059	.162	.035	-2.052	.154	4.9
0.8	135	2.120	.150	.054	-2.114	.177	5.0
0.85	0	2.071	.182	.040	-2.063	.170	8.0
0.85	45	2.043	.190	-.017	-2.034	.236	8.4
0.85	90	2.049	.203	.013	-2.039	.247	8.2
0.85	135	2.010	.191	.013	-2.001	.322	8.1
0.9	0	1.927	.111	.016	-1.924	.363	11.5
0.9	45	1.987	.118	.005	-1.984	.251	11.0
0.9	90	2.012	.230	-.062	-1.997	.252	10.7
0.9	135	1.977	.210	-.096	-1.963	.283	10.1
1.0	0	1.462	.135	.024	-1.456	.468	25.7
1.0	45	1.473	.188	.088	-1.459	.462	26.7
1.0	90	1.506	.197	.093	-1.490	.544	25.9
1.0	135	1.431	.291	.166	-1.391	.463	26.5

x/R	Ψ, deg	$\bar{v}_R/v_o$	$\bar{v}_x/v_o$	$\bar{v}_y/v_o$	$\bar{v}_z/v_o$	σ_{V_R}/v_o	σ_ϵ, deg
1.1	0	.729	.071	.068	-.722	.506	46.9
1.1	45	.843	-.104	-.013	-.837	.406	40.0
1.1	90	.875	.038	.192	-.853	.504	43.2
1.1	135	.790	.109	.004	-.782	.489	43.3
1.2	0	.497	.029	.017	-.496	.487	49.1
1.2	45	.459	.022	.085	-.451	.435	50.6
1.2	90	.453	.058	.175	-.413	.452	50.4
1.2	135	.387	.033	.141	-.359	.418	55.1
1.3	0	.286	.007	.232	-.167	.170	41.0
1.3	45	.276	-.000	.226	-.158	.161	39.2
1.3	90	.295	.018	.225	-.191	.170	41.4
1.3	135	.305	.022	.246	-.180	.180	38.4
1.4	0	.214	.117	.113	-.140	.116	47.7
1.4	45	.231	.138	.128	-.134	.133	48.0
1.4	90	.217	.124	.113	-.137	.112	48.0
1.4	135	.194	.109	.110	-.117	.130	53.6
1.5	0	.149	.018	.130	-.071	.089	27.7
1.5	45	.143	.019	.134	-.047	.071	29.6
1.5	90	.149	.028	.133	-.061	.086	30.1
1.5	135	.149	.027	.136	-.053	.084	30.7
1.6	0	.122	.001	.091	-.081	.077	52.8
1.6	45	.115	.013	.080	-.082	.087	55.9
1.6	90	.121	-.001	.083	-.087	.088	53.9
1.6	135	.115	.001	.080	-.082	.085	52.4

TEST CONDITION 2, $z/R = -1.5$
$\Omega R = 431$ ft/sec, $\theta_{75} = 10.75$ deg, $C_T = 0.0041$

0.45	0	1.100	.185	.111	-1.079	.169	12.0
0.45	45	1.121	.219	.128	-1.092	.137	11.0
0.45	90	1.166	.191	.197	-1.133	.146	7.2
0.45	135	1.136	.203	.167	-1.105	.162	11.2
0.5	0	1.309	.146	.154	-1.291	.251	7.5
0.5	45	1.375	.109	.146	-1.363	.215	5.4
0.5	90	1.405	.096	.165	-1.391	.189	6.6
0.5	135	1.370	.087	.195	-1.353	.182	6.1

x/R	Ψ, deg	$\bar{V}_R/v_o$	$\bar{v}_x/v_o$	$\bar{v}_y/v_o$	$\bar{v}_z/v_o$	σ_{V_R/v_o}	σ_ε, deg
0.6	0	1.280	.178	.053	-1.266	.162	4.1
0	45	1.285	.174	.068	-1.271	.132	4.4
0.6	90	1.274	.163	.075	-1.261	.124	3.7
0.6	135	1.277	.118	.117	-1.266	.101	3.5
0.7	0	1.716	.067	.136	-1.709	.227	4.4
0.7	45	1.678	.099	.083	-1.673	.225	5.5
0.7	90	1.668	.071	.113	-1.662	.273	3.3
0.7	135	1.705	.076	.144	-1.697	.225	3.1
0.8	0	2.171	.143	-.081	-2.165	.145	6.1
0.8	45	2.322	.267	-.040	-2.306	.199	5.1
0.8	90	2.295	.161	-.027	-2.289	.246	6.5
0.8	135	2.349	.123	.008	-2.346	.226	8.5
0.9	0	2.245	.278	-.059	-2.227	.243	5.8
0.9	45	2.314	.372	-.188	-2.276	.154	5.1
0.9	90	2.319	.356	-.160	-2.286	.207	6.9
0.9	135	2.307	.269	.167	-2.285	.302	12.3
1.0	0	2.082	.177	-.048	-2.074	.207	7.2
1.0	45	2.175	.251	-.024	-2.161	.196	6.3
1.0	90	2.122	.364	-.090	-2.088	.195	6.7
1.0	135	2.193	.475	-.194	-2.132	.197	6.3
1.05	0	1.942	.138	.065	-1.936	.407	14.3
1.05	45	1.831	.215	-.160	-1.811	.451	17.9
1.05	90	1.802	.271	-.082	-1.780	.352	16.9
1.05	135	1.700	.347	-.047	-1.664	.421	21.8
1.1	0	1.222	-.087	-.031	-1.219	.481	37.7
1.1	45	1.203	-.100	.008	-1.199	.365	28.5
1.1	90	1.079	.032	.037	-1.078	.463	35.6
1.1	135	1.033	.148	.289	-.981	.478	33.3
1.15	0	.924	.052	-.026	-.923	.477	38.5
1.15	45	.928	.057	-.088	-.922	.412	32.0
1.15	90	.923	.025	-.036	-.922	.349	22.1
1.15	135	.882	.206	.001	-.858	.470	36.2
1.2	0	.770	.166	.264	-.704	.432	41.3
1.2	45	.836	.269	.192	-.768	.429	39.1
1.2	90	.852	.130	.115	-.834	.521	42.7
1.2	135	.910	.086	.080	-.902	.428	37.4

x/R	ψ, deg	$\bar{V}_R/v_o$	$\bar{v}_x/v_o$	$\bar{v}_y/v_o$	$\bar{v}_z/v_o$	σ_{V_R/v_o}	σ_ϵ, deg
1.3	0	.723	.357	.212	-.591	.316	36.5
1.3	45	.694	.269	.142	-.624	.326	39.0
1.3	90	.784	.355	.176	-.676	.375	33.4
1.3	135	.709	.302	.166	-.619	.313	32.3
1.4	0	.285	.107	.208	-.162	.238	40.1
1.4	45	.305	.128	.216	-.174	.251	39.5
1.4	90	.338	.105	.242	-.212	.248	31.6
1.4	135	.346	.098	.252	-.215	.229	32.6
1.5	0	.102	.051	.032	-.082	.074	47.7
1.5	45	.091	.048	.036	-.069	.081	50.1
1.5	90	.094	.054	.039	-.067	.070	50.4
1.5	135	.090	.050	.046	-.060	.067	50.8
1.6	0	.127	.065	.101	-.042	.051	35.9
1.6	45	.121	.067	.090	-.045	.058	39.6
1.6	90	.118	.066	.088	-.042	.051	37.7
1.6	135	.121	.063	.098	-.032	.041	35.1
TEST CONDITION 3, $z/R = -1.5$							
$\Omega R = 452$ ft/sec, $\theta_{75} = 6.25$ deg, $C_T = 0.0020$							
0.45	0	.936	.007	-.059	-.934	.244	15.0
0.45	45	.896	.005	-.165	-.880	.246	18.0
0.45	90	.972	.028	-.031	-.971	.258	15.3
0.45	135	.975	.056	-.111	-.967	.290	15.9
0.5	0	.846	.113	.047	-.837	.256	18.5
0.5	45	.812	.078	.053	-.806	.198	24.1
0.5	90	.798	.072	.064	-.792	.149	17.8
0.5	135	.815	.071	.111	-.804	.202	20.6
0.6	0	.668	.043	.144	-.651	.169	20.1
0.6	45	.662	.059	.123	-.648	.182	16.7
0.6	90	.630	.080	.088	-.619	.188	21.9
0.6	135	.650	.060	.109	-.638	.160	18.6
0.7	0	.984	.150	.054	-.971	.115	5.7
0.7	45	.974	.137	.074	-.961	.104	6.3
0.7	90	.949	.123	.074	-.938	.120	8.0
0.7	135	.960	.126	.049	-.950	.107	6.1

x/R	ψ, deg	$\bar{v}_R/v_o$	$\bar{v}_x/v_o$	$\bar{v}_y/v_o$	$\bar{v}_z/v_o$	σ_{v_R/v_o}	σ_ϵ, deg
0.8	0	1.755	.300	.032	-1.729	.138	4.2
0.8	45	1.778	.291	.035	-1.753	.157	4.3
0.8	90	1.773	.264	.024	-1.753	.153	3.5
0.8	135	1.772	.245	.087	-1.753	.111	4.1
0.9	0	2.213	.329	-.102	-2.186	.088	3.0
0.9	45	2.198	.322	-.117	-2.171	.090	2.9
0.9	90	2.207	.329	-.137	-2.178	.084	2.9
0.9	135	2.191	.312	-.134	-2.164	.146	3.4
0.95	0	2.315	.317	-.106	-2.291	.099	3.9
0.95	45	2.276	.291	-.088	-2.256	.121	3.3
0.95	90	2.277	.273	.010	-2.261	.135	3.3
0.95	135	2.330	.290	-.054	-2.311	.103	3.3
1.0	0	2.310	.260	-.113	-2.293	.166	5.3
1.0	45	2.286	.248	-.053	-2.272	.167	7.5
1.0	90	2.304	.314	-.087	-2.281	.112	4.9
1.0	135	2.355	.294	-.073	-2.335	.143	4.5
1.05	0	2.262	.325	-.092	-2.237	.171	7.2
1.05	45	2.187	.280	-.093	-2.167	.269	8.8
1.05	90	2.196	.360	-.128	-2.162	.258	7.9
1.05	135	2.193	.395	-.206	-2.147	.339	9.1
1.1	0	2.151	.239	.075	-2.137	.327	15.3
1.1	45	2.127	.261	.013	-2.111	.246	14.9
1.1	90	2.148	.264	-.028	-2.131	.229	11.3
1.1	135	2.141	.306	.010	-2.119	.288	14.9
1.2	0	1.714	.348	.074	-1.677	.507	25.8
1.2	45	1.703	.160	-.015	-1.695	.497	20.6
1.2	90	1.569	.097	.134	-1.561	.485	31.9
1.2	135	1.601	.133	.102	-1.592	.400	27.8
1.25	0	1.218	.137	.088	-1.207	.456	35.3
1.25	45	1.269	.088	.112	-1.261	.417	30.2
1.25	90	1.235	.177	.138	-1.214	.517	32.8
1.25	135	1.139	.172	.164	-1.114	.502	37.3
1.3	0	.469	.020	.031	-.468	.340	50.2
1.3	45	.498	-.051	.082	-.488	.397	49.8
1.3	90	.538	-.144	.048	-.516	.343	40.9
1.3	135	.595	-.099	.098	-.579	.365	39.2

x/R	Ψ, deg	$\bar{v}_R/v_o$	$\bar{v}_x/v_o$	$\bar{v}_y/v_o$	$\bar{v}_z/v_o$	σ_{V_R}/v_o	σ_ε, deg
1.4	0	.377	.027	-.128	-.354	.202	26.3
1.4	45	.365	.050	-.131	-.337	.210	28.9
1.4	90	.372	.010	-.140	-.344	.184	24.1
1.4	135	364	.002	-.163	-.326	.158	26.0
1.5	0	.251	-.009	-.071	-.241	.106	43.2
1.5	45	.247	-.015	-.062	-.239	.117	44.9
1.5	90	.255	-.024	-.067	-.245	.090	41.3
1.5	135	.251	-.005	-.086	-.236	.100	43.4
1.6	0	.283	.073	-.139	-.235	.055	11.2
1.6	45	.292	.067	-.154	-.239	.060	9.7
1.6	90	.290	.068	-.149	-.239	.054	9.9
1.6	135	.293	.065	-.155	-.240	.056	10.7
TEST CONDITION 1, z/R = -2.0 ΩR = 634 ft/sec, Θ_{75} = 6.25 deg, C_T = 0.0020							
0.45	0	1.602	.107	-.077	-1.596	.353	9.5
0.45	45	1.628	.025	-.077	-1.626	.234	8.3
0.45	90	1.641	.066	-.020	-1.640	.270	6.3
0.45	135	1.653	-.029	-.043	-1.652	.272	7.0
0.5	0	1.585	.009	-.021	-1.585	.216	4.7
0.5	45	1.567	.010	-.024	-1.567	.242	6.2
0.5	90	1.576	.038	-.047	-1.574	.206	6.3
0.5	135	1.591	.025	-.024	-1.591	.223	6.6
0.6	0	1.778	.076	.088	-1.774	.179	8.8
0.6	45	1.760	.039	.046	-1.759	.157	9.1
0.6	90	1.803	.083	.090	-1.799	.209	6.6
0.6	135	1.767	.066	.076	-1.764	.116	10.3
0.7	0	1.852	.067	.012	-1.850	.290	14.2
0.7	45	1.908	.074	.009	-1.907	.248	9.5
0.7	90	1.922	.082	.011	-1.921	.340	10.5
0.7	135	1.914	.016	-.058	-1.913	.272	10.8
0.8	0	1.427	-.037	.055	-1.426	.414	22.4
0.8	45	1.328	-.016	.132	-1.322	.433	25.6
0.8	90	1.303	-.024	.048	-1.301	.395	28.1
0.8	135	1.291	.002	.078	-1.289	.417	25.8

x/R	ψ, deg	$\bar{v}_R/v_o$	$\bar{v}_x/v_o$	$\bar{v}_y/v_o$	$\bar{v}_z/v_o$	σ_{V_R/v_o}	σ_ε, deg
0.9	0	.653	.168	.166	-.609	.406	45.2
0.9	45	.663	.082	.153	-.640	.373	43.5
0.9	90	.652	-.022	.099	-.645	.369	43.8
0.9	135	.756	.103	.156	-.733	.368	36.4
0.925	0	.480	.059	.392	-.270	.263	36.3
0.925	45	.530	.084	.465	-.240	.233	31.4
0.925	90	.496	.031	.449	-.209	.203	28.7
0.925	135	.524	.115	.464	-.216	.252	31.8
1.0	0	.168	-.131	.095	-.044	.066	36.3
1.0	45	.159	-.126	.089	-.037	.067	38.5
1.0	90	.161	-.122	.097	-.040	.071	39.7
1.0	135	.156	-.115	.098	-.040	.075	40.2
1.1	0	.191	-.125	.125	-.072	.062	31.0
1.1	45	.191	-.128	.119	-.078	.061	26.2
1.1	90	.196	-.130	.122	-.081	.056	27.0
1.1	135	.197	-.131	.119	-.087	.058	25.3
1.2	0	.226	-.131	.145	-.113	.029	13.2
1.2	45	.224	-.130	.143	-.113	.032	15.3
1.2	90	.228	-.136	.146	-.109	.030	13.6
1.2	135	.222	-.131	.144	-.106	.032	15.7
1.3	0	.158	-.103	.077	-.092	.038	32.2
1.3	45	.166	-.101	.079	-.105	.035	27.0
1.3	90	.166	-.111	.082	-.092	.033	27.7
1.3	135	.166	-.107	.086	-.094	.037	27.8
1.4	0	.273	-.147	.186	-.137	.028	12.6
1.4	45	.271	-.146	.183	-.136	.036	14.7
1.4	90	.274	-.153	.182	-.137	.030	14.0
1.4	135	.276	-.151	.187	-.135	.039	14.4
1.5	0	.301	-.186	.210	-.109	.036	12.5
1.5	45	.300	-.185	.209	-.109	.040	14.3
1.5	90	.302	-.185	.211	-.111	.045	12.7
1.5	135	.303	-.183	.212	-.114	.042	13.2
1.6	0	.330	-.226	.226	-.083	.043	11.7
1.6	45	.328	-.225	.223	-.086	.044	10.7
1.6	90	.331	-.233	.216	-.092	.037	10.4
1.6	135	.333	-.227	.224	-.097	.042	9.9

TEST CONDITION 2, z/R = -2.0
ΩR = 450 ft/sec, θ_{75} = 10.75 deg, C_T = 0.0040

x/R	Ψ, deg	$\bar{v}_R/v_o$	$\bar{v}_x/v_o$	$\bar{v}_y/v_o$	$\bar{v}_z/v_o$	σ_{V_R/v_o}	σ_ϵ, deg
0.45	0	1.906	.254	.453	-1.833	.289	15.4
0.45	45	1.954	.247	.375	-1.901	.224	13.3
0.45	90	1.955	.165	.362	-1.914	.176	10.7
0.45	135	1.987	.190	.388	-1.939	.243	13.6
0.5	0	1.832	.168	.380	-1.785	.280	9.6
0.5	45	1.843	.166	.360	-1.800	.244	12.2
0.5	90	1.817	.123	.419	-1.764	.250	12.2
0.5	135	1.780	.101	.390	-1.734	.328	13.8
0.6	0	1.684	.153	.345	-1.641	.337	17.4
0.6	45	1.695	.170	.301	-1.659	.325	16.4
0.6	90	1.710	.108	.336	-1.673	.353	15.7
0.6	135	1.625	.110	.297	-1.594	.334	23.2
0.7	0	1.833	.258	.210	-1.802	.248	15.4
0.7	45	1.812	.247	.216	-1.782	.301	16.9
0.7	90	1.786	.344	.273	-1.731	.308	19.8
0.7	135	1.798	.157	.238	-1.775	.361	14.7
0.8	0	1.843	.479	.336	-1.748	.346	24.6
0.8	45	1.827	.336	.351	-1.761	.359	23.7
0.8	90	1.778	.376	.429	-1.684	.377	23.1
0.8	135	1.690	.270	.412	-1.616	.308	23.6
0.825	0	1.565	.276	.425	-1.481	.422	25.4
0.825	45	1.468	.271	.425	-1.410	.423	27.4
0.825	90	1.552	.227	.379	-1.488	.439	25.2
0.825	135	1.492	.189	.319	-1.445	.473	26.0
0.85	0	1.114	.284	.371	-1.011	.474	34.8
0.85	45	1.017	.404	.350	-.865	.470	38.2
0.85	90	1.027	.268	.374	-.918	.502	39.0
0.85	135	1.077	.367	.383	-.937	.571	39.5
0.9	0	.462	.122	.381	-.231	.203	37.2
0.9	45	.434	.086	.321	-.279	.234	40.1
0.9	90	.435	.071	.350	-.248	.171	37.0
0.9	135	.412	.102	.318	-.241	.162	38.6
1.0	0	.335	.053	.317	-.094	.115	26.9
1.0	45	.346	.043	.336	-.071	.135	26.6
1.0	90	.357	.066	.341	-.079	.127	26.1
1.0	135	.334	.070	.316	-.084	.116	24.7

x/R	ψ, deg	$\bar{v}_R/v_o$	$\bar{v}_x/v_o$	$\bar{v}_y/v_o$	$\bar{v}_z/v_o$	σ_{V_R}/v_o	σ_ϵ, deg
1.1	0	.349	.117	.299	-.137	.123	24.9
1.1	45	.337	.092	.296	-.132	.123	29.3
1.1	90	.346	.094	.302	-.141	.129	28.8
1.1	135	.376	.108	.325	-.156	.173	26.6
1.2	0	.292	.048	.268	-.107	.051	14.1
1.2	45	.286	.051	.259	-.109	.057	14.1
1.2	90	.288	.051	.265	-.100	.064	10.5
1.2	135	.286	.054	.262	-.102	.064	14.1
1.3	0	.322	-.023	.317	-.052	.057	11.2
1.3	45	.316	-.027	.310	-.053	.051	10.7
1.3	90	.311	-.025	.305	-.053	.054	12.8
1.3	135	.316	-.026	.311	-.046	.055	12.4
1.4	0	.206	-.027	.193	-.067	.074	39.4
1.4	45	.217	-.027	.205	-.067	.074	38.3
1.4	90	.219	-.032	.206	-.067	.080	36.6
1.4	135	.219	-.029	.205	-.071	.079	37.3
1.5	0	.259	-.026	.257	-.015	.081	23.1
1.5	45	.259	-.027	.257	-.018	.078	22.9
1.5	90	.257	-.032	.255	-.016	.073	23.7
1.5	135	.252	-.027	.250	-.011	.076	24.0
1.6	0	.294	-.066	.287	-.013	.103	21.7
1.6	45	.292	-.074	.282	-.019	.098	23.2
1.6	90	.302	-.075	.292	-.013	.093	20.0
1.6	135	.295	-.075	.284	-.025	.093	21.1

TEST CONDITION 3, $z/R = -2.0$
$\Omega R = 454$ ft/sec, $\theta_{75} = 6.25$ deg, $C_T = 0.0021$

0.45	0	1.674	.373	.517	-1.548	.413	26.8
0.45	45	1.619	.373	.421	-1.519	.503	24.5
0.45	90	1.697	.309	.418	-1.615	.422	21.7
0.45	135	1.697	.426	.552	-1.547	.434	24.8
0.5	0	1.487	.321	.476	-1.372	.472	29.1
0.5	45	1.646	.210	.474	-1.563	.455	26.8
0.5	90	1.588	.341	.442	-1.486	.408	28.8
0.5	135	1.575	.340	.469	-1.465	.377	25.4

x/R	Ψ, deg	$\bar{V}_R/v_o$	$\bar{v}_x/v_o$	$\bar{v}_y/v_o$	$\bar{v}_z/v_o$	σ_{V_R/v_o}	σ_ϵ, deg
0.6	0	1.293	.466	.538	-1.079	.400	30.7
0.6	45	1.271	.283	.488	-1.138	.399	32.6
0.6	90	1.216	.364	.439	-1.074	.409	31.4
0.6	135	1.281	.377	.420	-1.150	.385	29.1
0.625	0	1.277	.383	.491	-1.114	.398	31.5
0.625	45	1.256	.370	.422	-1.123	.369	32.3
0.625	90	1.246	.411	.413	-1.102	.363	32.5
0.625	135	1.242	.395	.393	-1.110	.403	33.9
0.7	0	1.128	.497	.664	-.764	.481	33.3
0.7	45	1.109	.350	.526	-.912	.461	33.1
0.7	90	1.122	.509	.510	-.861	.426	32.9
0.7	135	1.132	.500	.542	-.858	.446	32.4
0.8	0	.811	.521	.507	-.358	.481	40.4
0.8	45	.768	.470	.486	-.365	.482	43.0
0.8	90	.699	.432	.477	-.273	.451	48.9
0.8	135	.804	.491	.574	-.276	.460	37.8
0.9	0	.626	.427	.434	-.145	.422	39.4
0.9	45	.590	.409	.377	-.198	.462	43.7
0.9	90	.614	.438	.393	-.174	.474	41.6
0.9	135	.635	.429	.452	-.122	.400	38.3
1.0	0	.456	.269	.345	-.129	.231	38.4
1.0	45	.470	.252	.384	-.096	.173	37.3
1.0	90	.454	.252	.360	-.114	.174	38.5
1.0	135	.458	.254	.354	-.140	.221	37.1
1.1	0	.441	.260	.352	-.049	.158	38.5
1.1	45	.429	.286	.318	-.033	.151	40.3
1.1	90	.469	.279	.375	-.040	.161	33.0
1.1	135	.484	.307	.373	-.025	.155	33.2
1.2	0	.489	.231	.429	.040	.103	17.0
1.2	45	.494	.234	.433	.044	.090	16.7
1.2	90	.483	.237	.417	.058	.079	16.8
1.2	135	.466	.240	.396	.051	.070	20.6
1.3	0	.446	.161	.411	.063	.085	20.0
1.3	45	.449	.164	.413	.062	.088	19.5
1.3	90	.446	.167	.410	.053	.086	18.1
1.3	135	.453	.171	.416	.053	.101	18.2

x/R	Ψ, deg	$\bar{V}_R/v_o$	$\bar{v}_x/v_o$	$\bar{v}_y/v_o$	$\bar{v}_z/v_o$	σ_{V_R/v_o}	σ_ε, deg
1.4	0	.406	.147	.372	.075	.045	15.4
1.4	45	.400	.154	.363	.068	.048	14.5
1.4	90	.400	.147	.366	.064	.046	15.2
1.4	135	.405	.145	.371	.073	.048	14.5
1.5	0	.421	.118	.404	.008	.072	18.5
1.5	45	.414	.138	.390	.004	.071	18.4
1.5	90	.395	.116	.377	-.003	.069	19.2
1.5	135	.374	.115	.356	.004	.071	18.9
1.6	0	.455	.138	.425	-.084	.027	5.3
1.6	45	.457	.138	.427	-.086	.026	5.0
1.6	90	.460	.129	.434	-.077	.029	5.4
1.6	135	.463	.136	.435	-.082	.028	5.7